Cosmic ray propagation for various galactic magnetic field models

E. Roberts

COSMIC RAY PROPAGATION FOR VARIOUS GALACTIC MAGNETIC FIELD MODELS

by

E. ROBERTS, B.Sc.

A Thesis submitted to the
University of Durham for the
Degree of Doctor of Philosophy

April, 1973

ABSTRACT

A survey has been made of the information about the galactic magnetic field strength and configuration which has been obtained from a variety of astronomical measurements. These measurements comprise the polarization of starlight, the background synchrotron radiation emitted by relativistic electrons, the Zeeman splitting observed in absorption lines produced by clouds of neutral hydrogen and the Faraday rotation of the plane of the electric vector of linearly polarized radiation from extragalactic radio sources and pulsars.

Using these data four magnetic field models have been devised to represent the coherent galactic field. These are denoted models A, B, C, and D. Model A describes a field directed along the galactic spiral arms towards galactic longitude $\ell \sim 270^{\circ}$ above the galactic plane and towards $\ell \sim 90^{\circ}$ below the plane at the Sun. Model D also describes a longitudinal type of field but with no reversal above the galactic plane. The model C field has a helical configuration, while model B is a combination of model C near the Sun and model D at greater distances. A model has also been formulated for the irregular component of the magnetic field.

The trajectories of particles with energy above $5. 10^{17}$ eV have been followed through the coherent galactic field and, using the assumption that the sources are uniformly distributed within the galactic disc or spiral arms, predictions are made of the expected anisotropy of high energy cosmic rays of galactic origin reaching the Earth.

Measurements of the arrival directions at the Earth of extensive air shower primaries obtained by the Volcano Ranch, Haverah Park and Pilliga Forest experiments are then compared with the arrival direction distributions predicted assuming various percentages of primary particles to be of galactic origin. Assuming that the metagalactic cosmic rays are isotropic upper limits are obtained for the percentage of cosmic rays that could be of galactic origin.

Consideration of the irregular field component produces modifications in the values for these upper limits.

In general, assuming that the galactic field can be represented by a model such as A or D, together with irregularities, and that all primary cosmic rays are protons, it would appear that most cosmic rays of energy $\sim 6.10^{17}$ eV to 10^{19} eV must be of metagalactic origin.

PREFACE

The work described in this thesis was carried out in the period 1969 - 1972 while the author was a research student under the supervision of Professor A. W. Wolfendale in the Cosmic Ray Group of the Physics Department of the University of Durham.

The formulation of the coherent galactic magnetic field models, their use in calculating cosmic ray trajectories and in deducing predicted anisotropies, and the comparison with measurements was shared with the author's colleagues. The author was solely responsible for the comparison of model predictions with measurements of the Faraday rotation of radiation from the pulsars, and the work on the field irregularities except where indicated otherwise.

Reports were presented at the 12th International Conference on Cosmic Rays (Hobart, 1971) on the possibility of energetic cosmic rays arriving from the Crab Nebula (Osborne J.L., and Roberts, E., Proceedings; Hobart: University of Tasmania, Vol. **1**, 340) and on the anisotropy of cosmic rays of galactic origin above 10^{17} eV (Karakula, S., et al., Proceedings; Hobart: University of Tasmania, Vol. **1**, 310). The latter was also reported on by Karakula, S., et al., 1971, (J. Phys. A: Gen. Phys., Vol. 5, 904). The effects of the irregularities in the field were described by Osborne, J.L., et al., at the Third European Symposium on Cosmic Rays held in Paris in September 1972.

CONTENTS

Page

CHAPTER 1

INTRODUCTION

One of the basic problems associated with cosmic rays, particularly those of high energies ($\gtrsim 10^{16}$ eV) is the question of where they originate. Theories of high energy cosmic ray origin divide into two groups. Those which postulate that the majority of such cosmic rays are produced in the Galaxy and those which favour extragalactic sources.

Until the discovery of pulsars it was thought that cosmic rays of energy $\gtrsim 10^{18}$ eV could not be produced in the Galaxy. For the bulk of cosmic rays the proposed galactic sources included stars, novae, supernovae and the galactic centre. From considerations of maintaining a quasi-steady state for the distribution and energy of cosmic rays in the Galaxy, non-exploding stars were ruled out as sources for the bulk of particles with energy greater than $\sim 10^{9}$ eV/nucleon. It was thought possible that small explosions (giving $\lesssim 10^{55}$ ergs to cosmic rays) in the galactic nucleus or, perhaps, novae could supply sufficient power to make significant contributions to the cosmic ray flux in the Galaxy. However, on this basis, supernovae appear to be the most likely galactic source of the bulk of cosmic rays of all energies. Strong radio emission is also observed from supernovae which would seem to indicate that they are responsible for accelerating electrons, and probably the nuclear components of cosmic rays. Thus supernovae appear to be good candidates for the role of the main sources of cosmic rays in the Galaxy, although it is not definitely proved that they fulfil this role (Ginzburg and Syrovatskii, 1971). Although supernovae could produce the cosmic rays, the question of whether they can be produced with the required intensity, energy and charge spectra remains unresolved.

Various mechanisms have been proposed for accelerating cosmic rays in supernovae, including acceleration by shock waves produced during the explosion and acceleration in the supernova shell. In a supernova shell of radius

$\sim 4.10^{18}$cm, containing a field $\sim 10^{-3}$ gauss, particles could be accelerated up to energies $\sim 10^{17}$ eV /nucleon. (c.f. 10^{14} ev/nucleon for a typical nova). Thus this mechanism could not be responsible for producing cosmic ray particles up to energies $\sim 10^{19}$ eV, and prior to the discovery of pulsars it seemed that such particles must be of metagalactic origin.

The discovery of pulsars, which were subsequently identified as supernovae remnants, provided an alternative solution. Although the exact acceleration mechanism operating in pulsars is not yet clear they are very probably high energy cosmic ray sources (e.g. Gunn and Ostriker, 1969; Gold, 1969). (For a pulsar of radius $\sim 10^{6}$ cm with a magnetic field $\sim 10^{12}$ gauss, energies up to $3.\ 10^{20}$ eV/nucleon are possible).

In an alternative model Kulikov et al. (1969) suggested that high energy cosmic ray particles were formed in an explosion in the galactic nucleus $\sim 10^{6}$ years ago. By assuming that particle propagation is of a diffusional nature and by superimposing the energy spectra of particles with a range of Z values, they were able to reproduce the observed spectral shape. However, this diffusional approach is not really applicable when the radius of curvature of the particles is of the order of the disc thickness. Thus, this model would give incorrect predictions for the cosmic ray anisotropy in this energy region.

If high energy particles are of galactic origin it is unlikely that they will arrive at the Earth isotropically. Particles with energy $\gtrsim 10^{17}$ eV would not be completely trapped within the Galaxy by the galactic magnetic field and their arrival directions at the Earth would reflect the source distribution in the Galaxy and the effect of the magnetic field. (Syrovatskii, 1969). Thus if cosmic rays of energies $\gtrsim 10^{17}$ eV were found to arrive at the Earth with the appropriate degree of anisotropy this would be an indication that they could be of galactic origin.

Alternatively high energy cosmic rays could be of metagalactic origin, in which case they would presumably arrive at the Earth isotropically. Possible extragalactic sources include radio galaxies and quasars. The biggest problem encountered by such a hypothesis is a result of the existence of the 2.7°K blackbody relict radiation first detected by Penzias and Wilson (1965). If this radiation is indeed of Universal origin and if the cosmic rays pervade the whole universe, then the resulting interactions would produce a cut-off in the cosmic ray spectrum at $\sim 3.10^{19}$ eV. (Greisen, 1966; Zatsepin and Kuzmin, 1966). Hillas (1968) studied the effects of this radiation on cosmic rays in an evolving universe, in which the suggested extragalactic sources of cosmic rays (strong radio emitters) were more active in the past. He postulated that the interactions with the microwave radiation would have produced much greater energy loss, with lower threshold energies in the past, and calculated the energy loss by protons, in extragalactic space, due to interactions with microwave radiation both under present conditions and in a universe ten times smaller. Thence he predicted a steepening of the cosmic ray proton primary energy spectrum between 6.10^{15} eV and 3.10^{18} eV due to the effects of electron pair production. Assuming that at 10^{17} - 10^{18} eV most primary cosmic rays are protons (Linsley and Scarsi, 1962), Hillas suggested that the ankle of the primary energy spectrum, often attributed to a transition from galactic to extragalactic primaries, is actually a result of this proton-photon interaction. As a result of Π production a steepening of the spectrum was also predicted at $\sim 3.10^{19}$ eV, resulting in an effective cut-off in the spectrum at this energy.

However, this cut-off is not confirmed by air shower measurements - particles of higher energies having been detected by, for example, Andrews et al. (1968) and Brownlee et al. (1970a). In fact, the latter claim to have detected energies $\geq 10^{20}$ eV.

In general the absence of cut-off would only appear to be compatible with a universal relict microwave radiation if the high energy cosmic rays are of

local (i.e. effectively galactic) origin.

Attempts have been made to retain the theory of extragalactic origin by proposing that the ultra high energy ($\gtrsim 10^{19}$ eV) particles have a different source. For example it has been suggested that the ultra high energy primaries are neutrinos produced by secondaries of proton-microwave photon interactions (Berezinskii and Zatsepin, 1969; Berezinskii and Zatsepin, 1971).

One piece of evidence that would seem to be in favour of the extragalactic origin theory is the observed isotropy in the distribution of arrival directions at the Earth of E.A.S. primaries (e.g. Linsley, 1963; Brownlee et al., 1970). Analysis of the data to find anisotropies in the right ascension distribution has usually yielded negative results. Within the experimental limits high energy cosmic ray primaries arrive isotropically. The limits to the compatibility of this with high energy primaries being of galactic origin can be investigated by studying the anisotropies that would be present in the arrival direction distributions assuming various galactic source distributions and galactic magnetic field configurations. This forms the basis of the present work.

By collating the results of the various measurements of the galactic magnetic field it is possible to construct alternative field models to represent this field. Hence cosmic ray trajectories can be calculated for each model and assuming various source distributions within the Galaxy predictions for the arrival direction distributions can be made. Comparison with the extensive air shower arrival direction data yields a limit to the fraction of high energy cosmic rays that could be of galactic origin and yet not produce observable anisotropies.

CHAPTER 2

MEASUREMENTS OF THE GALACTIC MAGNETIC FIELD

2.1 Stellar polarization

Evidence for the existence of a magnetic field in the Galaxy was first found in the polarization of starlight.

Chandrasekhar (1946) had predicted that, if Thomson scattering by free electrons plays an important part in the transfer of radiation in the atmospheres of early type stars, then the continuous radiation emerging from these stars should be plane polarized.

While attempting to verify this Hiltner (1949) found that radiation from other types of stars is also polarized and concluded that the polarization is not associated with each individual star but is the effect on the radiation of passing through interstellar space. This polarization is independent of wavelength, the amount of polarization is greater near the galactic plane, and the plane of polarization is associated with the galactic plane. Hiltner suggested that this effect could be due to scattering of starlight by interstellar particles, the particles being unsymmetrical and elongated, and aligned by some force, such as a magnetic field.

Several mechanisms for aligning the interstellar particles have been suggested but they are usually based on the Davis and Greenstein mechanism (1951).

Davis and Greenstein calculated the various torques that might act on a grain of dust in a magnetic field $\sim 10^{-5}$ gauss and concluded that only paramagnetic relaxation has an appreciable effect. They considered both prolate and oblate spheroidal grains, consisting mostly of hydrogen compounds but also 12% iron by weight, and with mean radii 10^{-5} to 3.10^{-5} cm. These dust grains spin with an angular velocity of 10^{-5} to 10^{-6} rad/sec, due to equipartition of energy between dust and gas. To obtain the smallest rotation kinetic energy for their angular momentum the short axes of these grains

tend to become the axes of rotation. Paramagnetic absorption results in these axes becoming aligned parallel to the galactic magnetic field. Thus the maximum extinction coefficient is for light with its electric vector perpendicular to the magnetic field. The degree of alignment due to this mechanism was described by Davis and Greenstein by a distribution parameter F.

$$F = {}^{1}/_{3} - \langle \cos^2 a_z \rangle$$

where a_z is the angle between the axis of symmetry of a grain and the axis of symmetry of the orientating mechanism, $\langle \cos^2 a_z \rangle$ is the average over all grains. If there is no alignment F = 0, if the grains are all aligned with their axes of symmetry parallel to the field $F = -{}^{2}/_{3}$, and if the grains are all aligned with axes of symmetry perpendicular to the field $F = {}^{1}/_{3}$.

If the grains are prolate spheroids Davis and Greenstein predict

$$F = F_{\ell} = 6.3 \times 10^{6} \frac{B^2}{a N_H \cdot T^{\frac{1}{2}} T_g}$$

for small magnetic fields.

B is the magnetic flux density in gauss, a is the grain radius in μ, N_H the number of gas atoms per cm^3, T is the temperature of the interstellar gas, and T_g is the temperature of the dust grains. The above relationship holds so long as $|F_{\ell}| << {}^{1}/_{3}$. If $|F_{\ell}| >> {}^{1}/_{3}$ then the grains become completely aligned with $F = {}^{1}/_{3}$. If the grains are oblate spheroids F will be negative with a limiting value of $-{}^{2}/_{3}$ but the plane of polarization and order of magnitude of the effect will be unchanged.

Several modifications of this theory have been introduced by considering different types of grains. Henry (1958), considered ferromagnetic dust grains, with axial ratios of 2:1, consisting of monocrystals of iron or nickel, or of ferrites. Diamagnetic grains such as graphite flakes have also been studied.

Assuming $N_H T^{\frac{1}{2}} = 100$ (for neutral and ionized hydrogen regions between clouds), $T_g = 10^{\circ}K$, the grains will be practically completely aligned for fields much greater than

50 μgauss for graphite flakes

30 μgauss for paramagnetic grains

1·2 μgauss for ferrites

$1 \cdot 3 \times 10^{-2}$ μgauss for iron grains.

[$a \sim 4 \times 10^{-6}$ cm for iron grains and graphite flakes, and $a \sim 2 \times 10^{-5}$ cm for other grains] (Hall and Serkowski 1963).

Since other measuring techniques indicate magnetic fields $\sim 10^{-6}$ gauss it appears likely that the Davis and Greenstein method is applicable, producing polarization proportional to the square of the magnetic field.

Due to this uncertainty of the type of grain involved, the distribution of these grains and the alignment mechanism, the amount of polarization is not a reliable measure of the strength of the magnetic field, although the method may enable the orientation of the magnetic field in the local spiral arm of the Galaxy to be determined.

Hiltner (1949) found that stars of low galactic latitude tend to show polarization with the electric vector parallel to the galactic plane, indicating a magnetic field parallel to the plane of the Galaxy. Hoag (1953) measured the polarization of light from 92 stars and found that in the direction of the spiral arms the polarisation is small and randomly orientated, whereas light travelling perpendicularly to this direction experiences maximum polarization. This led to the conclusion that the magnetic field lies along the direction of the spiral arms of the Galaxy.

Since 1949 the polarization of the light from several thousands of stars has been investigated (Mathewson and Ford 1970).

Many models have been proposed for the configuration of the galactic

magnetic field. Basically, however, there are two types of model; the "quasi-longitudinal" models in which the magnetic field direction lies parallel to the spiral arm axis (e.g. Chandrasekhar and Fermi, 1953), and the "helical" models in which the magnetic field lies along helices wound round the spiral arms of the Galaxy. (Hoyle and Ireland 1961).

Optical polarization data appears to indicate that the local spiral arm magnetic field has a helical component (Ireland 1961, Mathewson 1968). Mathewson combined his polarization measurements of 1800 stars with those of several other observers, including Hiltner (1956) and Hall (1958), giving a total of nearly 7000 stellar polarization measurements, and plotted the electric vectors of the starlight (Figure 2.1).

The electric vector plotted at a particular latitude and longitude represents the projection of the magnetic field, in that direction, on the plane perpendicular to the line of sight. By trying different field configurations Mathewson found that the best fit to his data would be given by a local magnetic field of a helical form. In his model the field is wound in spirals, of pitch angle 7°, round coaxial elliptical cylinders whose axes lie in the direction of the local spiral arms (latitude $b = 0$, longitude $\ell = 90^{\circ}$ and 270°). The axial ratio of the cylinders is 3 and the helices are sheared through 40° anticlockwise looking from the North Galactic pole. The sun is 100 pc towards the galactic centre from the axis of the helices and 10 pc below the galactic plane.

However, Gardner et al. (1969c) interpret Mathewson's data as being consistent with a longitudinal field directed towards longitude $\ell = 50^{\circ}$. In this case for longitudes $\ell = 140^{\circ}$ and $\ell = 320^{\circ}$, the E vectors would be parallel to the galactic plane at all latitudes, whereas for $\ell = 50^{\circ}$ and $\ell = 230^{\circ}$ the polarization would be randomly orientated. Mathewson's data does show these characteristics but, as seen in the diagram many of the lines are curved which seems to indicate a better fit from a helical model

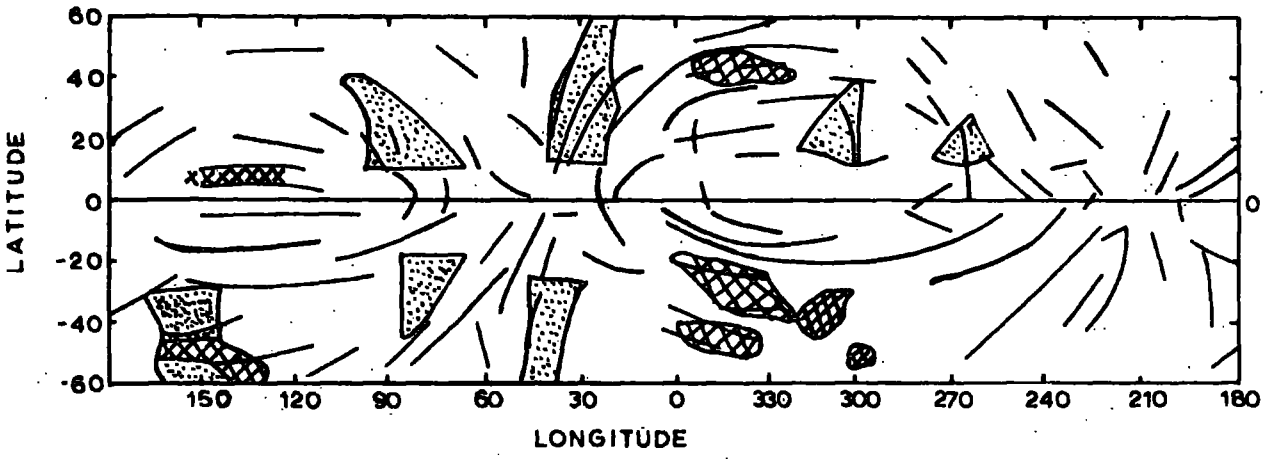

Figure 2.1. "Flow patterns" of E-vectors of optical polarization measurements.

Radio spurs are shaded.

Hatched areas are strongly polarized at 408 MHz

(Mathewson, 1968)

(Verschuur 1970). Seymour (1969) also concluded, from a statistical study of stellar polarization measurements, that the local spiral arm magnetic field is longitudinal but only 550 measurements were involved. Thus, the measurements of the polarization of starlight appear to indicate a local spiral arm magnetic field that is helical or has a helical component.

2.2 Synchrotron emission: Existence of halo field

2.2.1 Synchrotron mechanism

Relativistic electrons accelerating in the galactic magnetic field produce synchrotron radiation at radio frequencies. An electron of energy E GeV in a magnetic field of strength H gauss produces radiation with the spectrum maximum corresponding to frequency

$$\nu_m = \frac{eH}{2\pi mc}\left(\frac{E}{mc}\right)^2 \quad \text{Hz},$$

where m is the electron mass. So $\nu_m = 1{\cdot}61 \times 10^{13} HE^2$ Hz. In order to relate the measured intensities of synchrotron emission to the magnetic field, some knowledge of the distribution and energy spectrum of relativistic interstellar electrons is needed. If the electron spectrum is of the form $N(E)\,dE = kE^{-\gamma}dE$ where k is a constant, then it can be shown that the synchrotron emission has spectral index $\alpha = \frac{\gamma-1}{2}$ and is given by

$$J(\nu) \propto N(>E)\, E^{2}\nu^{(-\gamma+1)/2} H^{(\gamma+1)/2} \text{ ergs Hz}^{-1} \text{ cm}^{-3}$$

at frequency ν Hz where E is the energy of electrons corresponding to $\nu = \nu_m$ and N(>E) is the number of relativistic electrons with energy greater than E GeV (Biermann and Davis, 1960).

If the electron spectrum is known, then by measuring the synchrotron emission at various frequencies it is possible to evaluate the magnetic field. Many measurements have been made of the spectral index of radio emission, e.g. Costain (1960), Smith (1961), Large, Mathewson and Haslem (1961), and in the range 80 - 1500 MHz, $\alpha \sim 0{\cdot}6 \pm 0{\cdot}1$, giving $\gamma = 2{\cdot}2$.

Many measurements have been made of the electron energy spectrum at the earth using cloud chambers in balloons (e.g. Critchfield et al. (1952), Meyer and Vogt (1961), and Earl (1961)), and nuclear emulsion in balloons (e.g. Anand et al. (1968),(1970)) and counter techniques (e.g. Meyer and Muller, 1971).

Spectral index values obtained for the electron spectrum at the earth are $\sim 2{\cdot}8$.

e.g. γ = 2·7 - 2·8 at 5 - 600 GeV (Zatsepin, 1971)

γ = 2·8 at 10 - 1000 GeV (Meyer and Muller, 1971).

If it is assumed that this electron spectrum extends throughout interstellar space, allowing for the effect of solar modulation, the interstellar magnetic field strength can be calculated.

Due to a lack of knowledge of the exact form of the interstellar electron spectrum, and the distribution of these electrons in the Galaxy, an uncertainty is introduced into the value of the magnetic field deduced from synchrotron emission because $H^{(\gamma+1)/2} \propto \frac{1}{N(>E)}$.

An early estimate of the galactic field based on synchrotron observations was made by Davies (1965), who used measurements obtained by Mills (1959) to show that $N(>E)\ H^{1.6} = 2{\cdot}5 \times 10^{10}$, giving $H \sim 3 \times 10^{-5}$ gauss. However, later measurements of this type could give lower field estimates e.g. Anand et al. (1968b) give $H \sim 6 \times 10^{-6}$G.

2.2.2 Is there a galactic halo field?

Assuming a uniform electron density distribution synchrotron radiation can be used to map the relative magnetic field strengths in the Galaxy and it can give information in any direction of observation. Surveys of the synchrotron emission have been carried out by many workers including Davies and Hazard (1962) at 237 MHz, Pauliny-Toth and Shakeshaft (1962) at 404 MHz. Landecker and Wielebinski (1970) have composed a full sky map at 150 MHz.

Although the intensity of the radiation is greatest in the galactic plane, these surveys indicate that synchrotron radiation is also produced at high

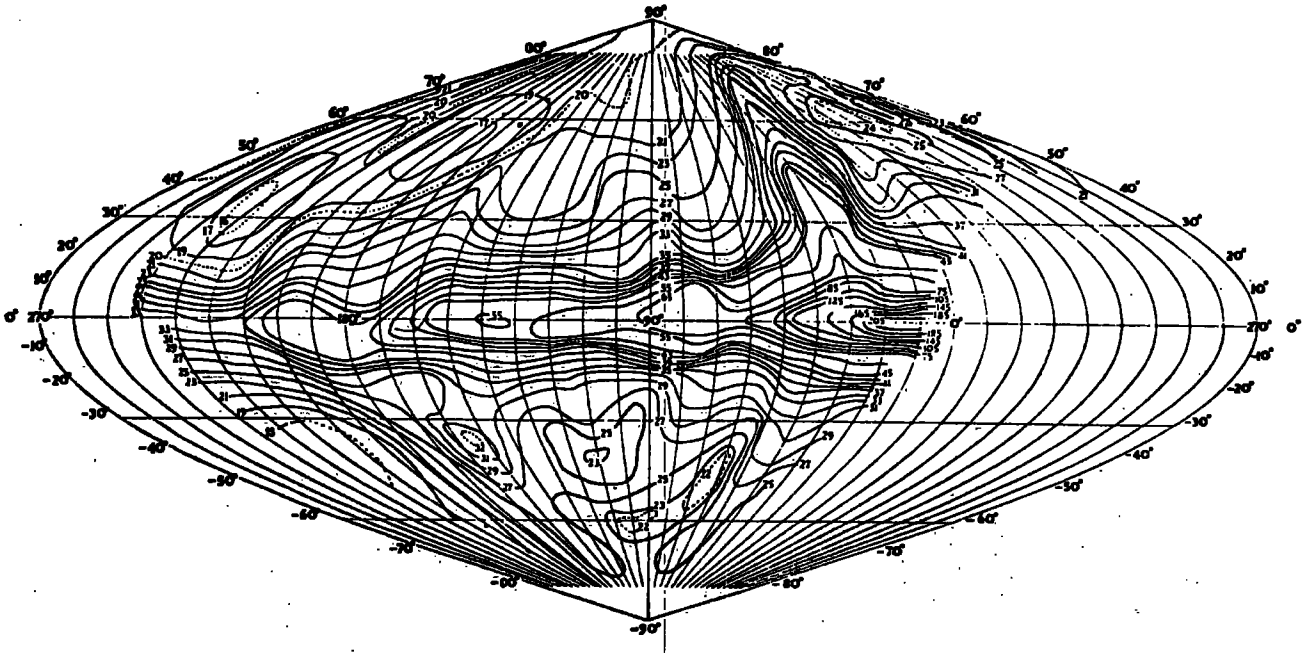

Figure 2.2. Contours of antenna temperature at 404 MHz from Pauliny-Toth and Shakeshaft (1962)

galactic latitudes (Figure 2.2). This could be due to the presence of a galactic halo magnetic field. Such a halo was originally postulated as a reservoir of Cosmic Rays, and later a halo was found in spiral galaxy M31 (Baldwin (1955)). However, not all spiral galaxies exhibit such a radio halo (Mathewson and Rome, 1963) and the question of whether our Galaxy possesses a halo or not is rather controversial.

Initially the suggestion that our Galaxy has a halo, of diameter 20 - 30 kpc, received much support on the basis of synchrotron measurements and cosmic ray containment theories, e.g. Baldwin (1955), Spitzer (1956), Woltjer (1965) and Parker (1965). However, it has been suggested that the structure seen in the background radiation at high latitudes is of a local nature, probably within the local spiral arm, and could be due to supernovae remnants (Davies, 1964). The presence of these radio spurs must be taken into account when investigating the synchrotron radiation to determine if a galactic halo exists. Surveys have been made to study these loops and spurs (Berkuijsen 1971) and it appears to be unlikely that there is a galactic halo field.

2.2.3 Field configuration

Synchrotron radiation is polarized perpendicularly to the direction of the magnetic field. If the magnetic field is uniform and there is an isotropic distribution of relativistic electrons, 72% polarization would be seen. In fact the observed polarization is only a few per cent. Also, at frequencies less than $\sim$ 1000 MHz Faraday rotation causes a reduction in the percentage polarization, except in the directions where there is no line of sight component of the magnetic field. Thus the radiation should exhibit optimum polarization in directions perpendicular to the magnetic field direction, and this fact was used by Mathewson and Milne (1964) to determine the magnetic field configuration in the local spiral arm. They found that

the polarized radiation at 400 MHz was confined to a band lying in a circle which went through the poles and cut the galactic plane at $\ell'' = 340^\circ$ and 160°, indicating a magnetic field directed along the local spiral arm the axis of which is directed towards 250° and 70°. However, Hornby (1966) postulated that Mathewson and Milnes' results are not inconsistent with a field in the local spiral arm of tightly wound helices, if these helices are sheared by differential galactic rotation so that the field direction is perpendicular to $\ell'' = 140^\circ$. Using model fields of this type, Hornby attempted to predict the intensity of synchrotron emission at 404 MHz and then compared the results with the Pauliny-Toth and Shakeshaft survey (1962). In general he found that this helical type of field model is compatible with the synchrotron measurements. Other surveys of the polarized radio emission have been made by Wielebinski and Shakeshaft (1964) at 408 MHz; Mathewson, Broton and Cole (1966) at 620 MHz, and Bingham (1966) at 1407 MHz.

Bingham and Shakeshaft (1967) devised a field model using these polarization measurements, taking into account the distribution of the intensity of synchrotron emission, and Faraday Rotation measurements of extragalactic sources. They concluded that in the galactic plane the magnetic field lies along the local spiral arm towards $\ell'' = 70^\circ$, but with a reversal of direction at positive latitudes. They suggest that this reversal of field could be due to an extension of the field above the galactic disc. If this extended part rotates more slowly than the galactic disc itself a reversal of field would be produced. However, Bingham and Shakeshaft admitted that a helical model would also explain the reversal of field at positive latitudes.

Mathewson (1968) attempted to show that his helical field model (Section 2.1) is compatible with measurements of the synchrotron radiation. In fact his model, derived from studies of optical polarization data, is very similar to that of Hornby (1966) derived from the synchrotron radiation measurements. Mathewson tried to show that the field directions in radio

spurs and loops supported his helical model. Synchrotron measurements show elongated regions of high emission intensity, that are strongly polarized with the magnetic field direction parallel to their length. Mathewson suggested that these spurs and ridges are due to the compression of magnetic lines of force, and can be used to determine the local magnetic field direction. Mathewson (1968) claimed that the field directions indicated by such features agree with those found from optical polarization measurements and fit his model (Fig. 2.1). However, objections to this have been raised (e.g. Spoelstra 1971) since not all radio spurs and regions of high polarization fit the model. Some of the polarization directions in these features are perpendicular to the helicies.

Mathewson also claimed that directions of zero or small line of sight magnetic fields predicted by such a helical model agree with those found from radio polarization measurements (Mathewson and Nicholls 1968). However optimum polarization should be observed where the helicies cross the galactic plane. This does not appear to be the case. It appears rather doubtful that radio spurs and regions of excess polarization are indicators of a helical structure. In fact synchrotron emission possibly cannot give much reliable information about magnetic field configuration for the large scale field.

2.3 The Zeeman Effect

The use of the Zeeman splitting of a spectral line, in the interstellar magnetic field, to determine the latter was first suggested by Bolton and Wild (1957). This method can be used to determine the magnetic fields in clouds of neutral hydrogen seen in absorption against strong radio sources. The splitting of the 21 cm absorption line can then be observed. However, the field measured is not necessarily representative of the general galactic field. In a weak magnetic field the 21 cm line, when observed in the direction of the magnetic field, is split into two components. These

components are circularly polarized in opposite directions.

The total splitting between these polarized components is $2{\cdot}8\ \mathrm{Hz}(\mu_G)^{-1}$ for the longitudinal field component. This is much smaller, for $H \sim 10^{-5}$ to 10^{-7} gauss, than the observed line widths. However to measure the splitting a device sensitive to the direction of the polarization can be used. The method used is to switch from the measurement of one sense of rotation to the other, and finding the change in the amount of light received ΔT, for all frequencies across the absorption line. Assuming that this line has a gaussian profile the maximum value of ΔT can be related to the frequency separation $\Delta\nu$ by

$$\Delta\nu = 0{\cdot}7\mu \frac{\Delta T_{max}}{T}$$

where μ and T are the half width and depth of the line (Galt et al., 1960). Early measurements of this type failed to produce any conclusive evidence for the existence of a magnetic field in any of the clouds measured. Galt, Slater and Shuter observed this absorption line using the radio source Cassiopeia A (see Figure 2.3). Their observed values are shown below. (Positive $\Delta\nu$ indicates a field directed away from the observer).

TABLE 2.1

Source	$\Delta\nu$ in Hz
Cass A	-24 ± 60
Cass A	$+10 \pm 60$
$\ell = 82{\cdot}2^{\circ}$, $b = -2{\cdot}38^{\circ}$	$+40 \pm 60$.

These show no significant Zeeman splitting and indicate a field $H < 5\ 10^{-5}$ gauss.

Other early measurements gave similar upper limits.

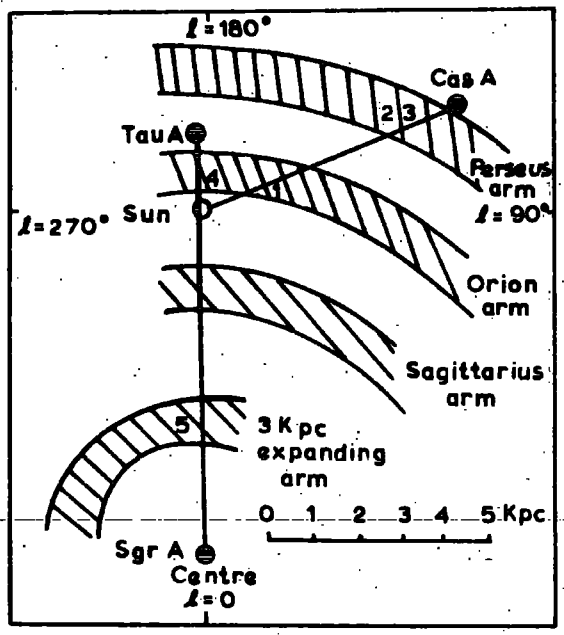

Figure 2.3. Diagram of absorbing clouds and sources from Davies et al (1960)

TABLE 2.2

(Positive field indicates a field away from the observer)

	Source (Figure 2.3)	Mean longitudinal field in absorbing cloud $\bar{H}_\ell$ in μG	cloud
Davies et al. (1960)	Cass A $\ell'' = 112^\circ$	+ 1 ± 4	1
"	Cass A $\ell'' = 112^\circ$	+ 1 ± 7	2
"	Cass A $\ell'' = 112^\circ$	+ 3 ± 7	3
"	Tau A $\ell'' = 185^\circ$	+10 ± 10	4
"	Sgt A $\ell'' = 0^\circ$	+14 ± 40	5
Davies et al. (1962)	Tau A	< 2·5	
	Tau A	< 5	
	Cass A	< 5	
	Cyg A	< 5	
Weinreb (1962)	Cass A	< 3	
	Tau A	< 5	
Davies et al. (1963a)	Cass A, Cyg A, Tau A and Sgt A	< 7	

These early experiments thus only gave an upper limit to the magnetic field.

However as the resolving powers of the apparatus used improved, values of $\bar{H}_\ell$ of 10·0 to 3·6 μgauss were detected going round the local arm in an anticlockwise direction (Davies et al., 1963b).

These measurements, however, indicated fields an order of magnitude smaller than those found from the synchrotron radiation technique, at that time (Davies and Shuter 1963). As mentioned in 2.2.1, lack of knowledge of the relativistic electron density makes the synchrotron method unreliable for estimating the field strength, so that the value of 10^{-5} gauss given by such measurements could be too high. However, at that time, it was

thought that the magnetic field was responsible for holding the gas and dust in the spiral arm and this would require a field of $\sim 10^{-5}$ gauss. The fields found from Zeeman splitting thus appeared to be too small, and several attempts were made to account for this by proposing that the fields in the clouds of neutral hydrogen are not representative of the general galactic field. Woltjer (1961) suggested that the dense clouds seen in absorption could be diamagnetic as they are more dense than the rest of the interstellar material and so could contain more heavy positive ions and electrons per cubic centimetre. Diamagnetism could be produced in the clouds by the action of surface currents in the outer layers of the cloud. Thus the field outside the cloud could be larger than that within it. Davies and Shuter (1963), however, showed that neutral hydrogen clouds could not support such large external fields but would collapse. Woltjer (1961) also postulated that the fields inside the absorbing clouds could consist of small closed loops of field ~ 1 pc in size. However, galactic rotation and cloud collision would result in the annihilation of such loops of field. It thus seemed likely that the field measured by Zeeman splitting techniques is of the order of the general interstellar magnetic field.

Recent values of $\bar{H}_\ell$ are shown in Table 2.3.

TABLE 2.3

	Position of Absorbing Cloud	$\bar{H}_\ell$ in μ gauss
Verschuur 1968 (Confirmed by Davies, R.D. et al., 1968)	Perseus arm in direction of Cass A	10 - 12 μ gauss
Verschuur 1969a	Perseus arm in direction of Tau A	$-3{\cdot}5 \pm 0{\cdot}7$ μ gauss
Verschuur 1969a	Orion arm (local arm)	$\lesssim 1, 2{\cdot}5, 4{\cdot}8$ μ gauss

These measurements are consistent with a field in a clockwise direction

around the spiral arm, observed from the North galactic pole.

Until recently it seemed that the Zeeman splitting of the 21 cm line would provide a direct measurement of the line of sight magnetic field, indicating field strength and direction. The field strengths found are independent of dust, relativistic electron, or thermal electron distributions and represent the field at a particular place, not an integrated value. This method also shows whether the line of sight component is directed towards or away from the observer, allowing some information on field directions to be found. Of course measurements can only be made from the absorption spectra of intense galactic radio sources, which results in a restricted sampling of the interstellar magnetic field and the complexity of the spectra makes estimation of the field difficult, but these were not thought to be insuperable difficulties. However, in 1969 it was postulated that these neutral hydrogen clouds contain "frozen in" magnetic fields (Verschuur 1969b). Verschuur suggests that the magnetic field may be stronger in the clouds as a result of amplification by contraction of the clouds and he proposes that the greater the density of the cloud the stronger the field strength in it. If a cloud contracts isotropically its density is proportional to radius^{-3} and the magnetic field strength is proportional to radius^{-2}. Thus the magnetic field is proportional to density $^{2}/3$. Verschuur (1970) attempted to show that the available data gives a reasonable fit to this (Figure 2.4) so that by extrapolating back to the average interstellar hydrogen density he finds a mean interstellar magnetic field of 1 - 3 μ gauss. Assuming that the clouds of hydrogen have "frozen-in" fields, Zeeman effect measurements probably cannot be used to give field strengths and directions in the general interstellar regions, and are of no value when attempting to construct a galactic magnetic field model.

	Direction	ℓ	b
1	Tau A	185°	-6°
2	Tau A		
3	Cas A	112°	-2°
4	Cas A		
5	Cyg A	76°	+6°
6	Cyg A		
7	M 17	15°	-1°
8	Orion A	209°	-19°
9	Orion A		

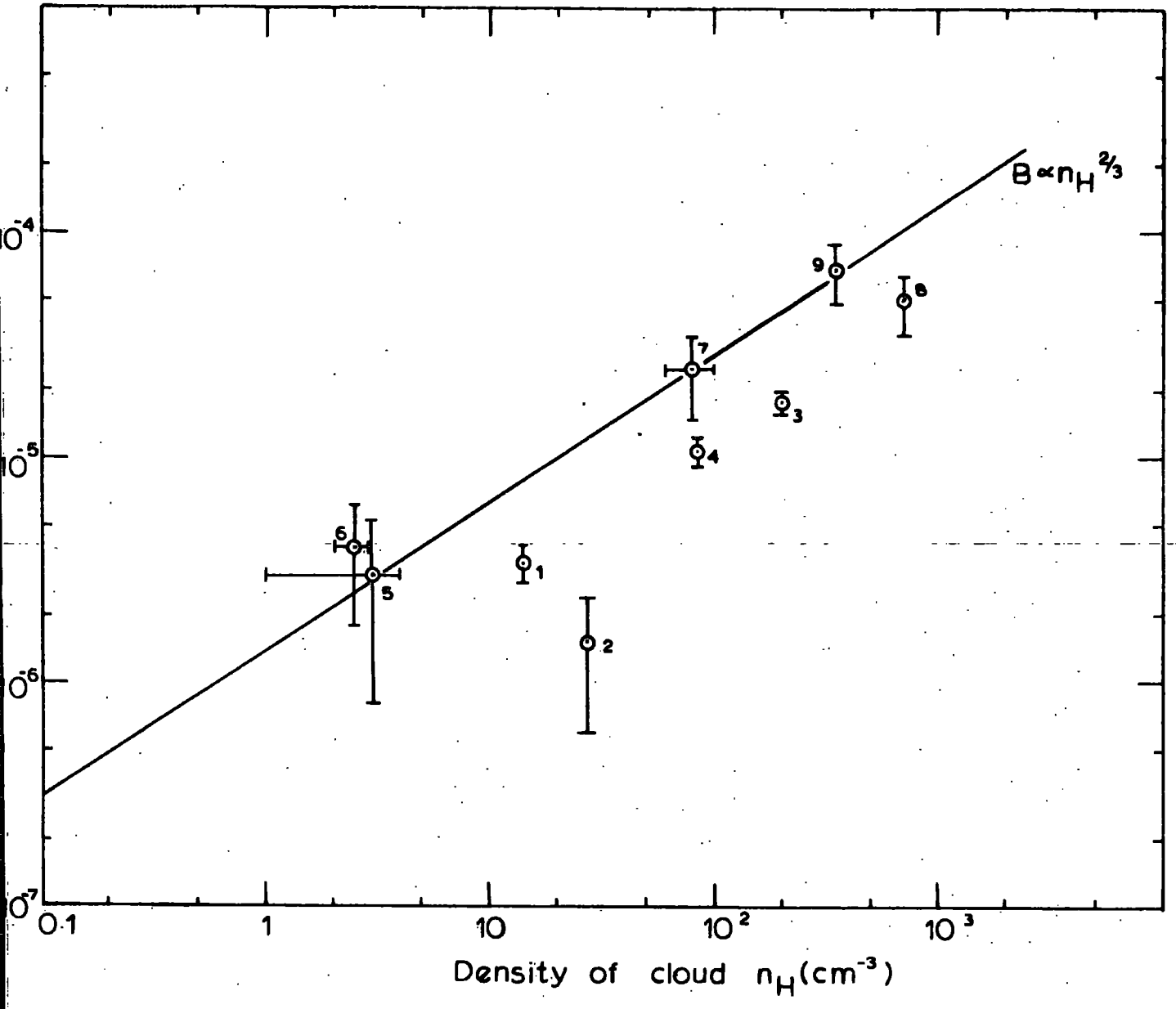

Figure 2.4. Magnetic Fields in neutral hydrogen clouds as a function of their density. (Verschuur 1970).

2.4 Faraday Rotation: Extragalactic sources

The plane of polarization of polarized radiation is rotated as it passes through a region of electrons in a magnetic field. This fact can be used to determine the interstellar magnetic field. The angle through which the plane is rotated, θ, is given by $\theta = 0{\cdot}81 \lambda^2 \int N_e H_\ell \, d\ell$ rad where λ is the wavelength of the radiation in metres, N_e is the electron density in cm^{-3}, H_ℓ is the line of sight component of the magnetic field in μgauss and ℓ is the depth, in parsecs, of the region in which rotation occurs. The magnetic field is determined by measuring the observed position angle of the plane of polarization of the radiation from a given radio source. This is done for several values of the wavelength and the resultant plot of θ against λ^2 gives the rotation measure (R.M.) θ/λ^2. Values of the rotation measure are typically 10 - 100 rad m^{-2}. By using a series of sources it is possible to find the rotation measure in many directions. A positive value of R.M. indicates a line of sight component of the field directed towards the observer. Then a knowledge of N_e and ℓ allow values of the magnetic field intensity to be found. However, it is necessary to know in which region Faraday rotation occurs and the electron density in that region. Early measurements of the position angle of the polarization from radio sources were made by

Mayer et al. (1962)
Haddock and Hobbs (1963)
Rose et al. (1963)
Seielstad et al. (1963)
Morris, Radhakrishnan and Seielstad (1964)
Hollinger et al. (1964)
Maltby and Seielstad (1966).

Measuring the position angle θ at several wavelengths for a given source allows the rotation measure for that source to be found. Some of the results obtained by Gardner and Whiteoak (1963) are shown in Figure 2.5.

It is important to know where this Faraday rotation is produced. Faraday rotation produced in the ionosphere must be taken into account. In fact,

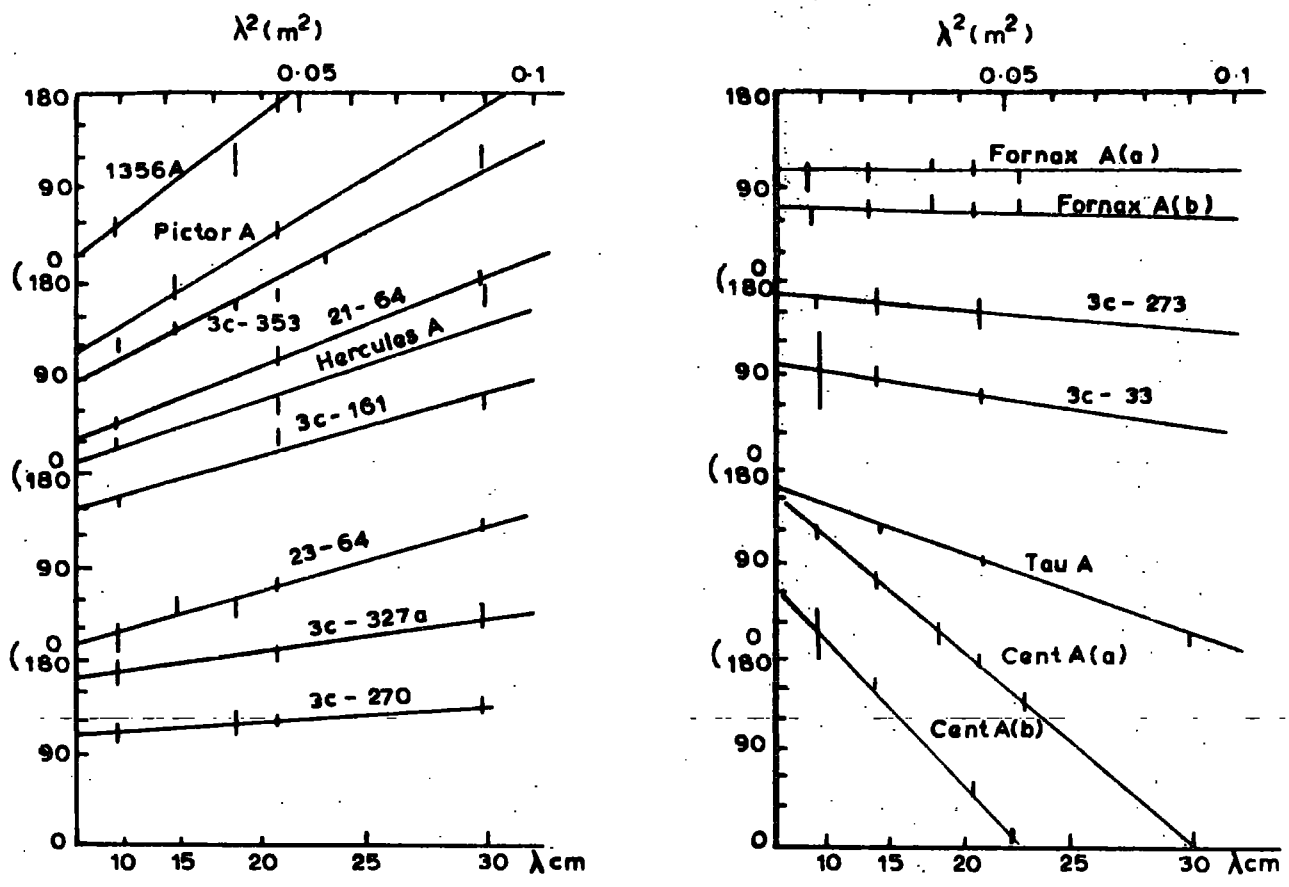

Figure 2.5. Position angle of the plane of polarization (Θ) plotted against wavelength^2. (λ^2).

Gardner and Whiteoak (1963)

the values of observed R.M. are about a hundred times the expected ionospheric effect and the position angles show little variation at different times of day or night, so that it would appear that the ionosphere does not play a significant part in the measured rotation (Cooper and Price 1962). Thus most of the observed Faraday rotation occurs in the outer regions of the source or in our Galaxy. Seielstad et al. (1964), finding a pronounced variation of R.M. with galactic latitude inferred that the rotation is produced mainly in the Galaxy, but this is far from conclusive.

Some sources which are only a few degrees apart show very different R.M.s (Gardner et al., 1969b) which may indicate large intrinsic Faraday rotations in the sources.

Assuming that most of the rotation is galactic, and if the electron density in the Galaxy is known, a value for the mean line of sight magnetic field to the edge of the Galaxy can be found. However, it is possible that the electron density is not uniform, resulting in an uneven sampling of the Galaxy's magnetic field. Thus although a value of $\int N_e H_\ell d\ell$ can be found this method is not reliable for obtaining magnetic field strengths. (However, if N_e is taken as $0{\cdot}05$ cm^{-3} then a value of $H_\ell \sim 5$ μgauss is obtained). The values of rotation measures found from sources in different directions give information about the distribution of thermal electrons and/or magnetic field in the Galaxy. Many observers have investigated the variation of rotation measure with galactic latitude and longitude. Morris and Berge (1964) collected the R.M.s of 37 sources and found a cyclical change of R.M. with longitude. At positive latitudes their results indicated a field away from the observer between longitudes 160° and 340°, and a field towards the observer at longitudes 340° to 160°. At negative latitudes the rotation measures were reversed. Morris and Berge interpreted these results as a helical form of field with the magnetic axis directed towards $\ell = 250^\circ$ and $\ell = 70^\circ$, which is the local spiral arm direction. As more rotation measures

were found their interpretation became more complicated. Gardner and Davies (1966), using the results of 86 measurements of R.M., attempted to draw contour lines of R.M. at 0, $\pm$ 20, $\pm$ 40 etc. rad/m^2. Once again the results indicated a magnetic field directed along the spiral arm, towards $\ell = 275^\circ$ at latitudes $b > + 20^\circ$ and towards $\ell = 95^\circ$ at latitudes $b < + 20^\circ$, thus indicating a longitudinal type of field with reversal of direction, a longitudinal field with some kind of anomaly, or a helical field component.

Similar results were obtained by Berge and Seielstad (1967) for 79 sources, and Gardner et al. (1967) for 133 sources, although as more rotation measures were included more irregularities in the overall pattern appeared.

Thielheim and Langhoff (1968) formulated a quasi longitudinal field model in an attempt to fit these early measurements. The field direction lies along the local spiral arm, in opposite directions on either side of the galactic plane, with the sun at 85 pc below the plane. In the local spiral arm, in the region of the sun, the field is towards $\sim\ell = 270^\circ$ above the plane and towards $\ell \sim 90^\circ$ below the plane.

Davies (1968) suggested that the field reversal at $b > 20^\circ$ could be due to a local irregularity, perhaps associated with Gould's belt, superimposed on a general galactic disc field parallel to the spiral arm.

Mathewson and Nicholls (1968) proposed that such R.M. would be observed if their helical model type of field was added to a longitudinal field along the spiral arm towards $\ell = 90^\circ$. The helical component would produce the reversal of direction, and the addition of the longitudinal component produces maximum and zero R.M.s at the longitudes expected from measurements. Since measurements of the polarization of starlight give information about the local field ($\sim$ few x 10^2 pc,) while Faraday rotation measurements measure the field to the edge of the Galaxy (where there is a magnetic field and electrons), Mathewson and Nicholls suggest that the helical component is a local perturbation of the general longitudinal

spiral arm field, perhaps associated with Gould's belt.

As more R.M.s are found (e.g. Gardner et al. (1969a) 366 sources) evidence for a reversal of field direction about the galactic plane becomes more tenuous (Gardner et al., 1969c), although little data is available at positive latitudes with $60^{\circ} < \ell < 180^{\circ}$. See Figure 2.6.

In conclusion it would seem that Faraday rotation measurements of the polarized radio emission from extragalactic sources, indicate a longitudinal field directed along the local spiral arm towards $\ell \sim 90^{\circ}$ with local perturbations, which could take the form of a helical component.

2.5 Faraday Rotation: Pulsar measurements

2.5.1 Introduction

When the Faraday rotations of extragalactic radio sources are measured a lack of knowledge of the electron density makes an estimate of field strength unreliable. This difficulty is removed when pulsars are used as the source of the polarized radio emission, as a value of $\int N_e \, d\ell$ can then be found, but Faraday rotation measurements have been made for only $\sim$ 20 pulsars mostly within 1 kpc of the sun. $\bar{H}_\ell$ the mean line of sight component of the magnetic field to the pulsar, weighted by the thermal electron density is then given by

$$\bar{H}_\ell = \frac{\int N_e H_\ell \, d\ell}{\int N_e \, d\ell}$$

2.5.2 The Dispersion Measure

It has been shown (e.g. J. G. Davies et al. 1968) that the arrival time, t, of a radio pulse from a pulsar is different at different frequencies, ν, due to passage through ionized hydrogen. For a uniform plasma

$$\frac{dt}{d\nu} = - \frac{8100}{\nu^3} \, D \quad \text{sec Hz}^{-1}$$

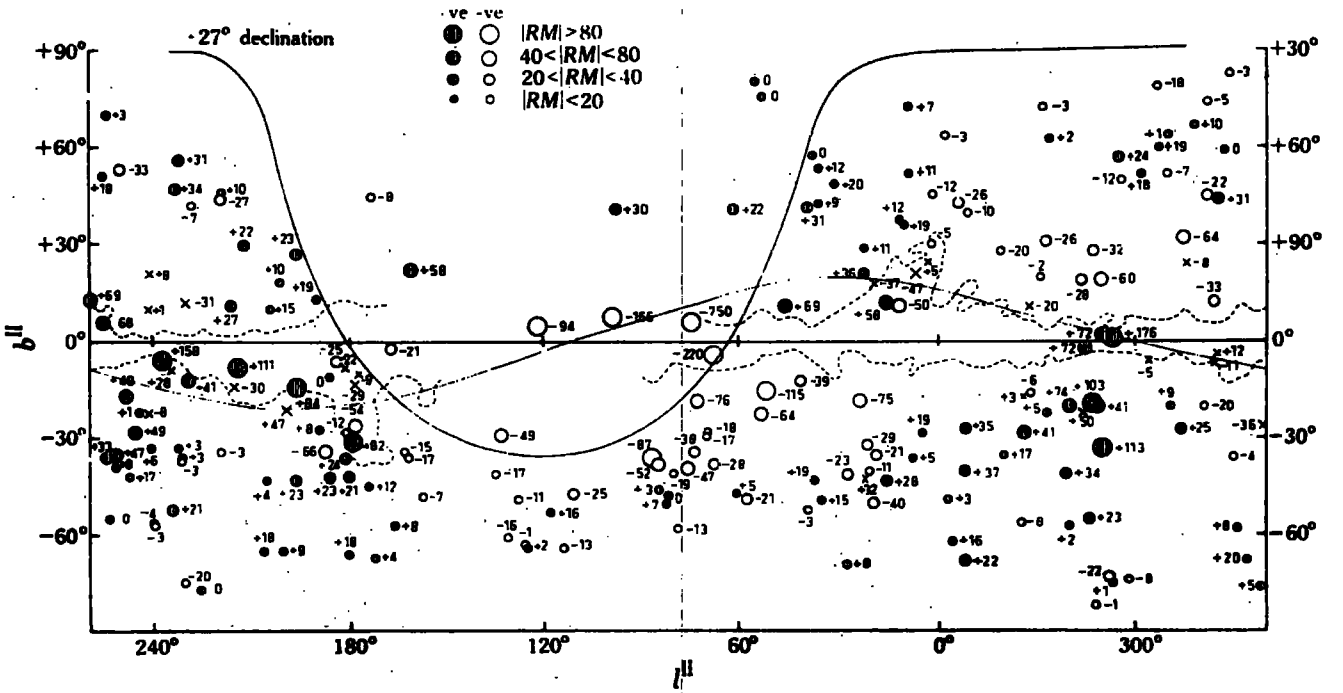

Figure 2.6. Distribution of rotation measures of extragalactic sources.
Gardner et al. (1969c)

where D is the dispersion measure in pc cm^{-3} and is equal to the line integral of the electron density to the source. $D = \int N_e d\ell$ pc cm^{-3}, where ℓ is the distance to the source in pc, N_e is the electron density in cm^{-3}.

Many measurements of dispersion measures of pulsars have been made e.g. Taylor (1969), Bridle and Venugopal (1969), Davies (1969), Goldstein and James (1969), Davies and Large (1970) and Manchester (1972).

2.5.3 Faraday Rotation measure

Two methods of measuring $\int N_e H_\ell d\ell$ have been applied to pulsars.

One is similar to that described in section 2.4 for extragalactic sources, and can be used even for weakly polarized pulsars. This method was first used by Smith (1968a) to measure the field in the direction of CP 0950 ($\ell = 229^\circ$, $b = 43^\circ$) and he obtained a value of $\bar{H}_\ell < 2 \times 10^{-7}$ gauss. (Mathewson (1969) suggested that this low value would be produced if the line of sight to the pulsar passed through both helical and longitudinal regions of field, although a randomly directed field would also give a small R.M.) Other early field measurements of this type were made by Smith (1968b), and Radhakrishnan (1969).

The second method can only be applied to strongly polarized radiation and does not give the field direction. The polarized radiation is observed at a frequency $\sim$ 150 M Hz with a detector sensitive to one plane of polarization. As the frequency of observation is varied through a band of width $\sim$ 5 MHz, a 'sinusoidal' variation of pulse amplitude with frequency is observed, the separation of the maxima giving a value for the rotation measure, e.g. Lyne and Rickett (1968), Staelin and Reifenstein (1969), Vitkevich and Shitov (1970), Shitov (1971).

2.5.4 Magnetic fields deduced from pulsar measurements

Some recent values of dispersion measure, rotation measure, and the deduced magnetic field are shown in Table 2.4. All these field calculations are made on the assumption that there is no intrinsic Faraday rotation in the source. Manchester (1972) states that since the form of variation of position angle across the pulse is independent of frequency, there is no differential rotation across the pulse. This would seem to indicate that there is no intrinsic Faraday rotation. However, at present, this question is rather uncertain, especially as strong magnetic fields very probably exist in pulsars.

The field values obtained are the mean line of sight components of the field, weighted according to the electron density. Verschuur (1970) suggests that if a dense neutral hydrogen cloud, containing a strong magnetic field, is included in the line of sight integral, then the measured field will be stronger than that expected from a coherent field model. Manchester (1972) found that low latitude pulsars with small dispersion measures, which are probably at short distances in the local arm, have stronger line of sight field components than those with large dispersion measures. This could indicate that the latter are at large distances and that the field varies randomly along the path to the pulsar, or the pulsar could lie in an interarm region where the field is weaker.

2.5.5 Field configuration derived from pulsar measurements

Manchester (1972) has interpreted his data as being consistent with a simple longitudinal field model; the field being directed along the local spiral arm towards $\ell = 90^{\circ}$ and with a field strength $\sim 3{\cdot}5$ μG locally. (Figure 2.7). These values do not appear to be compatible with a helical component in the local field.

TABLE 2.4

PULSAR DISPERSION MEASURES AND FARADAY ROTATION MEASURES

N.B. A positive R.M. and field indicates a field directed towards the observer.

Pulsar	Longitude	Latitude	Dispersion measure pc cm^{-3}	Rotation measure rad m^{-2}	$\bar{H}_{\ell}$ μG	Reference
0329	144°	- 1·2°	26·75 ± 0·05	63 ± 5	2·9 ± 0·23	Staelin and Reifenstein (1969)
			26·78 ± 0·005	-63·7 ± 0·4	-2·93 ± 0·02	Manchester (1972)
0525	183·8°	- 6·9°	49·3	36 ± 5	0·9 ± 0·125	Staelin and Reifenstein (1969)
			50·8 ± 0·1	-39·1 ± 0·2	- 0·961	Manchester (1971a)
			50·8 ± 0·1	-39·6 ± 0·2	- 0·96	Manchester (1972)
0531	184·2°	- 5·4°	56·8	-42·2 ± 0·6	- 0·92	Manchester (1971b)
			56·8	-42·3 ± 0·5	- 0·92 ± 0·02	Manchester (1972)
0628	237°	- 16·7°	34·36	45	1·6	Vitkevich and Shitov (1970)
				+ 47 ± 2	+ 1·6	Schwarz and Morris (1971)
0808	139·4°	+ 31·6°	5·84 ± 0·06	-11·7 ± 1·3	- 2·5 ± 0·3	Manchester (1972)
0818	236°	+ 13°	40·9 ± 0·1	- 2·8 ± 1·7	- 0·08 ± 0·05	Manchester (1972)
0833	263·6°	- 2·8°	63	+ 42	+ 0·8	Radhakrishnan and Cooke (1969)
0834	219·7°	+ 26·3°	12·9	+ 26 ± 5	+ 2·3	Schwarz and Morris (1971)
			12·90 ± 0·04	+ 24·5 ± 2·5	+ 2·3 ± 0·3	Manchester (1972)

TABLE 2.4 (continued)

Pulsar	Longitude	Latitude	Dispersion measure pc cm^{-3}	Rotation measure rad m^{-2}	H_{ℓ} μG	Reference
0950	228·9°	+ 43·7°	2·98 2·965 ± 0·007	< 0·5 + 1·8 ± 0·5	< ± 0·2 + 0·7 ± 0·3	Smith (1968b) Manchester (1972)
1133	242°	+ 69°	4·834 ± 0·007	+ 3·9 ± 0·2	+ 0·99 ± 0·06	Manchester (1972)
1237	252°	+ 87°	9·254 ± 0·008	- 0·6 ± 0·4	- 0·07 ± 0·05	Manchester (1972)
1508	91·3°	+ 52·3°	19·6 19·60 ± 0·02	+ 40 ± 30 + 0·8 ± 0·7	+ 2·4 + 0·05 ± 0·04	Lyne, Smith and Graham (1971) Manchester (1972)
1604	11°	+ 36°	10·72 ± 0·05	-	-	Manchester (1972)
1642	14·3°	+ 26·2°	35·7 35·71 ± 0·01	+ 48 ± 10 + 16·5 ± 2·5	+ 1·6 + 0·58 ± 0·09	Lyne, Smith and Graham (1971) Manchester (1972)
1706	6°	+ 14°	24·99 ± 0·08	-	-	Manchester (1972)
1818	26°	+ 5°	84·48 ± 0·08	+ 70·5 ± 7·5	+ 1·0 ± 0·1	Manchester (1972)
1911	31°	- 7°	89·41 ± 0·04	-	-	Manchester (1972)
1929	47·4°	- 3·9°	3·6 3·176	< 4 - 8·6 ± 1·8	< 1·4 - 3·3 ± 0·7	Lyne, Smith and Graham (1971) Manchester (1972)

TABLE 2.4 (continued)

Pulsar	Longitude	Latitude	Dispersion measure pc cm^{-3}	Rotation measure rad m^{-2}	$\bar{H}_{\ell}\mu G$	Reference
1933	$52{\cdot}3^{\circ}$	$-\ 2{\cdot}0^{\circ}$	159 $158{\cdot}53 \pm 0{\cdot}05$	$-\ 36 \pm 10$ $-\ 1{\cdot}9 \pm 0{\cdot}4$	$-\ 0{\cdot}3$ $-\ 0{\cdot}015 \pm 0{\cdot}003$	Lyne, Smith and Graham (1971) Manchester (1972)
2016	68°	$-\ 3{\cdot}9^{\circ}$	$14{\cdot}16 \pm 0{\cdot}03$	$-\ 34{\cdot}6 \pm 1{\cdot}4$	$-\ 3{\cdot}0 \pm 0{\cdot}2$	Manchester (1972)
2021	88°	$+\ 8^{\circ}$	$22{\cdot}580 \pm 0{\cdot}004$	$-\ 6{\cdot}5 \pm 0{\cdot}9$	$-\ 0{\cdot}36 \pm 0{\cdot}05$	Manchester (1972)
2045	31°	$-\ 33^{\circ}$	$11{\cdot}51 \pm 0{\cdot}01$	$-\ 10{\cdot}8 \pm 0{\cdot}4$	$-\ 1{\cdot}15 \pm 0{\cdot}04$	Manchester (1972)
2111	89°	$-\ 1{\cdot}3^{\circ}$	~ 100 $141{\cdot}4 \pm 0{\cdot}4$	$-\ 182 \pm 20$ $-\ 223{\cdot}7 \pm 2{\cdot}2$	$-\ 2{\cdot}2$ $-\ 1{\cdot}95 \pm 0{\cdot}03$	Lyne, Smith and Graham (1971) Manchester (1972)
2218	98°	$-\ 8^{\circ}$	$43{\cdot}52 \pm 0{\cdot}05$	$-\ 35{\cdot}3 \pm 1{\cdot}8$	$-\ 1{\cdot}00 \pm 0{\cdot}05$	Manchester (1972)
2303	98°	$-\ 27^{\circ}$	$49{\cdot}9 \pm 0{\cdot}2$	-	-	Manchester (1972)

Figure 2.7. Mean line of sight magnetic field components for pulsars plotted in galactic coordinates. (Manchester 1972).
Circle diameter ∝ field strength (for fields > 0.3 μgauss).

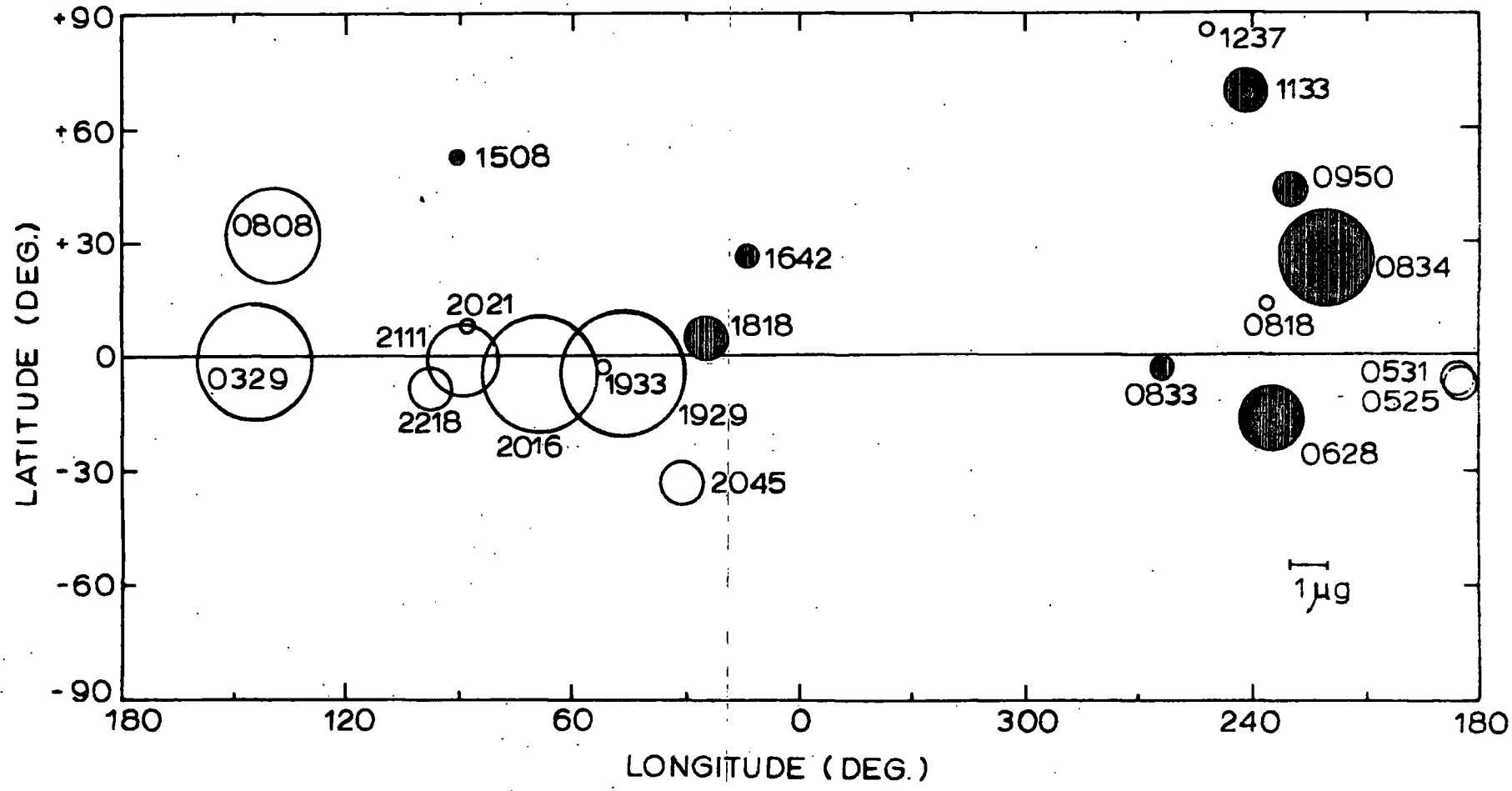

For positive R.M. (field towards the observer) the circles are filled
For negative R.M. (field away from observer) the circles are open

2.6 Conclusions

It seems reasonable to assume that the galactic magnetic field is connected with the gas distribution of the Galaxy, so that the field is strongest in the spiral arm regions. Four types of spiral arm field configurations have been deduced from measurements.

Thielheim and Langhoff (1968)'s model of a longitudinal field in the direction of the spiral arm axis, reversing in direction about the galactic plane, and directed, at the Earth, towards $\ell = 270^{\circ}$ above the plane and $\ell = 90^{\circ}$ below the plane, was based on about 40 extragalactic Faraday rotation measures, and is not confirmed by the pulsar measurements. A completely helical local spiral arm field is in agreement with measurements of stellar polarizations, if this method is a reliable way of finding the magnetic field. Extragalactic Faraday rotation measurements are not incompatible with such a field. However, it seems more likely that the helical field is a local perturbation of a longitudinal field directed along the spiral arm. To discover the extent of this helical component Mathewson and Ford (Mathewson 1969; Mathewson and Ford 1970) divided stellar polarization data for 7000 stars into distance intervals 0 - 50 pc, 50 - 100 pc, 100 - 200 pc, 200 - 400 pc, 400 - 600 pc, 600 - 1000 pc, 1000 - 2000 pc and 2000 - 4000 pc. From the electric vector plots (section 2.1), the helical component was deduced to be contained in a region extending $\sim$ 400 pc along the spiral arm in both directions from the sun (Figure 2.8). Pulsar Faraday rotation measurements do not support this model.

A longitudinal field in the direction of the local spiral arm ($\ell \sim 90^{\circ}$ at the sun), is indicated by pulsar measurements and is not incompatible with extragalactic rotation measurements.

The local spiral arm coherent field thus appears, to the author, to be of a longitudinal type, directed along the spiral arm towards $\ell = 90^{\circ}$, with perturbations, possibly of a helical nature. Smaller scale irregularities

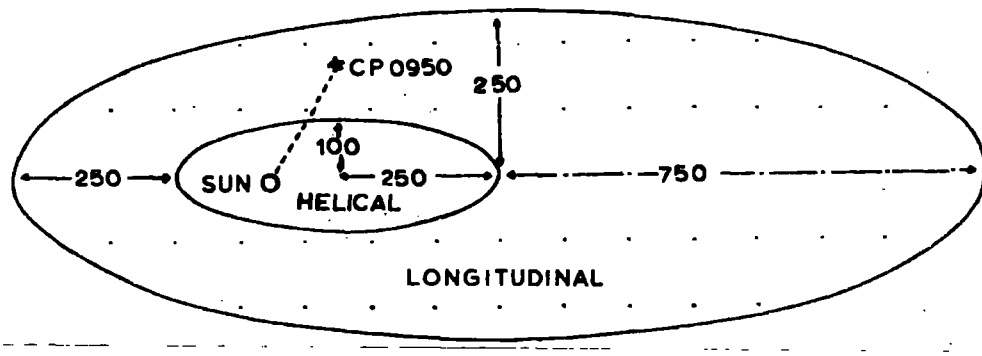

Figure 2.8. Spacial distribution of the helical and longitudinal magnetic fields. (Mathewson 1969)

($\sim$10 - 100 pc) probably also exist associated with turbulence in the interstellar medium. (Parker 1968, Parker 1969).

CHAPTER 3

MODELS OF THE FIELD

Information about the magnetic field within a few kpc of the Sun, which is obtained from experimental measurements, indicates several possible field configurations. To obtain models for the large scale galactic magnetic field much extrapolation is needed, so four such models, denoted A, B, C and D, have been considered.

3.1 Mathematical formulation of models

(N.B. All distances are in kpc)

3.1.1 Field Model A

This is the field model described by Thielheim and Langhoff (1968), based on extragalactic Faraday rotation measures. It is a quasi-longitudinal model, with the field direction lying along the spiral arms, towards $\ell = 270^{\circ}$ above the galactic plane and $\ell \sim 90^{\circ}$ below the plane, at the Sun. The model does not include any halo structure, as too little is known about this, and is not intended to describe the field configuration near the galactic centre, as this region has little effect on cosmic rays reaching the Earth.

In cylindrical coordinates R, ϕ and Z (R is the distance from the galactic centre in the galactic plane, Z is perpendicular to the galactic plane) the spiral arm axes are defined by

$$\phi_R = \frac{b}{k} R \arctan \frac{R}{k} + \phi_o$$

(see Figure 3.1). $\phi_o = 0$ or Π, giving the two arms, the Sun lying on the $\phi_o = \Pi$ arm. The constants are b = 1 and k = 1·5. At large distances from the galactic centre the separation between the two arms becomes constant. In this model the Sun is situated at R = 10 kpc, $\phi = 6{\cdot}5^{\circ}$, and is 85 pc below the galactic plane (Figure 3.1). The magnetic field in the plane is directed along the spiral arms, the direction being given by the unit vector

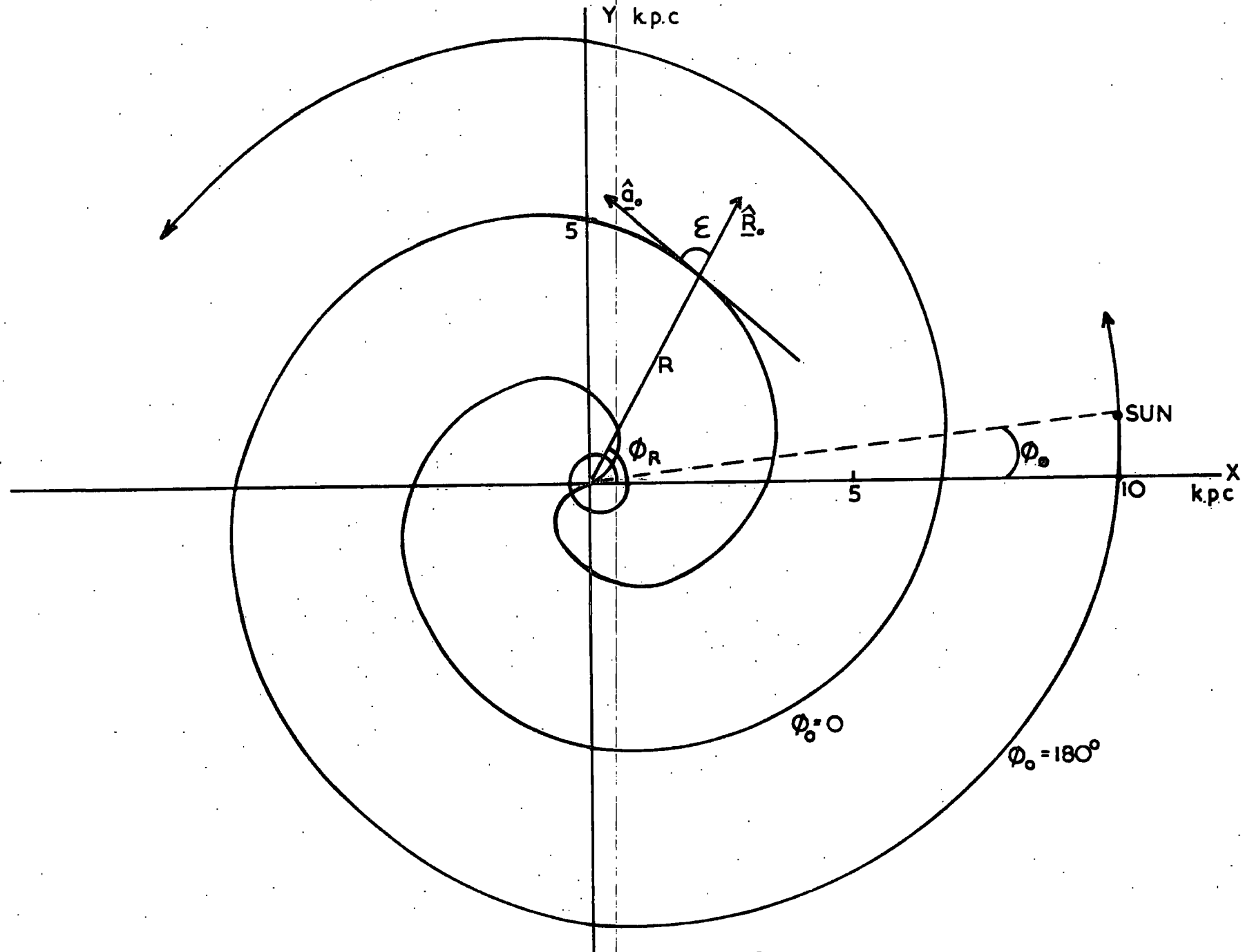

Figure 3.1. Representation of the spiral arms of the Galaxy.

$$\hat{a}_o = \hat{R}_o \cos\varepsilon + (\hat{Z}_o \times \hat{R}_o) \sin\varepsilon$$

where $\hat{R}_o$ is a unit vector in the R direction, $\hat{Z}_o$ is a unit vector in the Z direction, so that $\hat{Z}_o \times \hat{R}_o$ is a unit vector in the ϕ direction.

ε is the angle between the tangent vector to the spiral arm and the radius vector (Figure 3.1).

$$\tan\varepsilon = R\frac{d\phi}{dR} = \left(\frac{b}{k} R \arctan\frac{R}{k} + \frac{bR^2}{k^2+R^2}\right)$$

Thielheim and Langhoff (1968) propose that the total magnetic field is given by

$$\underline{H} = \hat{a}_o H_{a_o} + \hat{Z}_o H_{Z_o}$$

$$H_{a_o} = 50Z \left[\exp - \left(\frac{Z}{Z_o}\right)^2\right]\left[\left(\exp - \left(\frac{R}{R_o}\right)^2\right)\left(1 - \exp - \left(\frac{R}{R_1}\right)^2\right)\right] \times \left[1 + a^2 \cos^2(\phi - \phi_R)\right] \mu G.$$

Z_o = 0·175 kpc., R_o = 10 kpc., R_1 = 2 kpc., and a = 2. The mean field strength is $\sim$ 5 μG.

The $Z \exp - \left(\frac{Z}{0{\cdot}175}\right)^2$ term describes a field which decreases rapidly outside the galactic disc and which reverses in direction about the galactic plane. Figure 3.2 shows the z dependence of H_{a_o} along the Z axis through the Sun.

The $\left[\left(\exp - \left(\frac{R}{10}\right)^2\right)\left(1 - \exp - \left(\frac{R}{2}\right)^2\right)\right]$ term describes a field varying along the spiral arm length. Figure 3.3. shows the R dependence of H_{a_o} at Z = - 0·085 kpc parallel to the axis of the spiral arm. Thus $|H_{a_o}|$ is zero at the centre of the Galaxy, reaches a maximum value at R = 3·6 kpc and becomes negligible at R greater than about 18 kpc.

The $\left[1 + 4\cos^2(\phi - \phi_R)\right]$ term describes a field which has its maximum value on the arm axis (where $\phi - \phi_R = n\pi$), and reduces to 0·2 times

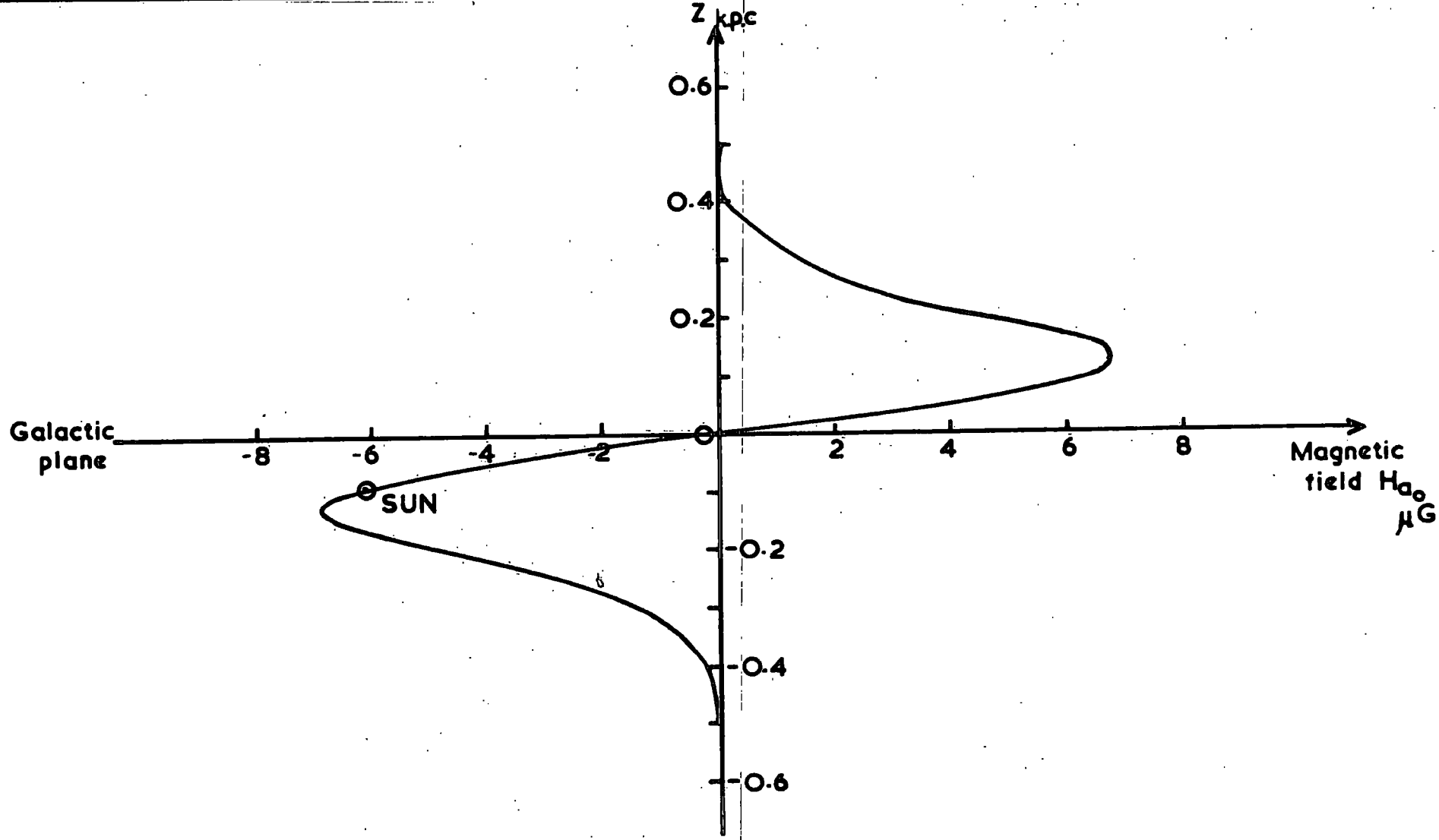

Figure 3.2. The Z dependence of the H_{a_o} along the Z axis through the sun. Field model A.

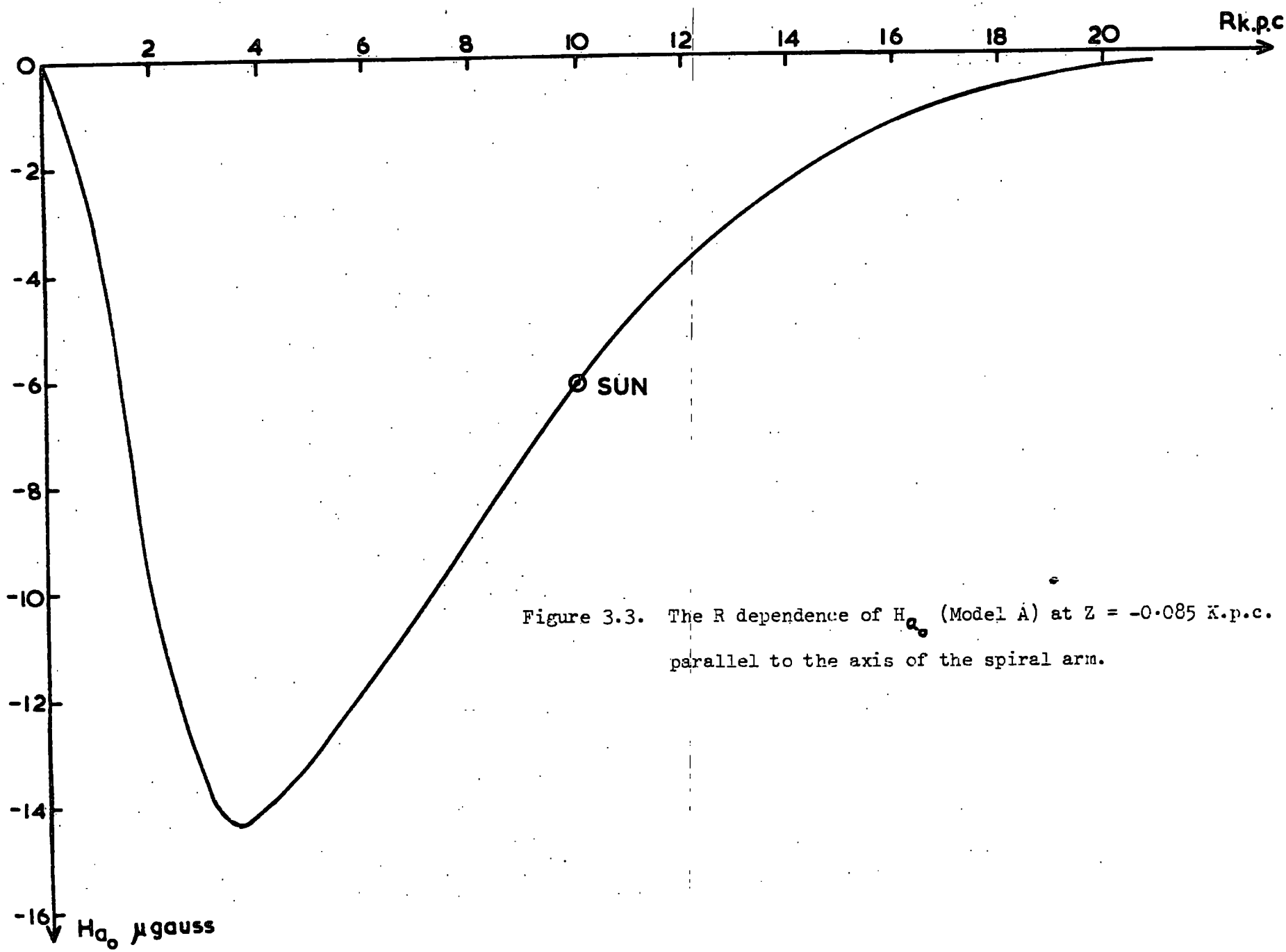

Figure 3.3. The R dependence of H_{a_o} (Model A) at Z = -0·085 K.p.c. parallel to the axis of the spiral arm.

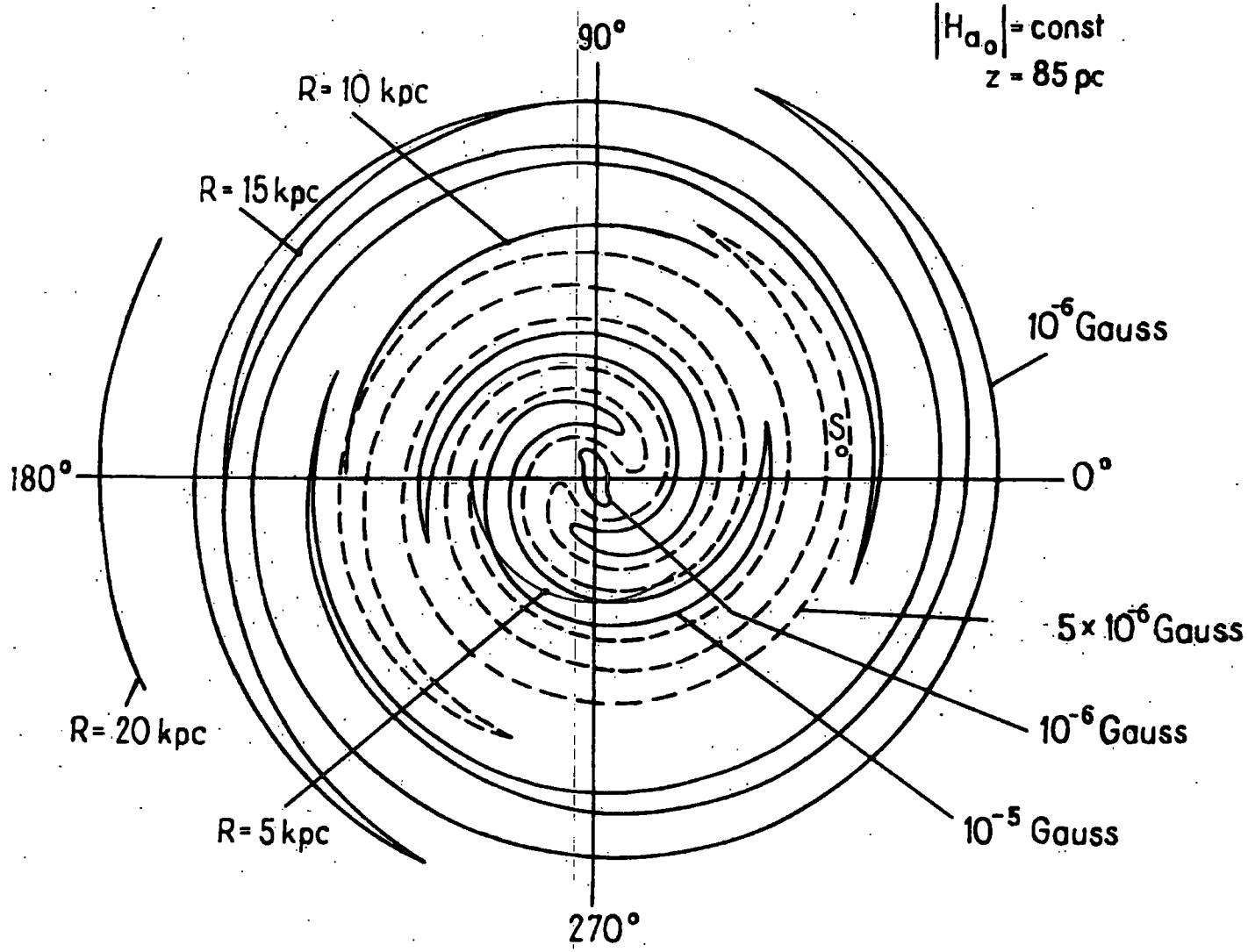

Figure 3.4. Lines $|H_{a_o}|$ = constant in the plane of Z = -0.085 kpc. Model A (Thielheim Langhoff, 1968).

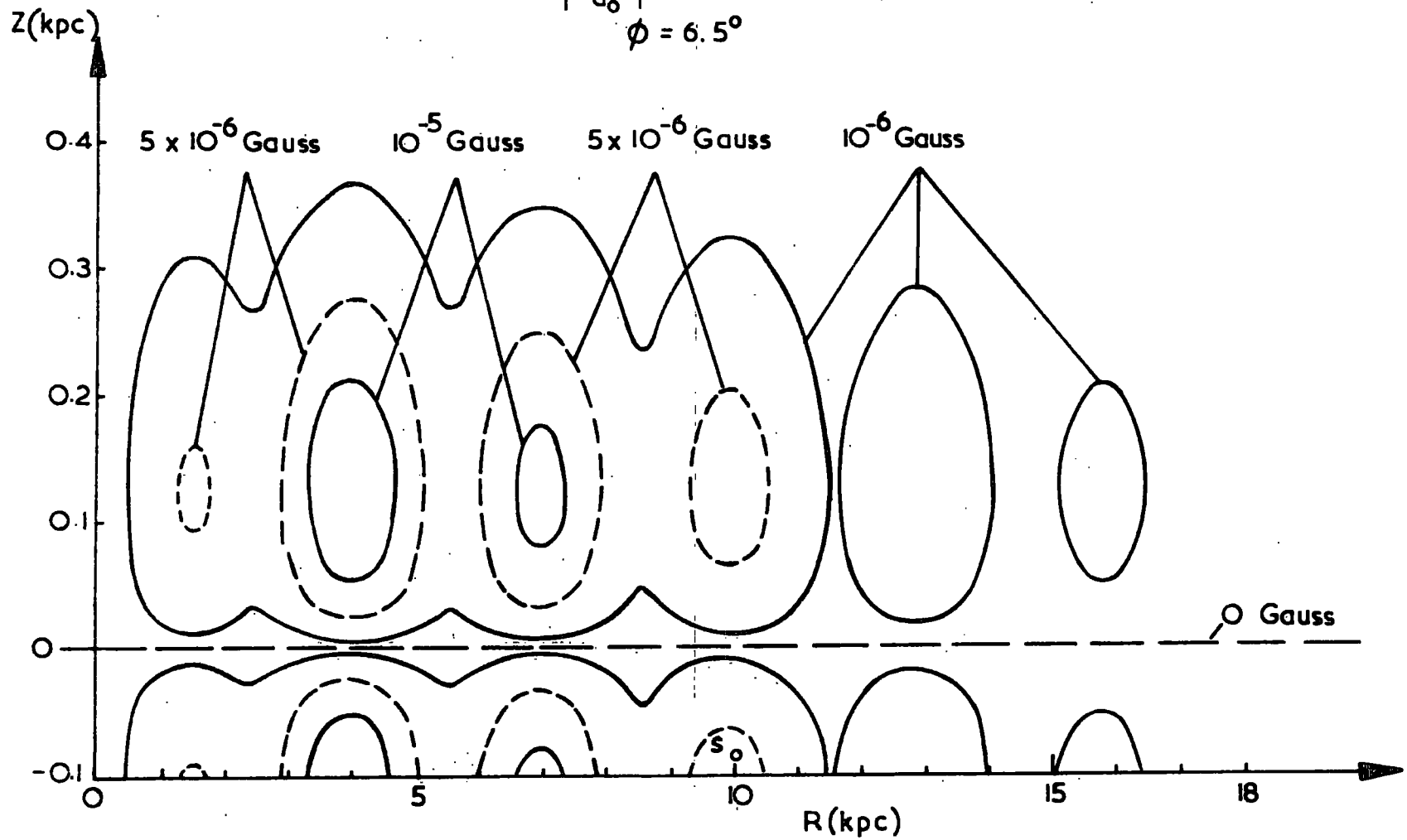

Figure 3.5. Lines $|H_{a_o}|$ = constant in plane $\phi = 6.5^{\circ}$ Model A. (Thielheim and Langhoff, 1968)

this value midway between adjacent arms. Figures 3.4 and 3.5 show contours of $|H_{a_o}|$ = constant, in the planes Z = - 0·085 kpc and $\phi = 6{\cdot}5^{\circ}$ respectively (Thielheim and Langhoff 1968).

In the galactic plane, at a point with coordinates x_1, y_1; H_X and H_Y the field strengths in the X and Y directions respectively are given by

$$H_X = \frac{H_{a_o}}{R} \left[x_1 \cos\varepsilon - y_1 \sin\varepsilon \right]$$

and

$$H_Y = \frac{H_{a_o}}{R} \left[x_1 \sin\varepsilon + y_1 \cos\varepsilon \right]$$

The field perpendicular to the galactic plane, denoted by H_{z_o} is obtained by setting Div $\underline{H}$ = 0 (Thielheim and Langhoff 1969).

$$H_{z_o} = \tfrac{1}{2} H_{a_o} \frac{Z_o^2}{ZR(1+t^2)^{\frac{1}{2}}} \times \left\{ \left[\frac{1}{1+t^2} \left(1 - \frac{2bk^2R^2t}{(k^2+R^2)^2} \right) - \frac{2R^2}{R_o^2} \right] + \frac{2R^2}{R_1^2} \left[\exp\left(\frac{R}{R_1} \right)^2 - 1 \right]^{-1} \right\}$$

where $t = \tan\varepsilon$

However, values of H_{z_o} are $\sim$ 1% or less of those of H_{a_o}.

3.1.2 Field Model C

This model consists of a helical form of magnetic field, based on the interpretation of stellar polarization data by Mathewson and Nicholls (1968). Their results indicated a local field which is helical in form, but in this model the helical field is taken to extend throughout the Galaxy. The field lines wind around the spiral arms from the galactic centre out to R = 15 kpc.

The spiral arm axes are described by the function $\phi_R = CR + \phi_o$ where C = 0·943. $\phi_o = 0$ or π. This function produces a similar spiral arm configuration, near the Sun, to that generated by the spiral function of Thielheim and

Langhoff (1968), but its use simplifies computation.

The field directions lie tangential to right handed helices of pitch angle 7°, wound round tubes coaxial with the spiral arms. The tubes are of elliptical cross section, the ellipses having axial ratio 3, with their major axes lying in the galactic plane. The axes of the helices are sheared through 40° anti-clockwise (looking downwards from the north), from the direction of the axis of the arm. Figures 3.6 and 3.7 show the locus of such a helix with minor axis of length 0·6 kpc. Every point in the region of this helical field is considered to be lying on a helix, with the field direction tangential to the helix at that point.

The method used to determine the field direction and strength at any point is described in Appendix I.

Figure 3.8 shows contours of $|H|$ = constant in the plane $\phi = 0$, for the helical model. $|H|$ is the field strength in μ.G.

In this model the Sun is 0·1 kpc towards the galactic centre from the arm axis, and is 0·01 kpc below the galactic plane.

3.1.3 Field Model D

Field model D consists of a longitudinal field directed towards $\ell = 90^{\circ}$.

The spiral arms are defined as for model A with the Sun situated at $R = 10$ kpc, $\phi = 6{\cdot}5^{\circ}$, and $Z = 0$.

The mathematical formulation of the magnetic field is the same as for model A except that H_{a_o} is given by

$$H_{a_o} = -3{\cdot}8 \left[\exp -\left(\frac{Z}{0.24}\right)^2\right]\left[\left(\exp -\left(\frac{R}{10}\right)^2\right)\left(1 - \exp -\left(\frac{R}{2}\right)^2\right)\right]$$

$$\times \left[1 + 4\cos^2(\phi - \phi_R)\right]. \ \mu G$$

This gives a field which does not reverse its direction across the galactic plane, but has approximately the same magnitude and extent as field model A.

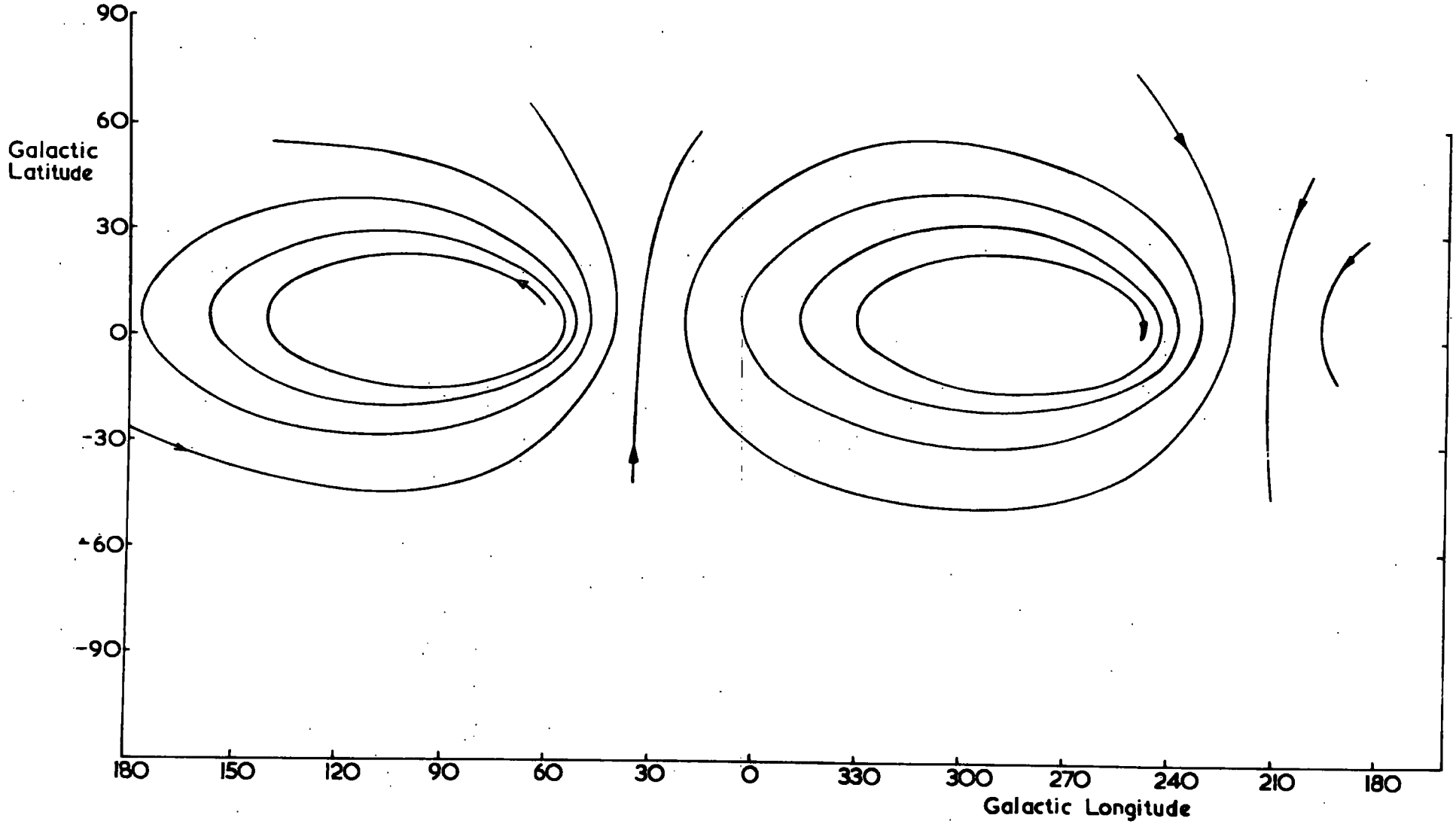

Figure 3.6. Locus of a helical magnetic line of force, such as described in section 3.1.2., with minor axis of length 0.6 kpc.

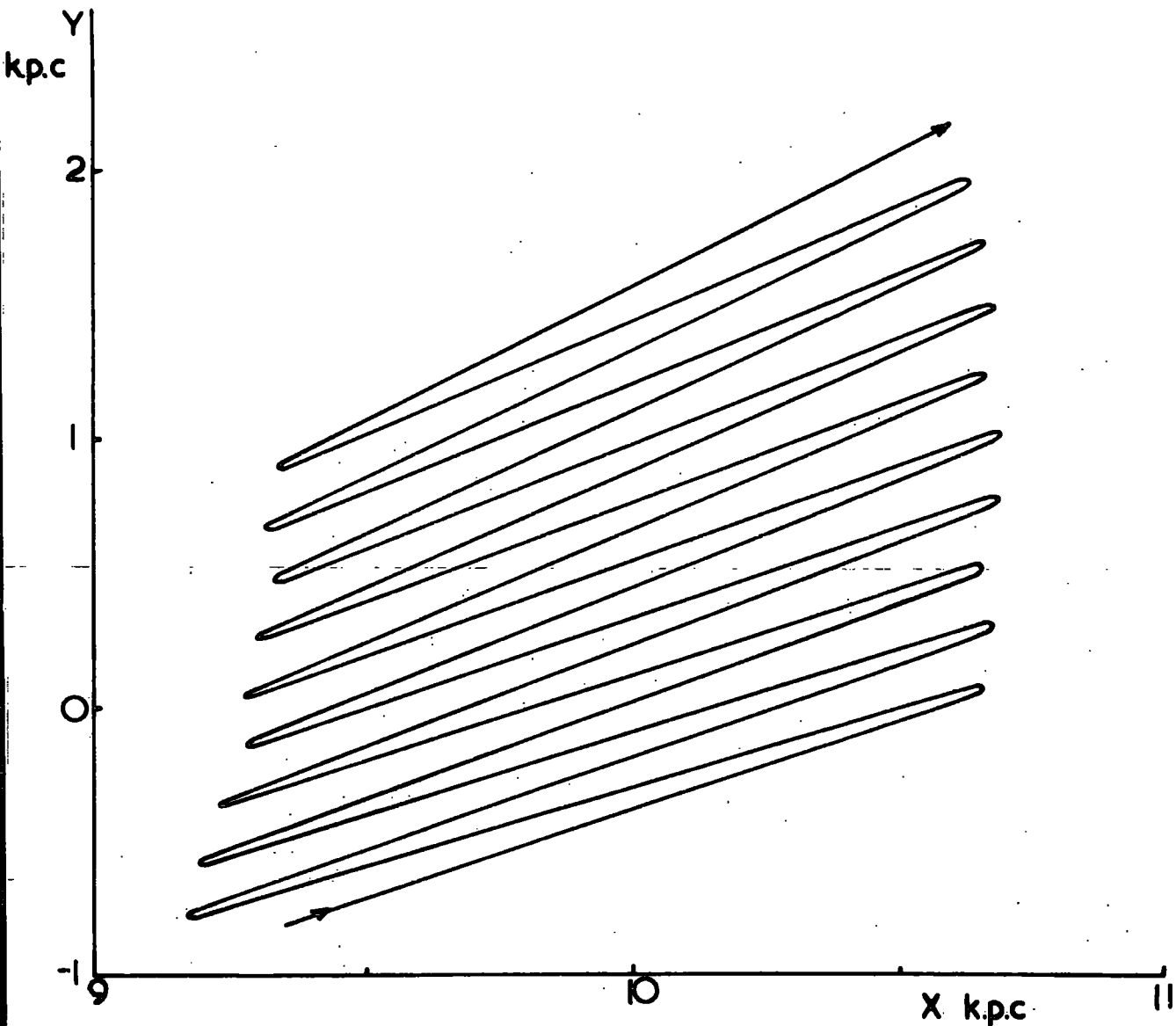

Figure 3.7. Locus of a helical magnetic line of force, such as described in section 3.1.2., with minor axis of length 0.6 kpc.

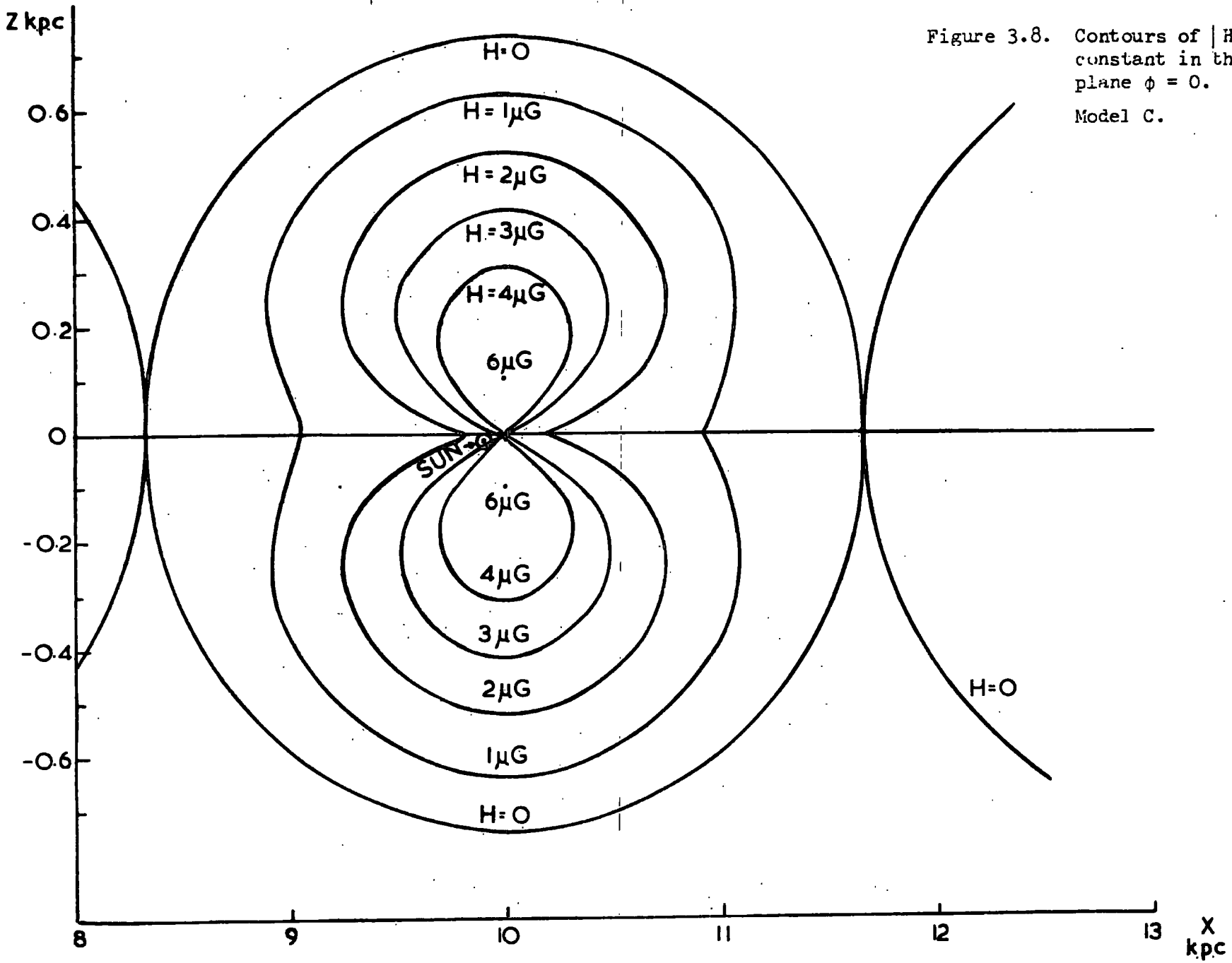

Figure 3.8. Contours of $|H|$ = constant in the plane $\phi = 0$.

Model C.

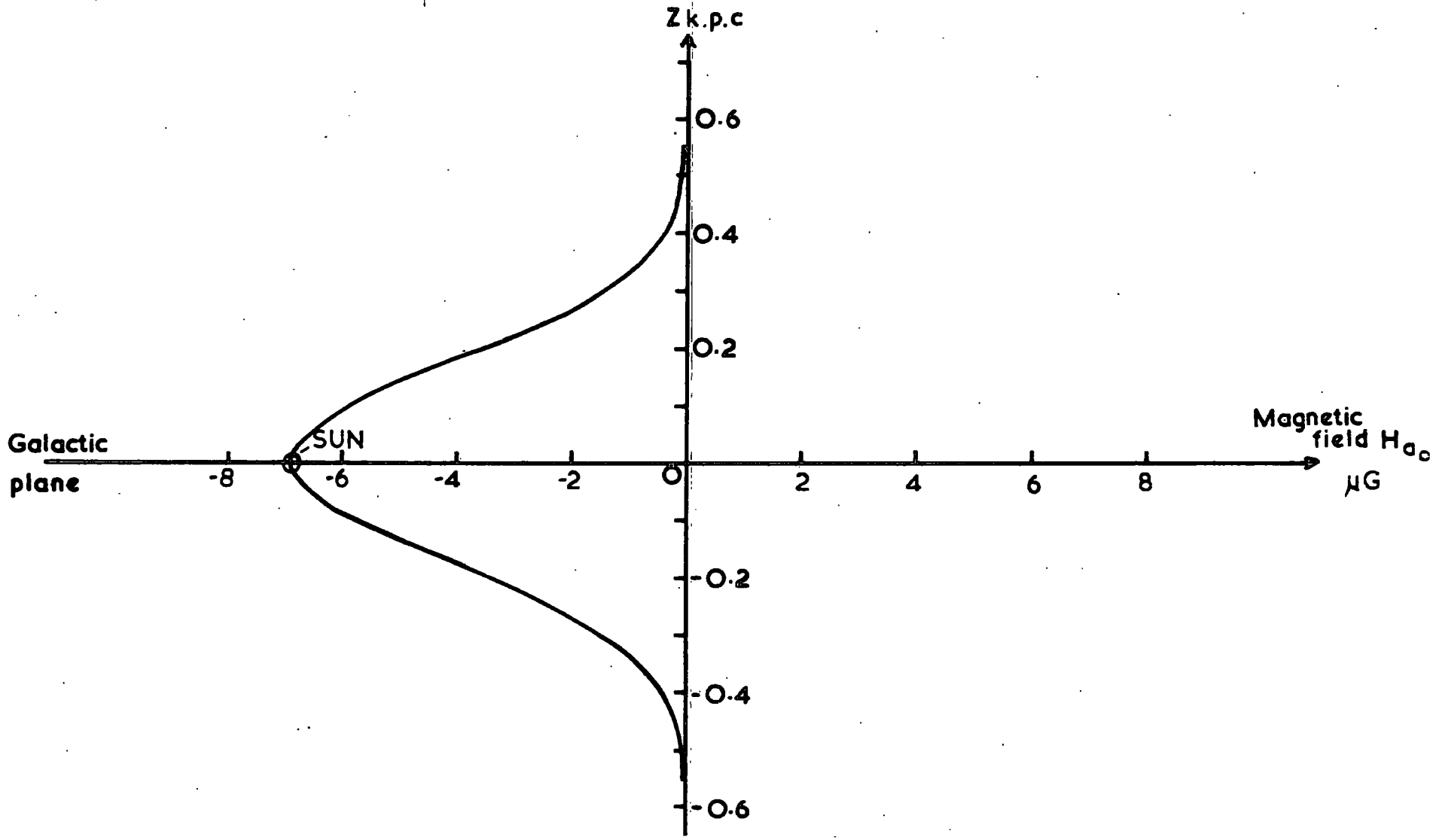

Figure 3.9. The Z dependence of H_{a_o} along the Z axis through the sun. Field Model D.

Figure 3.9 shows the Z dependence of H_{a_o} along the Z axis through the Sun. The maximum field strength on this axis is the same as for model A (see Figure 3.2).

3.1.4 Field Model B

Mathewson and Nicholls (1968) proposed that rotation measures of extra-galactic sources, and the optical polarization measurements of distant stars indicate that the general spiral arm magnetic field is longitudinal, with only a local helical component. The helical field exists within a tube which has an elliptical cross section with major axis 0·5 kpc and which extends $\pm$ 0·5 kpc along the spiral arm from the Sun. Within this region the field is as described for model C, while outside the field is as described for model D. Since these models are only intended to be representations of the actual field, a smooth transition between the two regions was not defined.

However, it is possible that the helical region is not as extensive as suggested above but is merely a local perturbation of a longitudinal field, such as represented by field model D.

3.2 Comparison of model predictions with measurements of the Faraday rotation of radiation from pulsars

Calculations were made of the mean line of sight magnetic field between the Earth and various pulsars, using the models of the galactic magnetic field described above, and the results compared with values found experimentally from measurements of the rotation measure and dispersion measure of these pulsars.

The calculations were repeated for three different electron density distributions

1. $N_e1 = 0{\cdot}062\ cm^{-3}$ (Mills, 1970)

2. $N_e2 = 0{\cdot}092 \exp - (Z^2/(1{\cdot}443 \times 10^{-2}))\ cm^{-3}$ (R.D. Davies, 1969)

3. $N_e3 = 0{\cdot}05 \exp - (|Z|\ /0{\cdot}152)\ cm^{-3}$ (Prentice and ter Haar, 1969)
   where Z is in kpc.

In each case the line integrals

$$\int_0^L N_e H_\ell \, d\ell \quad \text{and} \quad \int_0^L N_e \, d\ell$$

were calculated until $\int_0^L N_e \, d\ell$ reached the experimental value of the dispersion measure of the pulsar (i.e. the effective distance of the pulsar was found in each case)

Then $$\bar{H}_\ell = \int_0^L N_e H_\ell \, d\ell \Big/ \int_0^L N_e \, d\ell$$

was calculated and compared with the experimental values tabulated in Table 2.4. The value of $\bar{H}_\ell$ calculated using electron density distributions N_e1, N_e2, and N_e3 are shown in Tables 3.1, 3.2, and 3.3 respectively. (Positive fields are directed towards the observer, negative fields away from the observer.)

The large experimental dispersion measures of some pulsars lying away from the galactic plane may be due to the presence of HII regions.

In these calculations, the expressions for N_e2 and N_e3 give a rapid decrease in electron density above and below the plane, and this may result in the terminal value of $\int_0^L N_e \, d\ell$ never being reached. This is particularly true in the case of field model A, (with the Sun at Z = -85 pc) for pulsars at negative latitudes (e.g. 0525, 0531, 1933, 2045 and 2218). For model A it would probably be more reasonable if the maximum of the electron density distribution occurred nearer the plane of the Sun.

The effective distance to the pulsar is also very dependent on the electron density distribution relative to the position of the Sun. N_e1, N_e2, and N_e3 each predict different effective distances to the pulsars at high latitudes. As a result predicted values of $\bar{H}_\ell$ can be considerably different. In the case of model A, a reversal of field direction may occur along the

TABLE 3.1

MEAN LINE OF SIGHT MAGNETIC FIELDS BETWEEN THE SUN AND VARIOUS PULSARS, CALCULATED USING $N_e l = 0{\cdot}062\ cm^{-3}$

PULSAR	EFFECTIVE DISTANCE kpc.	MEASURED $\bar{H}_l$ μ.G.	$\bar{H}_l$ μ.G.			
			MODEL A	MODEL B	MODEL C	MODEL D
0329	0.435	-2.93	-3.47	+0.41	+1.16	-3.22
0525	0.800	-0.96	+0.24	+1.86	+2.30	+0.84
0531	0.810	-0.92	+0.28	+1.65	+2.07	+0.89
0628	0.560	+1.6	+4.27	+4.42	+4.62	+4.88
0808	0.100	-2.5	-2.61	-1.40	-1.40	-3.43
0818	0.665	-0.08	+0.70	-1.92	-4.35	+5.17
0833	0.810	+0.8	+6.42	+3.71	+2.47	+6.90
0834	0.215	+2.3	+1.64	-4.50	-4.50	+4.27
0950	0.055	+0.7	+2.73	-2.64	-2.64	+4.16
1133	0.085	+0.99	+1.11	-2.61	-2.61	+2.29
1237	0.155	-0.07	+0.02	-1.05	-1.37	+0.32
1508	0.320	+0.05	+1.44	-1.31	+0.96	-3.22
1604	0.180	-	-0.35	-0.14	+0.85	-1.57
1642	0.580	+0.58	+0.44	-0.97	+1.53	-1.59
1706	0.410	-	-0.24	-0.84	+0.65	-1.32
1818	1.370	+1.0	-0.90	-2.35	+0.40	-2.78
1911	1.445	-	-2.19	-2.50	-0.97	-2.85
1929	0.065	-3.3	-4.53	-1.07	-1.07	-5.68
1933	2.570	-0.015	-3.57	-3.92	-0.48	-4.49
2016	0.235	-3.0	-5.96	-1.16	-1.16	-6.83
2021	0.370	-o.36	-4.81	+1.27	+1.27	-6.98
2045	0.190	-1.15	-2.73	-2.27	-2.13	-3.30
2111	1.620	-2.0	-6.71	-5.24	-1.86	-6.84
2218	0.705	-1.0	-6.36	-3.33	-1.70	-6.24
2302	0.810	-	-	-2.06	-1.30	-3.25

TABLE 3.2

MEAN LINE OF SIGHT MAGNETIC FIELDS BETWEEN THE SUN AND VARIOUS PULSARS, CALCULATED USING $N_e 2 = 0{\cdot}092 \text{ Exp} - (Z^2/(1{\cdot}443 \times 10^{-2}))\text{cm}^{-3}$

LSAR	MEASURED $\bar{H}_\ell$ μ.G.	MODEL A		MODELS B, C, and D			
		EFFECTIVE DISTANCE kpc	$\bar{H}_\ell$ μ.G.	EFFECTIVE DISTANCE kpc	$\bar{H}_\ell$ μ.G.		
					MODEL B	MODEL C	MODEL D
29	-2.93	0.520	-3.41	0.300	+1.46	+1.46	-3.34
25	-0.96	* *	* *	0.655	+2.37	+2.73	+0.94
31	-0.92	* *	* *	0.620	+2.11	+2.52	+0.99
28	+1.6	* *	* *	* *	* *	* *	* *
08	-2.5	0.085	-2.69	0.070	-1.29	-1.29	-3.45
18	-0.08	0.505	+1.53	0.595	-3.26	-4.31	+5.51
33	+0.8	1.455	+6.30	0.575	+2.41	+2.02	+6.98
34	+2.3	0.170	+1.96	0.155	-4.06	-4.06	+4.40
50	+0.7	0.050	+2.76	0.040	-2.18	-2.18	+4.17
53	+0.99	0.070	+1.24	0.060	-2.54	-2.54	+2.33
17	-0.07	0.115	+0.08	0.150	-1.39	-1.55	+0.34
18	+0.05	0.300	+0.68	* *	* *	* *	* *
14	-	0.140	-0.45	0.135	+0.28	+0.43	-1.61
12	+0.58	0.555	+0.21	* *	* *	* *	* *
16	-	0.325	-0.29	0.300	-0.67	+0.44	-1.36
18	+1.0	1.060	-1.14	1.050	-2.59	+0.39	-3.24
11	-	* *	* *	* *	* *	* *	* *
19	-3.3	0.070	-4.54	0.045	-1.06	-1.06	-5.67
13	-0.015	* *	* *	2.045	-4.27	-0.55	-5.09
15	-3.0	0.295	-6.00	0.160	-1.08	-1.08	-6.82
11	-0.36	0.325	-4.81	0.255	+0.67	+0.67	-7.02
15	-1.15	* *	* *	0.165	-2.01	-1.91	-3.39
1	-2.0	2.710	-6.68	1.135	-4.64	-1.97	-6.97
18	-1.0	* *	* *	0.585	-2.59	-1.59	-6.45

Indicates pulsars lying away from the galactic plane, such that $\int_0^L N_e d\ell$ never reaches its terminal value.

TABLE 3.3

MEAN LINE OF SIGHT MAGNETIC FIELDS BETWEEN THE SUN AND VARIOUS PULSARS, CALCULATED USING $N_e 3 = 0.05 \exp - (|Z|/0.152)$ cm $^{-3}$

PULSAR	MEASURED $\bar{H}_\ell$ μ.G.	MODEL A		MODELS B, C, and D			
		EFFECTIVE DISTANCE kpc	$\bar{H}_\ell$ μ.G.	EFFECTIVE DISTANCE kpc	$\bar{H}_\ell$ μ.G.		
					MODEL B	MODEL C	MODEL D
0329	-2.93	1.015	-2.95	0.605	-0.39	+0.96	-3.07
0525	-0.96	* *	* *	2.290	+1.26	+1.55	+0.57
0531	-0.92	* *	* *	1.765	+1.14	+1.49	+0.64
0628	+1.6	* *	* *	* *	* *	* *	* *
0808	-2.5	0.155	-1.81	0.145	-1.32	-1.32	-3.38
0818	-0.08	1.420	-0.79	* *	* *	* *	* *
0833	+0.8	2.580	+5.54	1.315	+4.50	+3.01	+6.74
0834	+2.3	0.330	+0.38	0.440	-2.44	-4.37	+3.87
0950	+0.7	0.090	+2.20	0.070	-2.99	-2.99	+4.14
1133	+0.99	0.125	+0.52	0.145	-2.08	-2.54	+2.20
1237	-0.07	0.335	-0.10	* *	* *	* *	* *
1508	+0.05	* *	* *	* *	* *	* *	* *
1604	-	0.280	-0.00	0.415	-0.48	+1.16	-1.39
1642	+0.58	* *	* *	* *	* *	* *	* *
1706	-	0.645	-0.05	0.885	-0.78	+0.72	-1.14
1818	+1.0	2.34	-0.12	4.230	-1.94	+0.07	-2.28
1911	-	* *	* *	* *	* *	* *	* *
1929	-3.3	0.135	-4.60	0.085	-1.07	-1.07	-5.68
1933	-0.015	* *	* *	* *	* *	* *	* *
2016	-3.0	0.570	-6.18	0.330	-1.24	-1.24	-6.82
2021	-0.36	0.595	-3.23	0.550	+0.38	+1.74	-6.90
2045	-1.15	* *	* *	0.640	-1.97	-2.22	-2.63
2111	-2.0	4.96	-5.79	2.580	-5.28	-1.45	-6.45
2218	-1.0	* *	* *	2.115	-3.11	-1.43	-4.97

** Indicates pulsars, lying away from the galactic plane, such that $\int_0^L N_e d\ell$ never reaches its terminal value.

line of sight, resulting in a reduction of $|\bar{H}_\ell|$. (e.g. 0818:- N_e2 gives the effective distance as 0·505 kpc and $\bar{H}_\ell$ as + 1·53 μG; N_e1 gives 0·665 kpc and + 0·7 μG; and N_e3 gives 1·42 kpc and - 0·79 μG.)

However, the exact form of the electron density distribution is not known and since most of the pulsars lie near the galactic plane, N_e1 probably gives a satisfactory distribution. Field values calculated using N_e1 have been used in the following analysis.

Figure 3.10 shows values of $\bar{H}_\ell$ calculated using field model A and N_e1, plotted against experimental values. There appears to be some correlation between measured and predicted values, especially in the case of those pulsars for which the entire line of sight distance is below the plane. Of the pulsars considered few have large enough positive values of latitude and effective distance, for the line of sight distance to include a sufficient distance above the galactic plane, for the field reversal to be apparent. Only if the electron density is much less than 0·062 cm^{-3} would the reversal of field above the plane have any real effect on the rotation measures of the pulsars at positive latitudes.

Thus the fact that the experimental Faraday rotation measures show no reversal at positive latitudes does not necessarily rule out this field model. In fact, there is a correlation of 0·72 between the predicted and measured field strengths. The best fit to the experimental values is given if the field strengths predicted by model A (H_A), are reduced to 0·59 H_A.

As expected the field strengths predicted by models B and C are the same for pulsars near the Sun.

As the distance to the pulsar increases the model B values approach those obtained using model D (H_D). Figures 3.11, 3.12 and 3.13 show the values of $\bar{H}_\ell$ calculated using models B, C and D respectively. The rotation measures predicted by models C and B do not appear to be compatible with measurements,

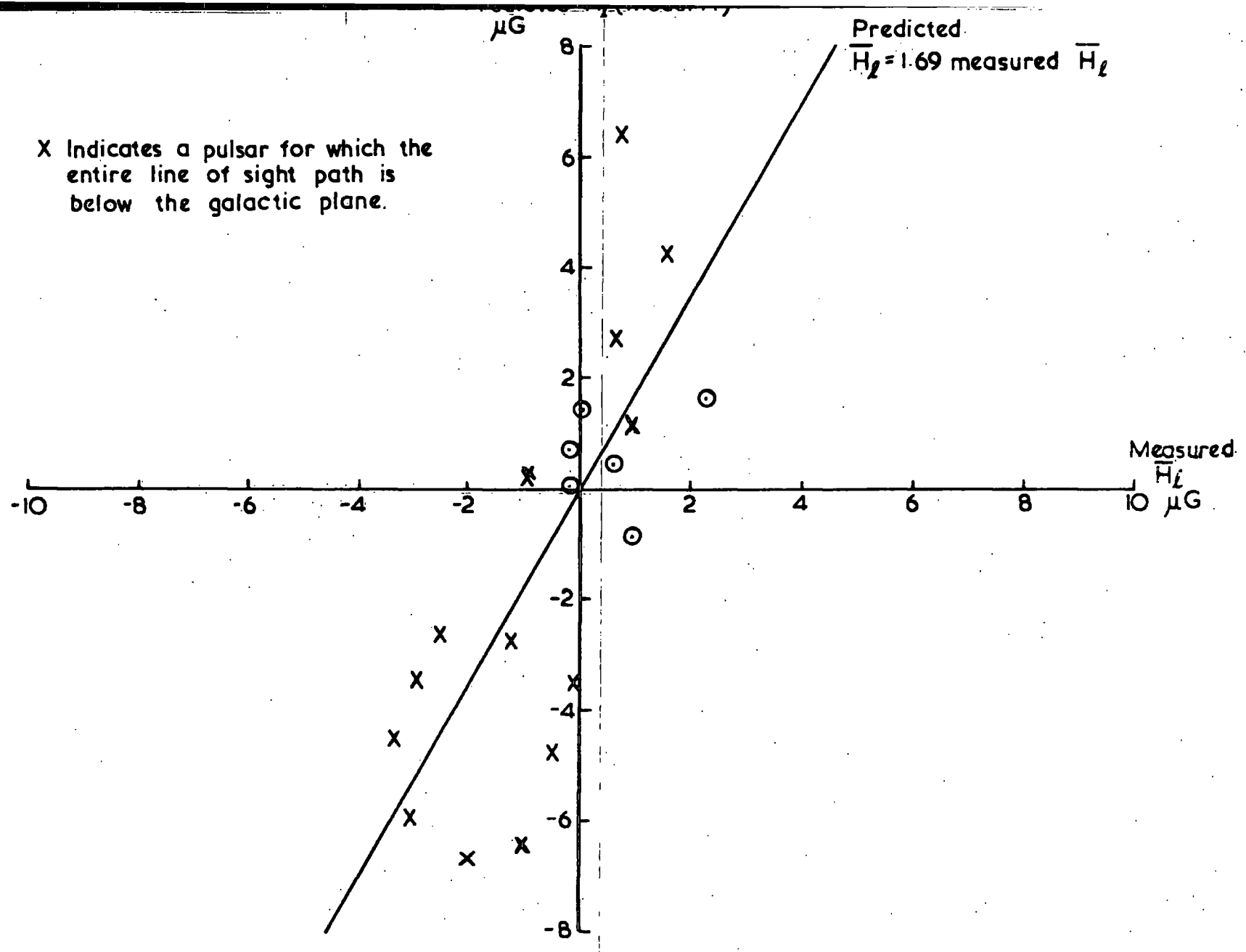

Figure 3.10. Values of $\bar{H}_\ell$ (Model A. H_e')

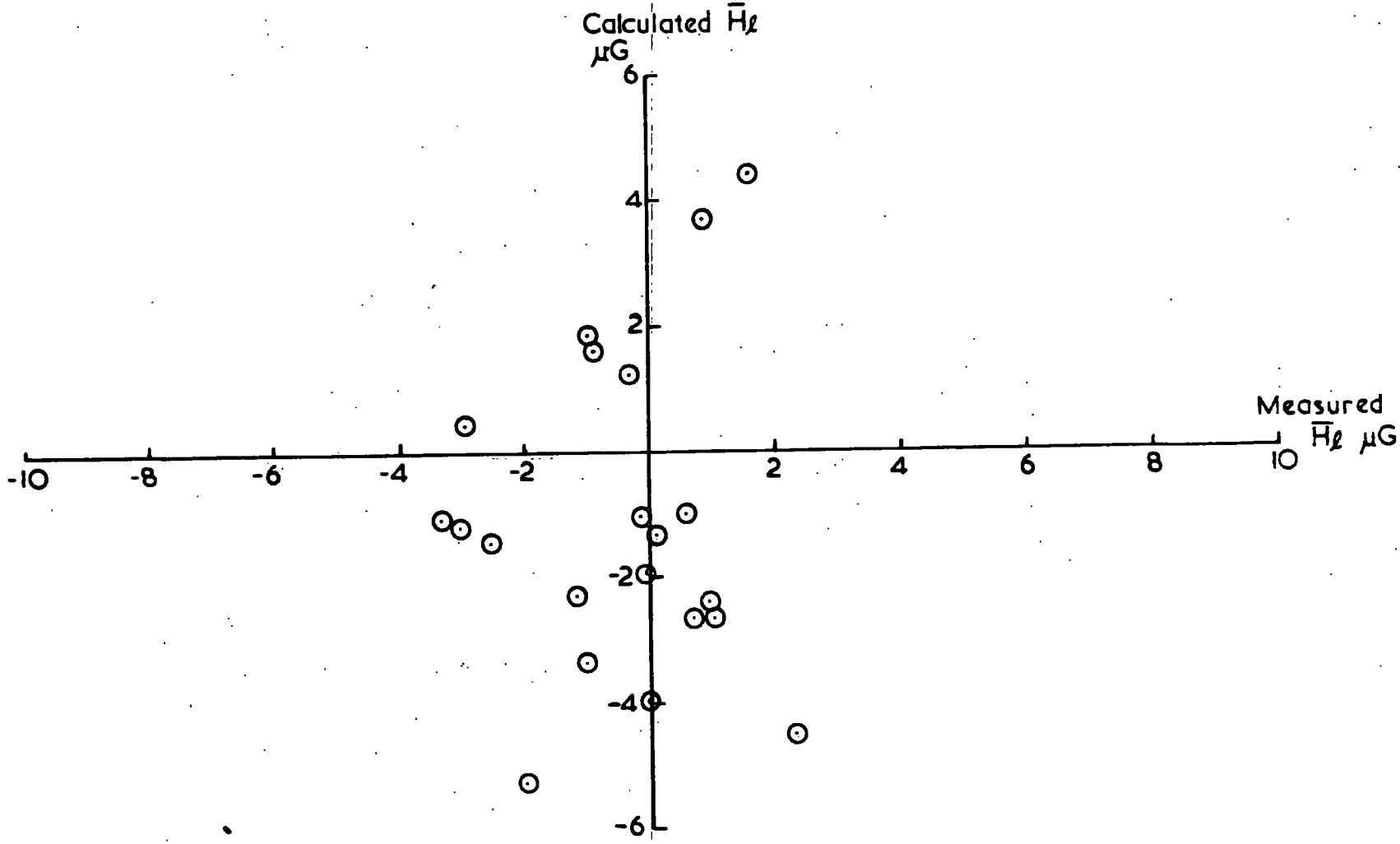

Figure 3.11. Values of $\bar{H}_\ell$ calculated using $N_e 1$ and Field Model B.

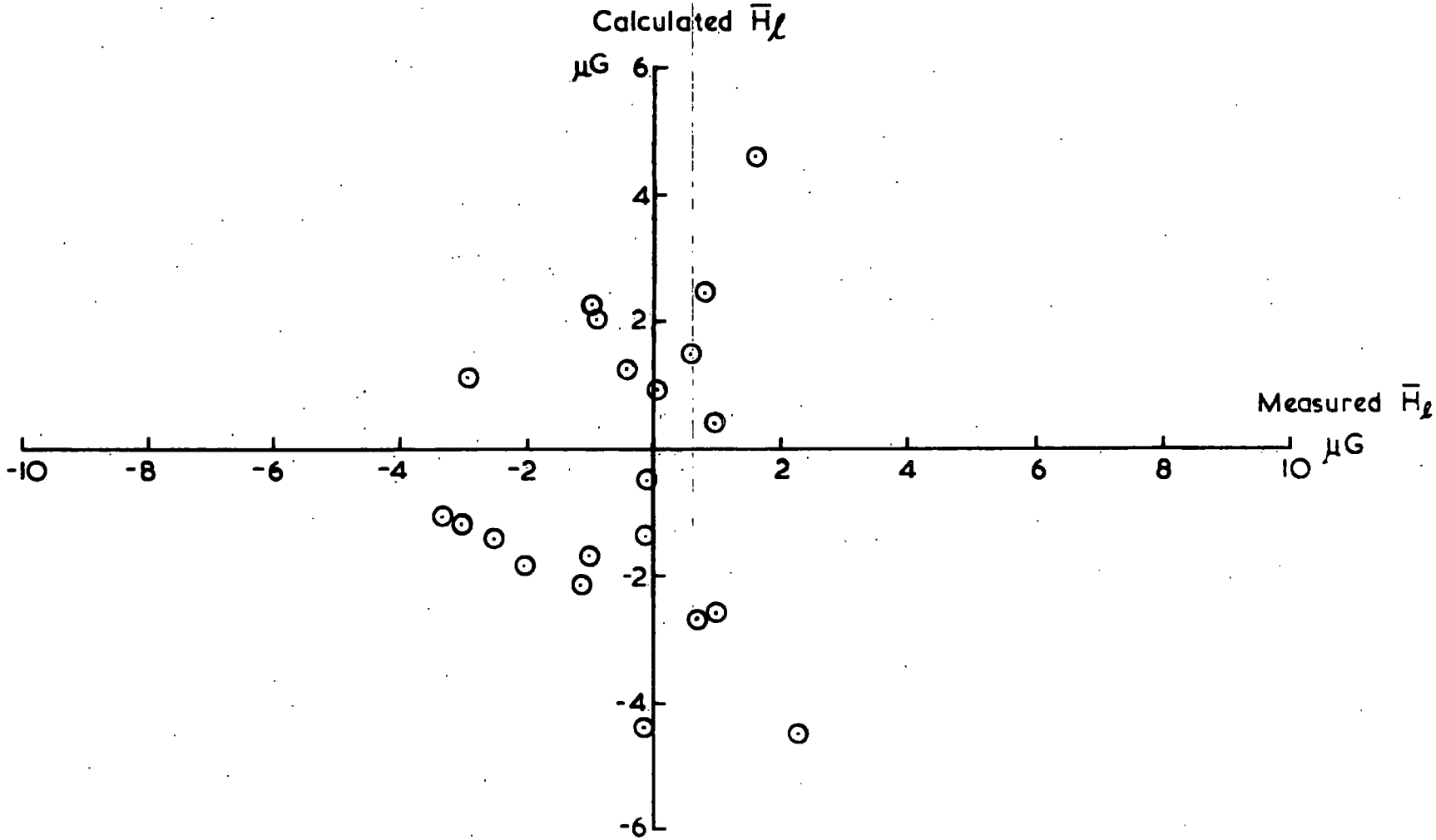

Figure 3.12. Values of $\bar{H}_\ell$ calculated using $N_e 1$ and Field Model C.

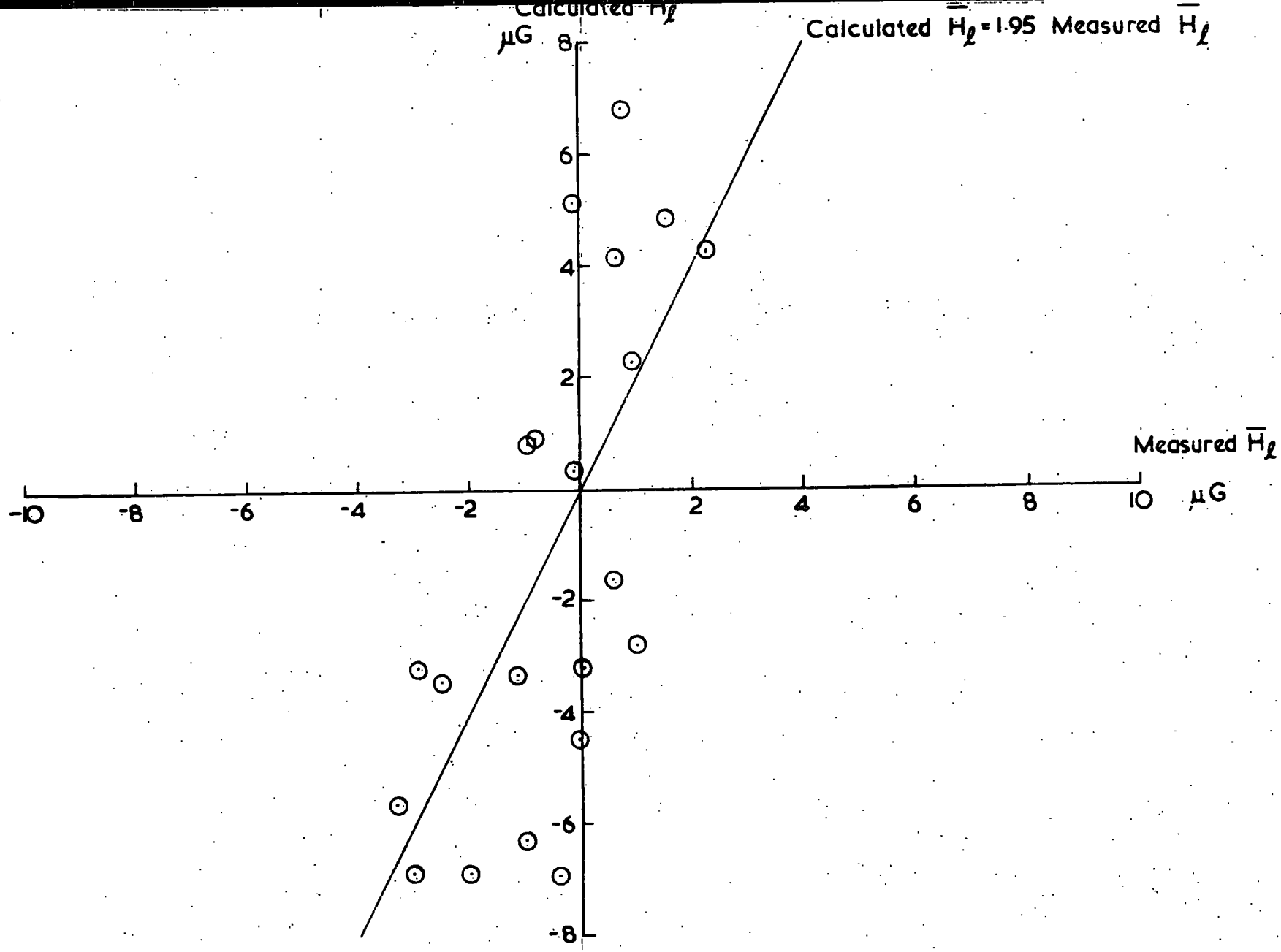

Figure 3.13. Values of $\bar{H}_\ell$ calculated using $N_e 1$ and Field Model D.

and if a helical component exists it is probably smaller in extent than that of model B.

TABLE 3.4

Field Model	Correlation with predictions	Least squares best fit
A	0·72 (significant correlation)	$H_A = 1{\cdot}69\ H_{exp}$
B	0·045	-
C	0·017	-
D	0·67 (significant correlation)	$H_D = 1{\cdot}95\ H_{exp}$

As can be seen from Table 3.4 pulsar rotation measurements are best explained by a model A, or model D, type field, but they seem to suggest a smaller field strength than used in these models.

CHAPTER 4

CALCULATION OF TRAJECTORIES OF PARTICLES ARRIVING AT THE EARTH FROM VARIOUS REGIONS OF THE GALAXY

4.1 Introduction

Cosmic ray particles reach the Earth after travelling through the galactic magnetic field. The force acting on them due to this field causes them to spiral about the field lines with a Larmor radius of $R_L \sim \frac{E \times 10^{-21}}{ZH}$ pc, where E is the energy of the particle in ev, Z is the atomic number and H is the magnetic field strength in gauss.

If this radius is small compared with the size of any irregularities in the magnetic field then quasidiffusional motion occurs. Clouds of stronger magnetic field than the surrounding regions act as scattering centres for the particles.

Particles with higher energies, such that the radius of curvature is larger than this but smaller than the characteristic scale of the regular magnetic field, move, in effect, along the lines of force. This type of motion probably occurs for protons of energy between $\sim 10^{15}$ eV and 10^{17} eV.

However, for protons of energy $E \gtrsim 10^{17}$ eV, in a field $\sim 10^{-6}$ G, the Larmor radius is large compared with the scale of the regular field and quasi-rectilinear motion occurs. At lower energies within this region the particles are trapped within the Galaxy. However, at $\sim 10^{18}$ eV (for protons), R_L is of the order of the thickness of the galactic disc and at higher energies the particles can escape from the Galaxy. For energies $\gtrsim 10^{19}$ eV the trajectories approximate to straight lines. The transition from complete trapping of particles in the Galaxy, to complete escape is of interest when considering whether these high energy particles originate in the Galaxy or are of extra-galactic origin. The exact effect of the magnetic field on the paths of the particles depends on the configuration of the magnetic field. To investigate this the trajectories of particles reaching the Earth were calculated utilizing each of the magnetic field models described above. In practice this is done

by following the trajectories of antiparticles from the Earth until they interact with the interstellar gas (A distance $\sim$ 500 kpc if the gas density is 1 cm^{-3}), or until they leave the Galaxy.

This method was used by Thielheim and Langhoff (1968, 1969), for their field model (model A), to calculate 18 individual proton trajectories at several energies. They found that protons of energy 10^{20} eV and 10^{19} eV travel along straight paths from the edge of the galactic region. Thus at these energies the pathlength in the Galaxy was found to be quite short in most directions.

Protons of energy 10^{17} eV were found to be completely trapped, by the magnetic field, in the spiral arms of the Galaxy. Thus protons arriving at the Earth from all the directions considered were found to have long pathlengths in the Galaxy at this energy.

Thielheim and Langhoff also found that particles with energies corresponding to protons of energy 10^{18} eV appear to come from the hemisphere around the anti-centre, and no such particles reach the Earth from the galactic centre. At this energy there is also a wide distribution in the lengths of paths within the Galaxy.

If it is assumed that the cosmic ray sources are uniformly distributed in the Galaxy, then the intensity of cosmic rays from a certain direction will be proportional to the pathlength in the Galaxy of particles from that direction, if their motion is quasirectilinear.

Thus, these results indicate that protons of galactic origin reach the Earth comparatively isotropically at 10^{20} eV, 10^{19} eV and 10^{17} eV, and anisotropically at 10^{18} eV.

However, only 18 trajectories were calculated at each energy and only one field model was used by Thielheim and Langhoff. To extend these results a larger number of trajectories have been calculated for each of the field models (A, B, C and D).

4.2 Calculation of trajectories

An electronic computer was used to calculate the trajectories of protons, or particles of the same rigidity, arriving at the Earth after travelling through the galactic magnetic field. Each path was calculated by following an antiproton of a particular energy leaving the Earth in a certain direction. The trajectories were calculated in short steps of distance, over which the acceleration was assumed to be constant.

The force, $\underline{p}$ due to a magnetic field $\underline{H}$ μG, acting on a particle of charge q coulombs and velocity $\underline{V}$ m/sec is given by

$$\underline{p} = 10^{-10}\, q\, (\underline{V} \times \underline{H}) \text{ newtons.}$$

This produces an acceleration of $\frac{p}{E} c^2$ m/sec^2 where E is the particle energy in joules, and c is the velocity of light in m/sec. Hence it can be shown that

$$\frac{\underline{a}}{c^2} = 9.25 \times 10^{-17}\, (\underline{U} \times \underline{H})\, \frac{Z}{E} \text{ (kpc)}^{-1}$$

where $\underline{a}$ is the acceleration of the particle in kpc/sec^2, c is the velocity of light in kpc/sec, $\underline{U}$ is a unit vector in the direction of the velocity of the particle, $\underline{H}$ is the magnetic field in μG, Z is the atomic number of the particle (taken to be negative for antiparticles), and E is the energy of the particle in eV.

During the calculation of the trajectory of a particle, its acceleration was calculated at the beginning of each step, using the expression above. Since in fact, the acceleration is not constant over the steplength, an effective acceleration was found. This was equal to the acceleration at the midpoint of the step and was calculated by interpolation using the accelerations at the beginning of the step and the two previous steps. This effective acceleration was then used in the calculation of the position and the direction of motion of the particle at the end of the step.

By calculating the trajectories of particles in a uniform magnetic field, it was found that step sizes of 0·01 kpc were small enough for energies of 2×10^{18} ev and above. At lower energies smaller step sizes were needed.

Initially the particle trajectories were followed until the particles were more than 20 kpc from the galactic centre. Some of these trajectories are shown in figures 4.1, 4.2, 4.3, 4.4, and 4.5. In these figures the trajectories are identified by numbers 1 to 11, which correspond to the directions listed in Table 4.1.

α = galactic longitude - $173{\cdot}5^{\circ}$ for field models A and D

α = galactic longitude - 180° for field models B and C.

TABLE 4.1

Trajectory number	Direction in which the particle leaves the Earth	
	α	Galactic latitude (b")
1	-	90°
2	0°	45°
3	0°	0°
4	45°	0°
5	90°	0°
6	90°	45°
7	135°	0°
8	180°	0°
9	225°	0°
10	270°	0°
11	315°	0°

Field model A has only a small effect on the trajectories of particles with $E/Z = -3 \times 10^{18}$ eV. The particles leaving the Earth at b"= $\pm 45^{\circ}$ orb" $\sim 0^{\circ}$ and $90^{\circ} \lesssim \alpha \lesssim 270^{\circ}$ (i.e. trajectories 7, 8 and 9) tend to escape from the

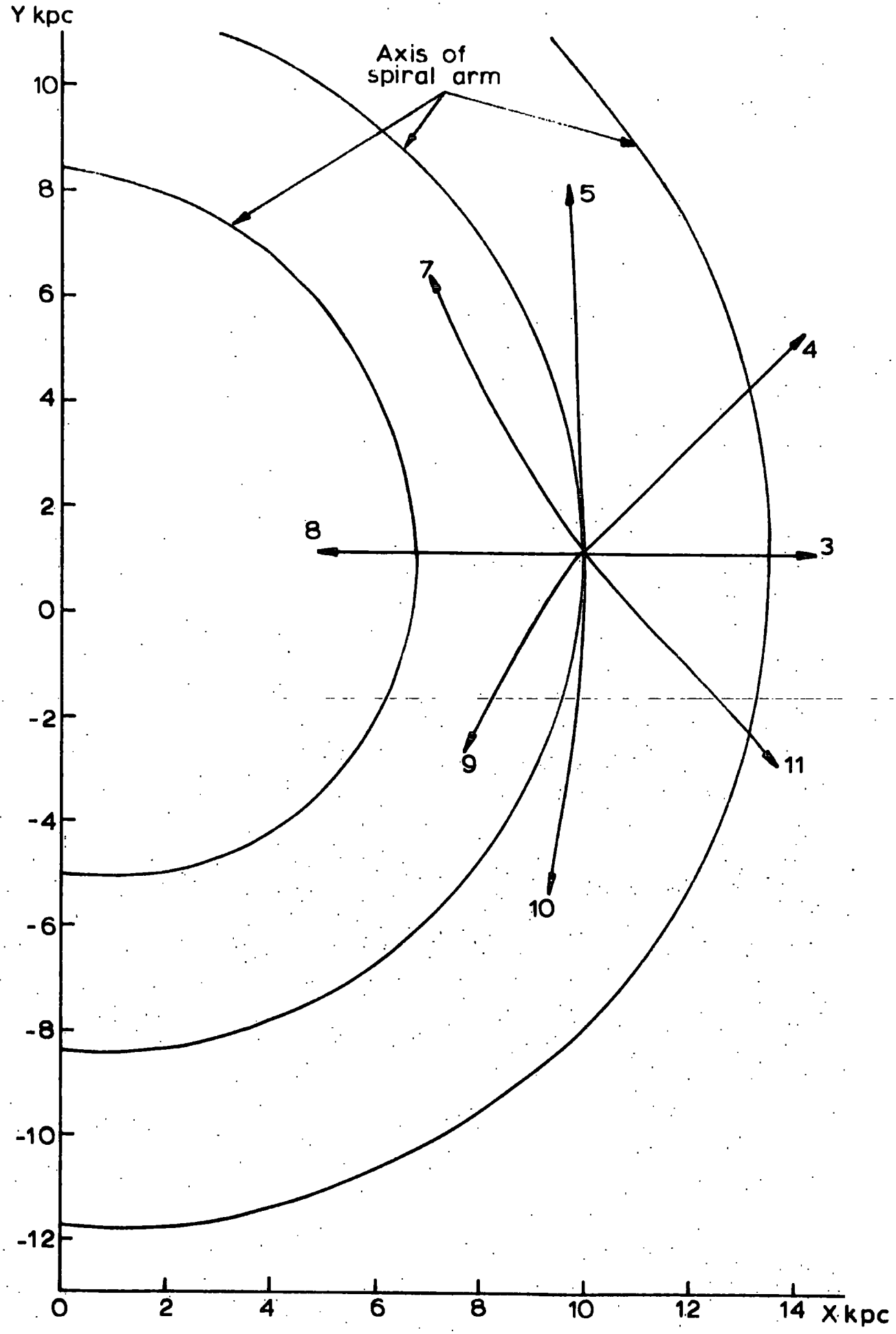

Figure 4.1. Trajectories in field model A. $E/Z = -3 \times 10^{18}$eV

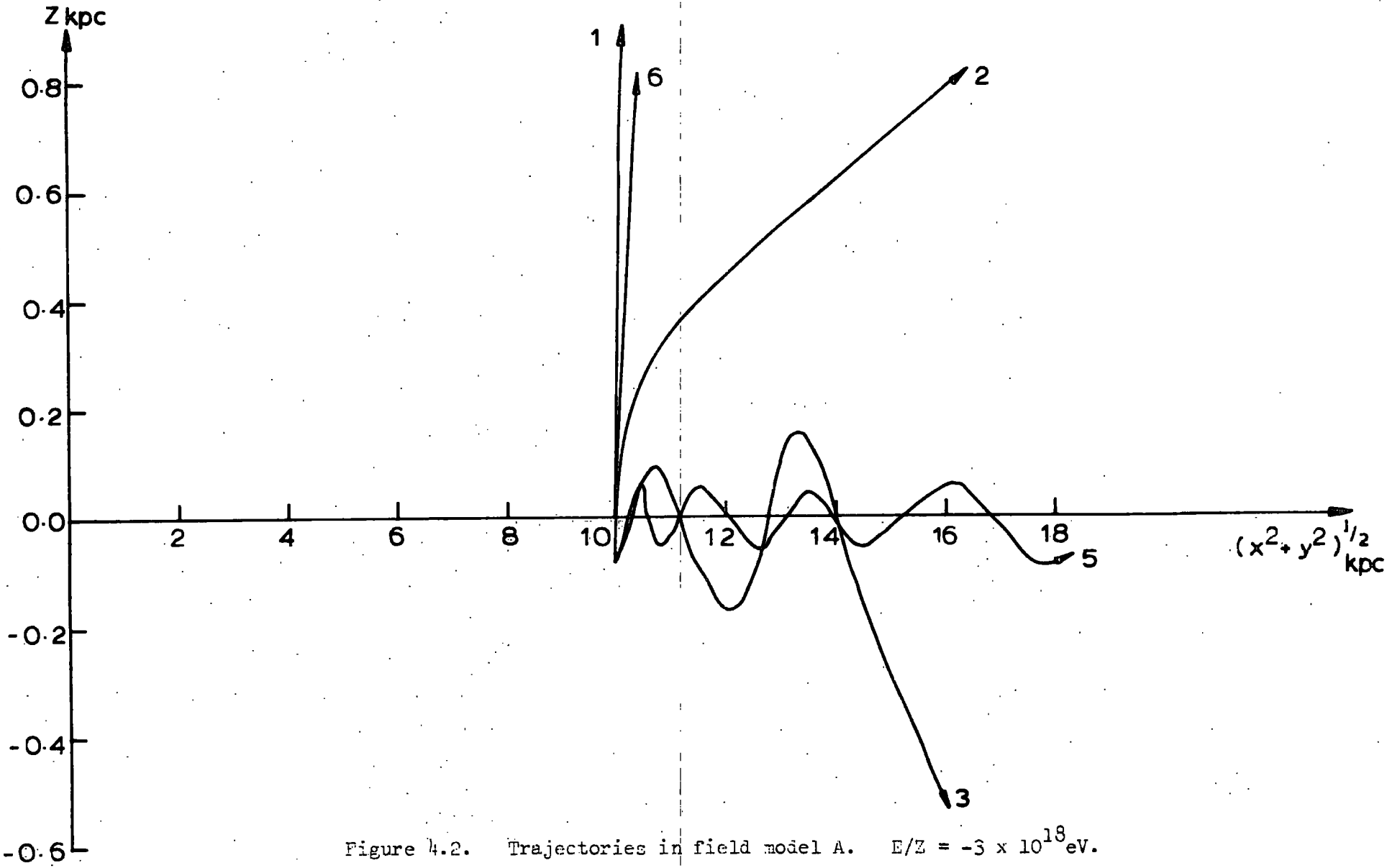

Figure 4.2. Trajectories in field model A. $E/Z = -3 \times 10^{18}$eV.

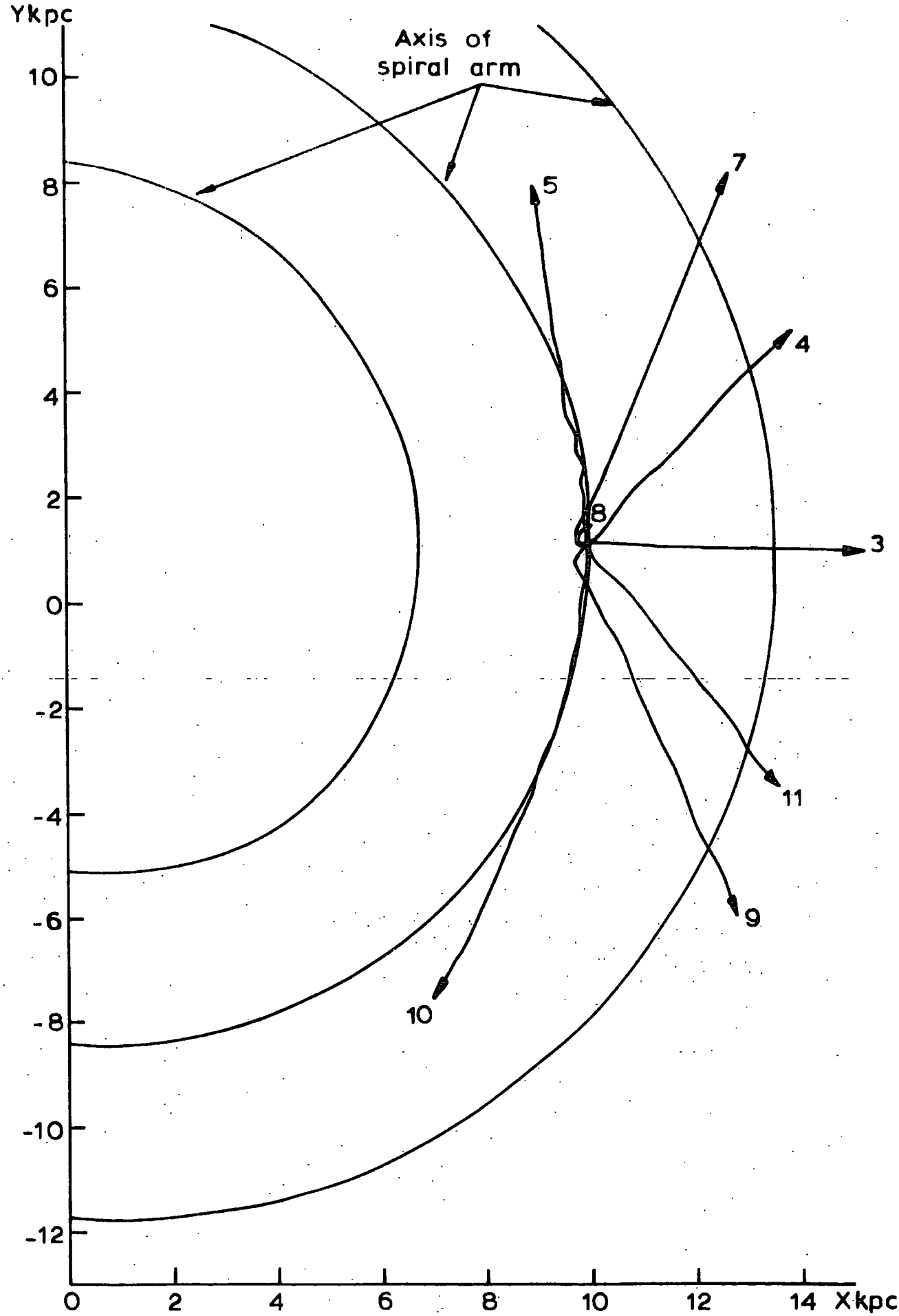

Figure 4.3. Trajectories in field model A. $E/Z = \sim 10^{18}$eV

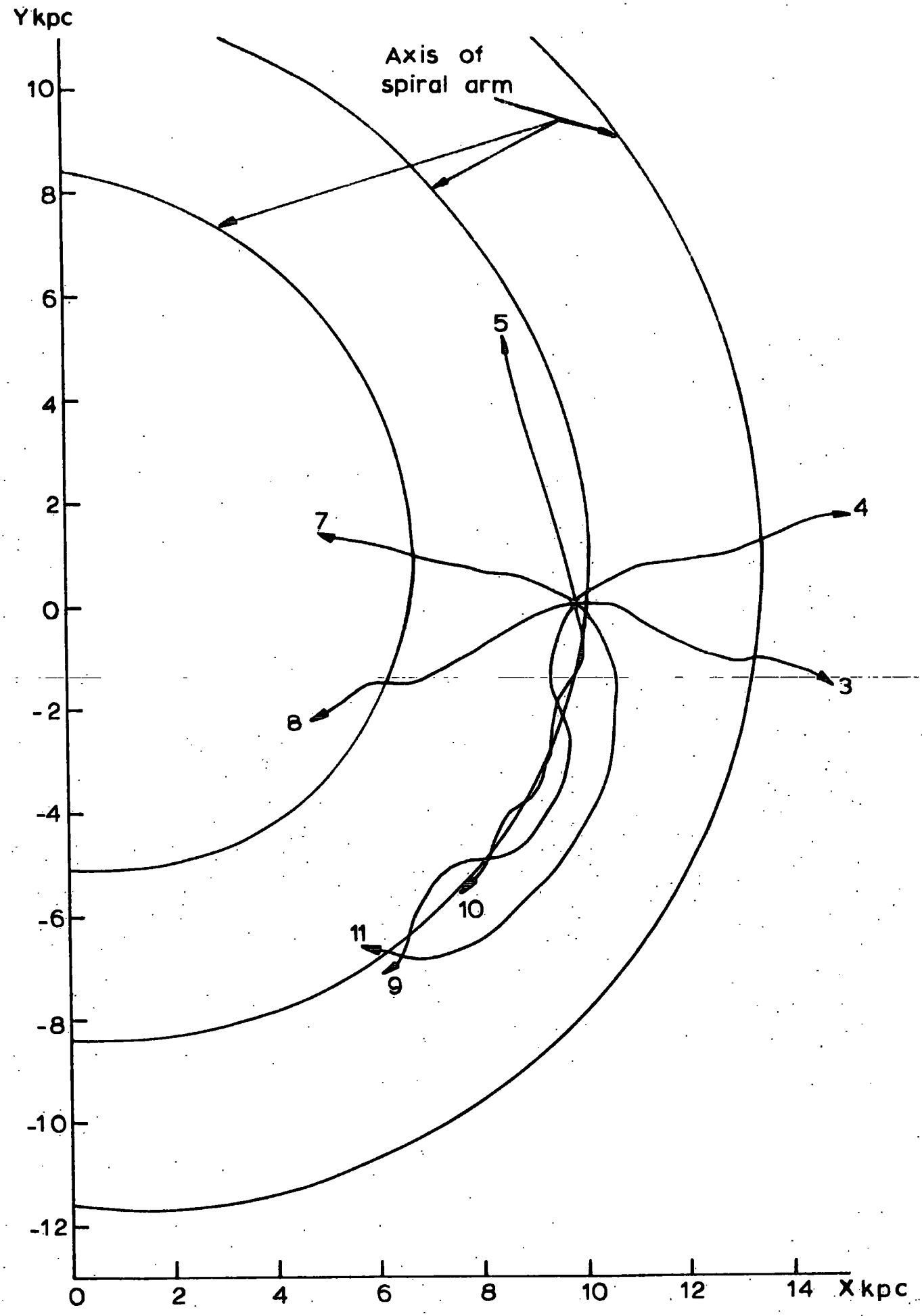

Figure 4.4. Trajectories in field model C. $E/Z = -3 \times 10^{18}$ eV

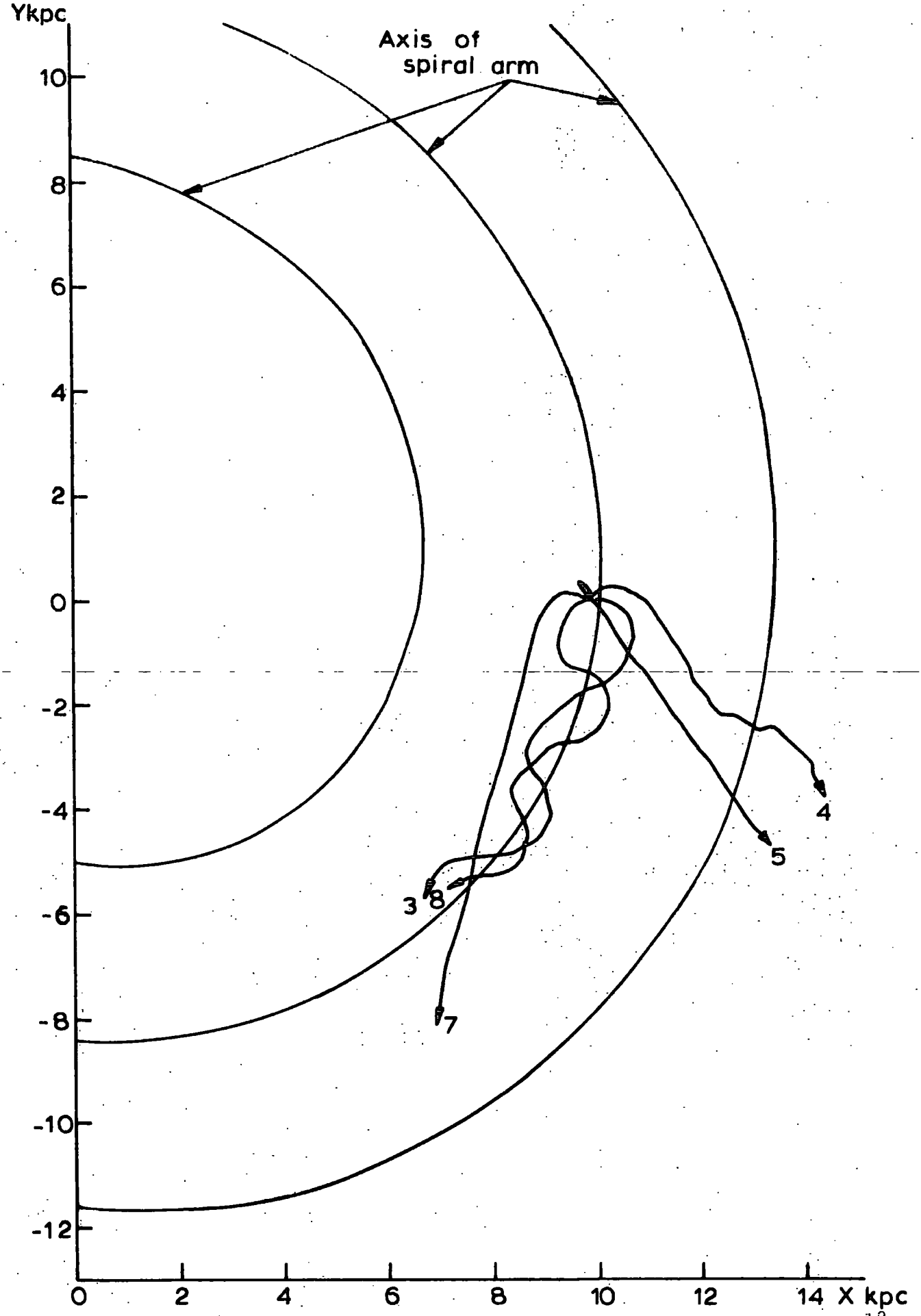

Figure 4.5 Trajectories in field model C. $E/Z = -10^{18}$ eV

galactic disc, while those leaving the Earth at $b'' \sim 0^\circ$ and $-90^\circ \leq \alpha \leq 90^\circ$ (i.e. trajectories 3,4,5, 10 and 11) tend to make small oscillations about the galactic plane. This oscillation is probably caused by the particle being initially deflected across the galactic plane, where the reversal of field direction produces oscillations, which continue until the particle reaches a region where the field is weak enough to allow it to escape. The effect of field model A on the trajectories of particles with $E/Z = -10^{18}$ eV is much bigger. The particles are much more easily trapped within the region of the galactic disc and some (i.e. trajectories 5 and 10) spiral about the galactic arm. Trajectories 7, 8 and 9 are bent steeply downwards so that particles following them cannot reach the galactic centre. These results agree with those of Thielheim and Langhoff (1968, 1969).

Field model C is more effective in the trapping of particles within the disc and spiral arms. Even at $E/Z = -3 \times 10^{18}$ eV some trapping in the disc occurs of particles leaving the Earth at $b'' \simeq \pm 45^\circ$. At this energy trajectories 3 and 4 are similar to those in field model A in that the particles oscillate about the galactic plane. (A reversal of field direction about the galactic plane also occurs in this model). Particles following trajectories 5, 7 and 8 escape from the disc. However, some particles, such as those following trajectories 9, 10 and 11 are trapped spiralling about the galactic arm. At $E/Z = -10^{18}$eV this trapping in the spiral arms is more widespread and it is noticeable that the trajectories tend to follow the spiral arm towards the galactic centre. This effect may be produced by the reversal in direction of the Z component of the field about the surface perpendicular to the galactic plane, through the spiral arm axis.

In later calculations the trajectories were followed until $R = (X^2+Y^2)^{\frac{1}{2}} > 15$ kpc or $|Z| > 1$kpc. Beyond this the magnetic field is weak and the particles have effectively left the Galaxy.

To relate these trajectories to cosmic ray anisotropies at the Earth,

some knowledge of the distribution of cosmic ray sources within the Galaxy is required.

4.3 Distribution of cosmic ray sources in the Galaxy

If cosmic rays of energy $\gtrsim 10^{17}$ eV reaching the Earth are of galactic origin then their most probable sources are pulsars or possibly the galactic nucleus.

Pulsar distances obtained from dispersion measures or absorption by neutral hydrogen at 21 cm show that most observed pulsars lie within 1 or 2 kpc of the sun (e.g. R.D. Davies, 1969), and their measured positions indicate that they lie mainly in the galactic disc (Hewish, 1970).

However it has been suggested (e.g. Mills, 1970; Cavallo, 1971) that most pulsars are situated within the galactic spiral arms. Since the form of the source distribution affects the predicted cosmic ray anisotropy at the Earth these calculations were done for both a uniform distribution of sources in the disc and for a uniform distribution of sources in the spiral arms. That is, in each direction the length of the trajectory lying within the disc (or the pathlength in the disc) and the length of the trajectory lying within the spiral arms were calculated.

It is also interesting to know if particles of these energies ($\gtrsim 10^{17}$ eV) produced in the galactic nucleus can reach the Earth in the presence of a magnetic field such as those described above, and what the cosmic ray anisotropy at the Earth would be if these cosmic rays do come from the galactic nucleus. Thus for each trajectory the following pathlengths were calculated.

(1) The pathlength within 1, 2 and 3 kpc of the galactic centre

(2) The pathlength in the disc defined by $|Z| < 0.3$ kpc

(3) The pathlength in the spiral arms defined, for simplicity, as having a rectangular cross section of 0.6 kpc by 1.2 kpc.

4.4 Trajectories calculated

Trajectories were followed from the Earth in the 146 directions listed below.

TABLE 4.2

Directions of trajectories followed

Galactic latitude	α
$\pm 90^\circ$	
$\pm 75^\circ$	From 0° at 90° intervals to 270°
$\pm 60^\circ$	From 0° at 45° intervals to 315°
$\pm 45^\circ$	From 0° at 30° intervals to 330°
$\pm 30^\circ$	From 0° at 22.5° intervals to 337.5°
$\pm 15^\circ$	From 0° at 18° intervals to 342°
0°	From 0° at 15° intervals to 345°

This set of trajectories was calculated using each of the field models for several different values of -E/Z between $4.5\ 10^{17}$ eV and 10^{20} eV. At lower energies the trajectories require so many steps that this method of calculation is impracticable, while at higher energies the trajectories are effectively straight lines.

The following combinations of energies and field models were used.

TABLE 4.3

Energies and field models for which trajectories were calculated

- E/Z in eV	Field Model
$4.5\ 10^{17}$	A
$6\ \ 10^{17}$	A
$7.5\ 10^{17}$	A,B,D
10^{18}	A,B,C,D
$2\ \ 10^{18}$	B,D
$3\ \ 10^{18}$	A,B,C,D
$6\ \ 10^{18}$	B,C
$8\ \ 10^{18}$	C
10^{19}	A,B,C,D
$3\ \ 10^{19}$	A
10^{20}	A

Pathlength calculations were also done using modified forms of these basic models.

For example the trajectory calculations performed using model A with the Sun at R = 10 kpc were repeated for the Sun at R = 9 kpc in an attempt to discover how sensitive the pathlengths are to changes in this parameter. Pathlengths were also found at $E/Z = -7.5\ 10^{17}$ eV and $E/Z = -10^{18}$ eV using field model A with $H_{z_o} = 0$. Since H_{z_o} is typically $\sim \frac{1}{100} \times H_{a_o}$ this change would not be expected to produce much alteration in the results. In fact both these adjustments were found to have a negligible effect on the pathlengths and their distribution over the galactic latitude-longitude sphere.

A modification was also made to field model A to determine the effect of a halo field. Obviously if a halo magnetic field exists it will affect anisotropies considerably. Although, at present, there is not generally considered to be much evidence in support of a halo field it is difficult to prove that it definitely does not exist. Even if a halo field does exist so little is known about its possible structure that it is difficult to construct a model for this field. In this case a halo field model was produced by modifying model A such that the field strength is constant for $|Z| > 0.28$ kpc at a value $\sim 2\mu G$ and the flux lines in this halo follow the spiral arm direction.

Trajectories were found using this model for $-E/Z = 10^{18}$ eV, 3.10^{18} eV and 10^{19} eV.

Field model C was adapted by using a field strength with a gaussian dependence on b, and it was found that the pathlength distribution is effectively the same as for the unmodified field, indicating that the helical form of the field is more influential than the exact distribution of field strength.

4.5 Cosmic rays from the galactic nucleus

The possibility of cosmic rays from the galactic centre reaching the Earth can be determined for each field model from these trajectory calculations.

In general there is an energy band within which no particles can reach the Earth from the galactic centre. At higher energies the particles travel along almost straight paths and may hit the Earth, while at lower energies particles can travel along the spiral arms from the centre to the Earth.

For field model A this 'forbidden' band is given by $7.\ 10^{17}$ eV $\lesssim E/Z \lesssim 3.\ 10^{19}$ eV. For the other models the lower limit to this band occurs at higher energies. Particles with $E/Z \lesssim 10^{18}$ eV for models D and B, and $\lesssim 10^{19}$ eV for model C can reach the Earth by travelling along the spiral arms.

The addition of a halo field would make particle transfer from the galactic centre to the Earth easier.

However, in each case, cosmic rays exclusively from the galactic centre would produce large anisotropies at the Earth - larger in fact, than the anisotropies produced by cosmic rays coming from sources uniformly distributed in the galactic disc or spiral arms.

4.6 Pathlength distributions

The distribution over the galactic latitude-longitude sphere was found for pathlengths in the galactic disc and for pathlengths in the spiral arms. For all the field models and energies considered pathlengths in the disc were found to have a similar distribution to those in the spiral arms but to be approximately twice as long.

From the 146 trajectories calculated in each case, it was possible to interpolate to produce contour maps of the maximum pathlength in the disc or spiral arms of particles arriving at the Earth in a given direction. These maps were plotted on an equal area projection in celestial coordinates to facilitate later comparison with measured cosmic ray anisotropies.

Figures 4.6 to 4.19 show some of these maps although not all the contours are marked.

For field model A the longest pathlengths are in the spiral arm directions

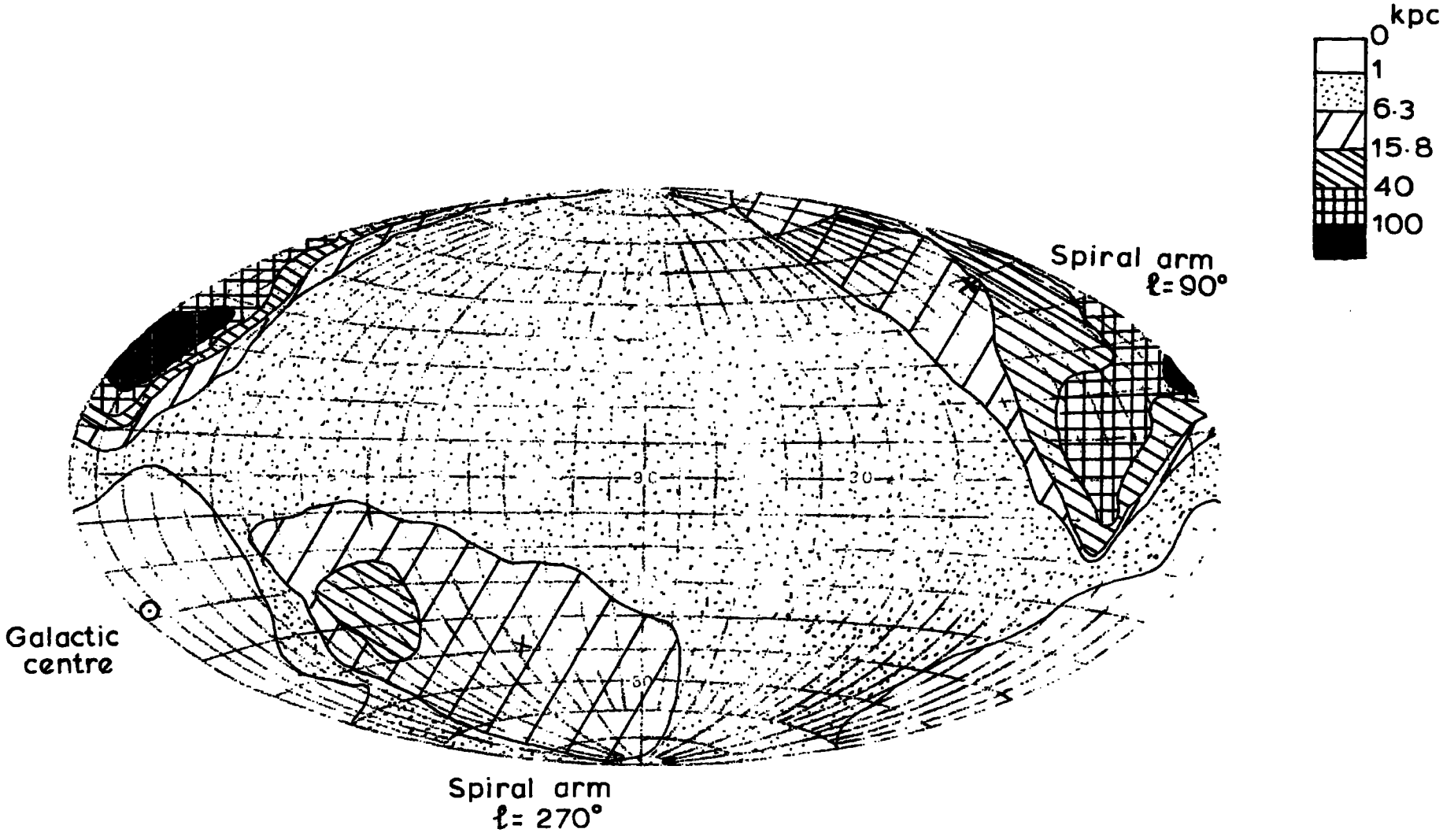

Figure 4.6. Plot in celestial coordinates of pathlengths in the spiral arms for field A. $^{E}/_{Z} = 6.10^{17}$eV.

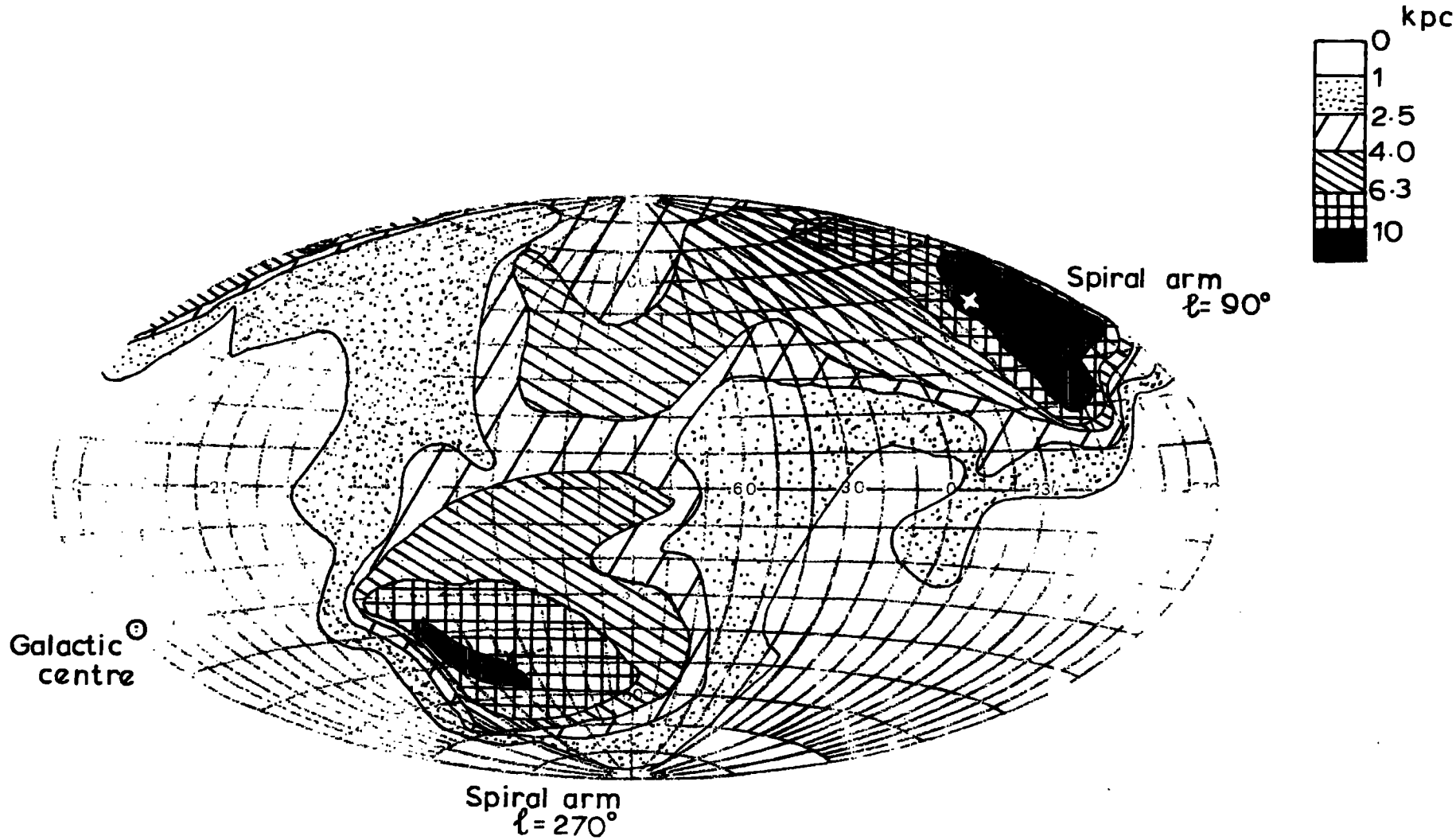

Figure 4.7. Plot in celestial coordinates of pathlengths in the spiral arms for field A. $E/Z = 10^{18}$ eV.

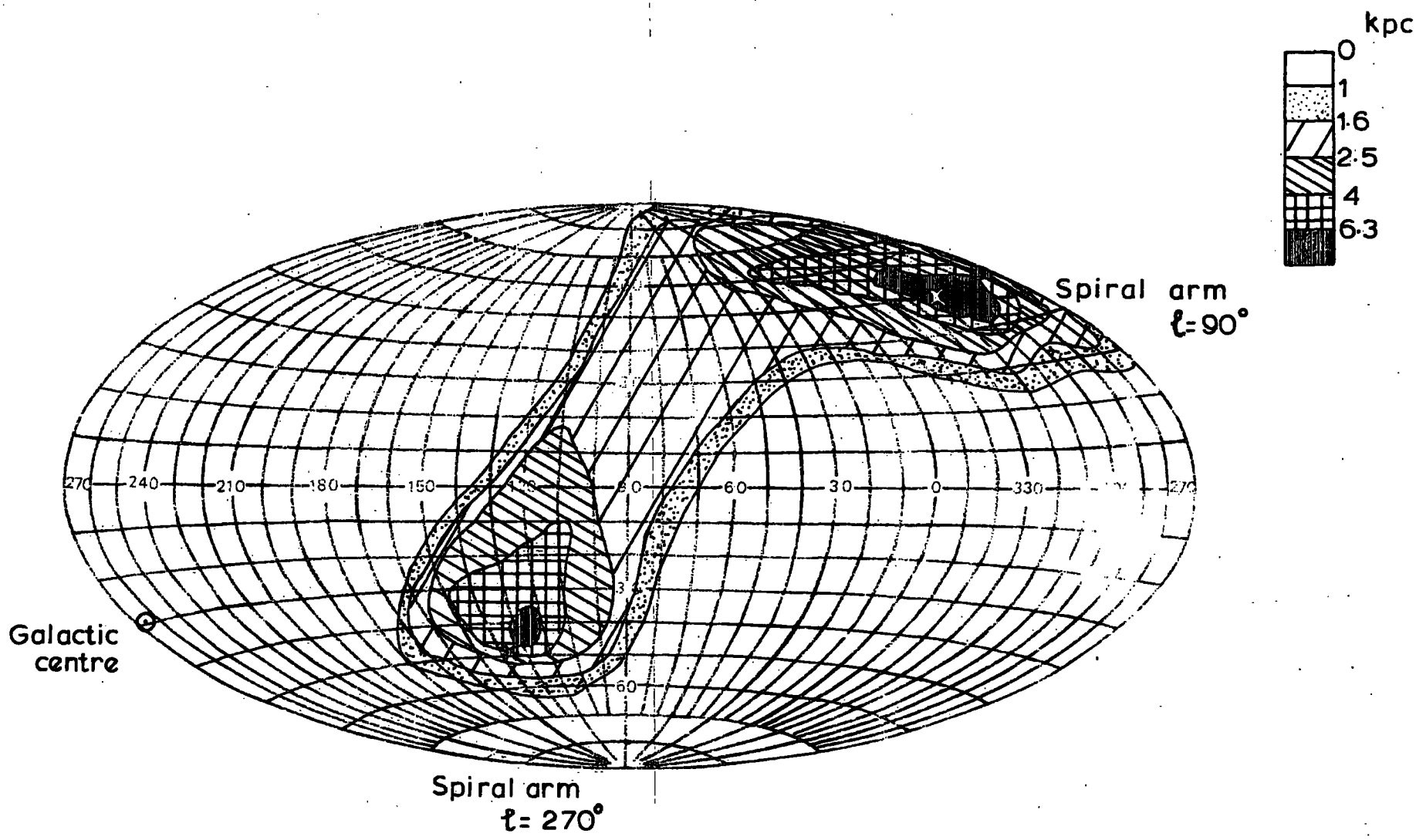

Figure 4.8. Plot in celestial coordinates of pathlengths in the spiral arms for field A. $E/Z = 3\ 10^{18}$eV.

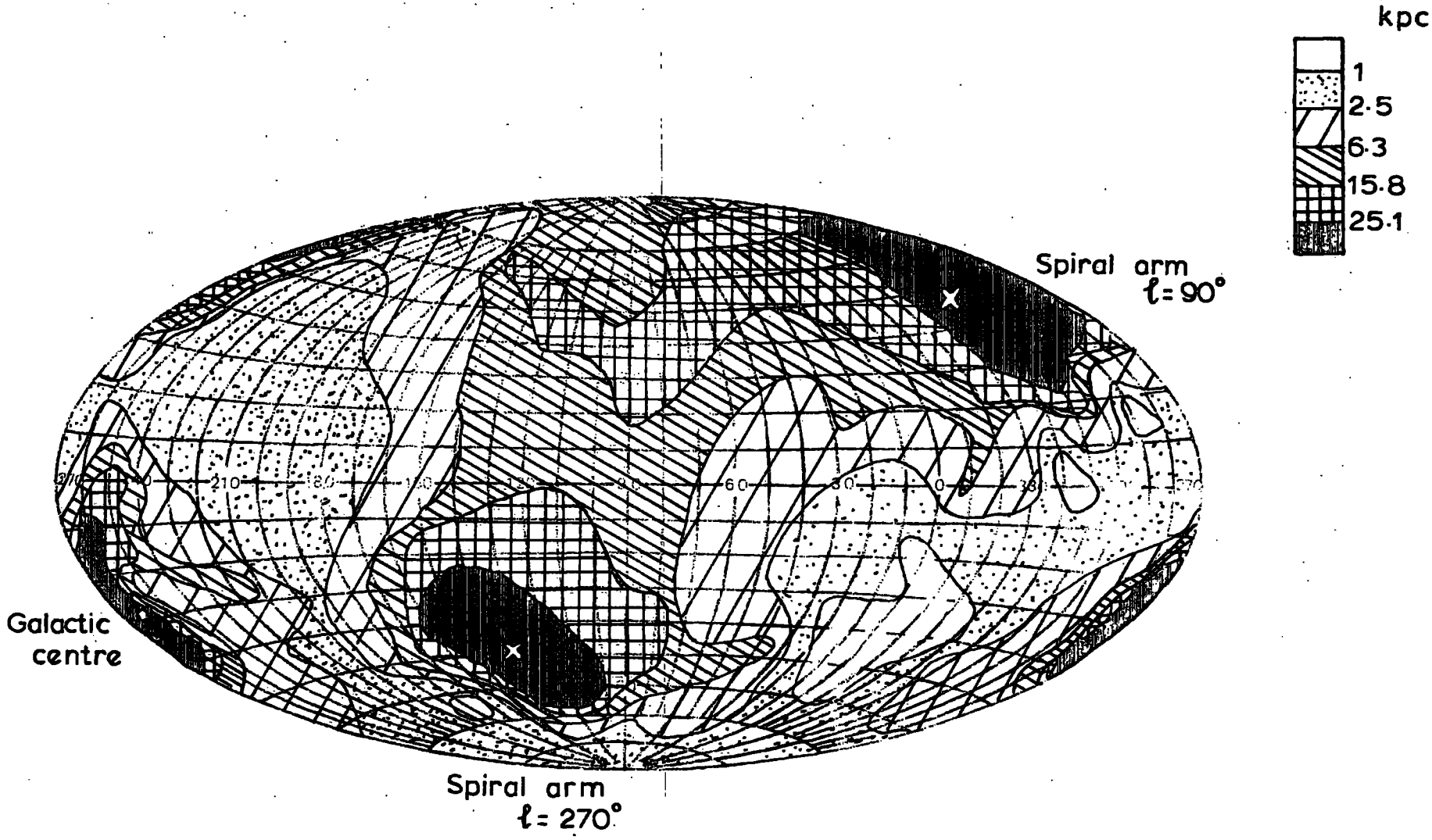

Figure 4.9 Plot in celestial coordinates of pathlengths in the disc for field A + 'halo'. $E/_Z = 10^{18}$eV.

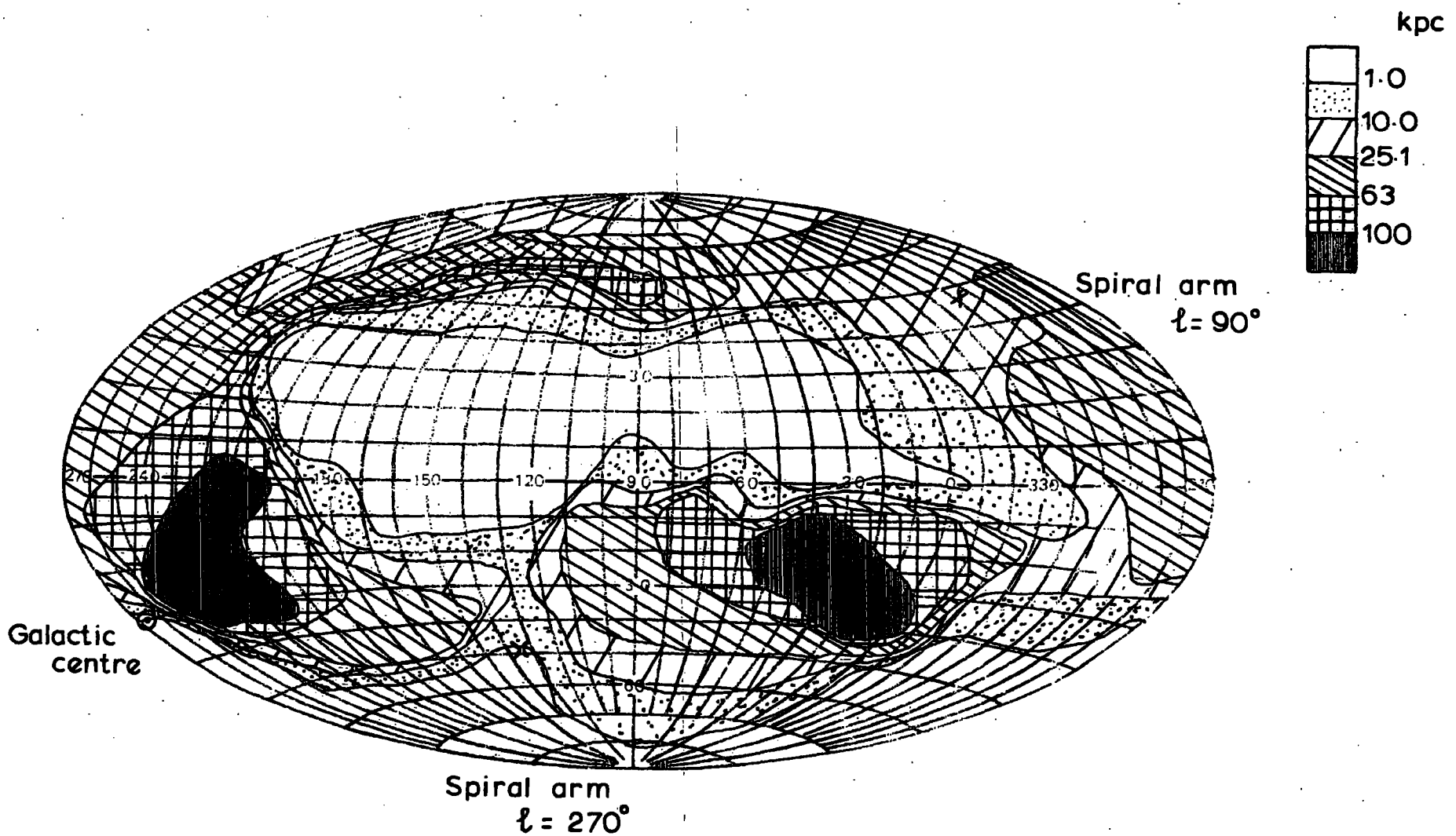

Figure 4.10 Plot in celestial coordinates of pathlengths in the disc for field B. $E/_Z = 7{\cdot}5\ 10^{17}$ eV

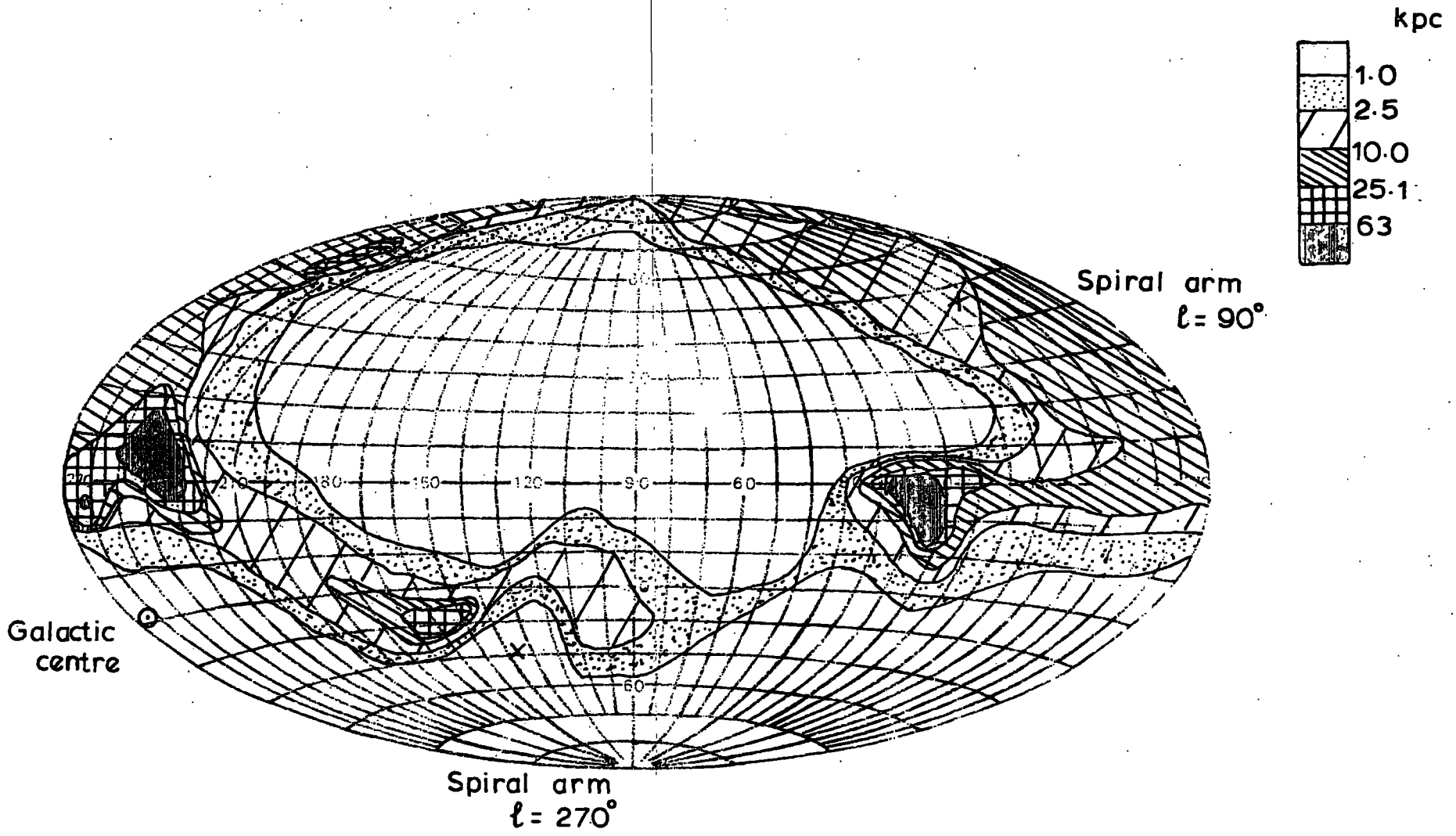

Figure 4.11 Plot in celestial coordinates of pathlengths in the disc for field B. $E/Z = 10^{18}$ eV.

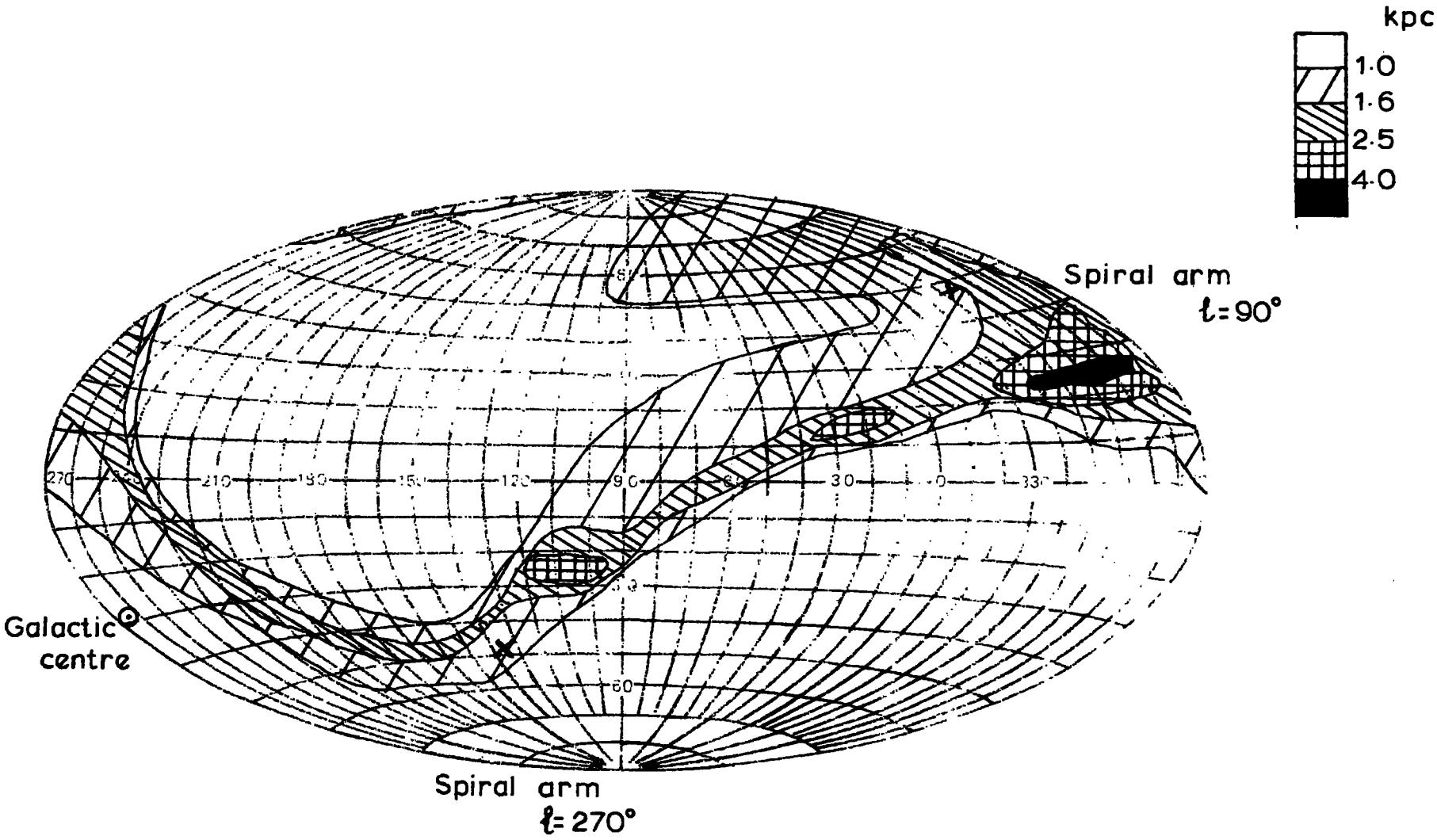

Figure 4.12 Plot in celestial coordinates of pathlengths in the disc for field B. $E/Z = 3\ 10^{18}$eV.

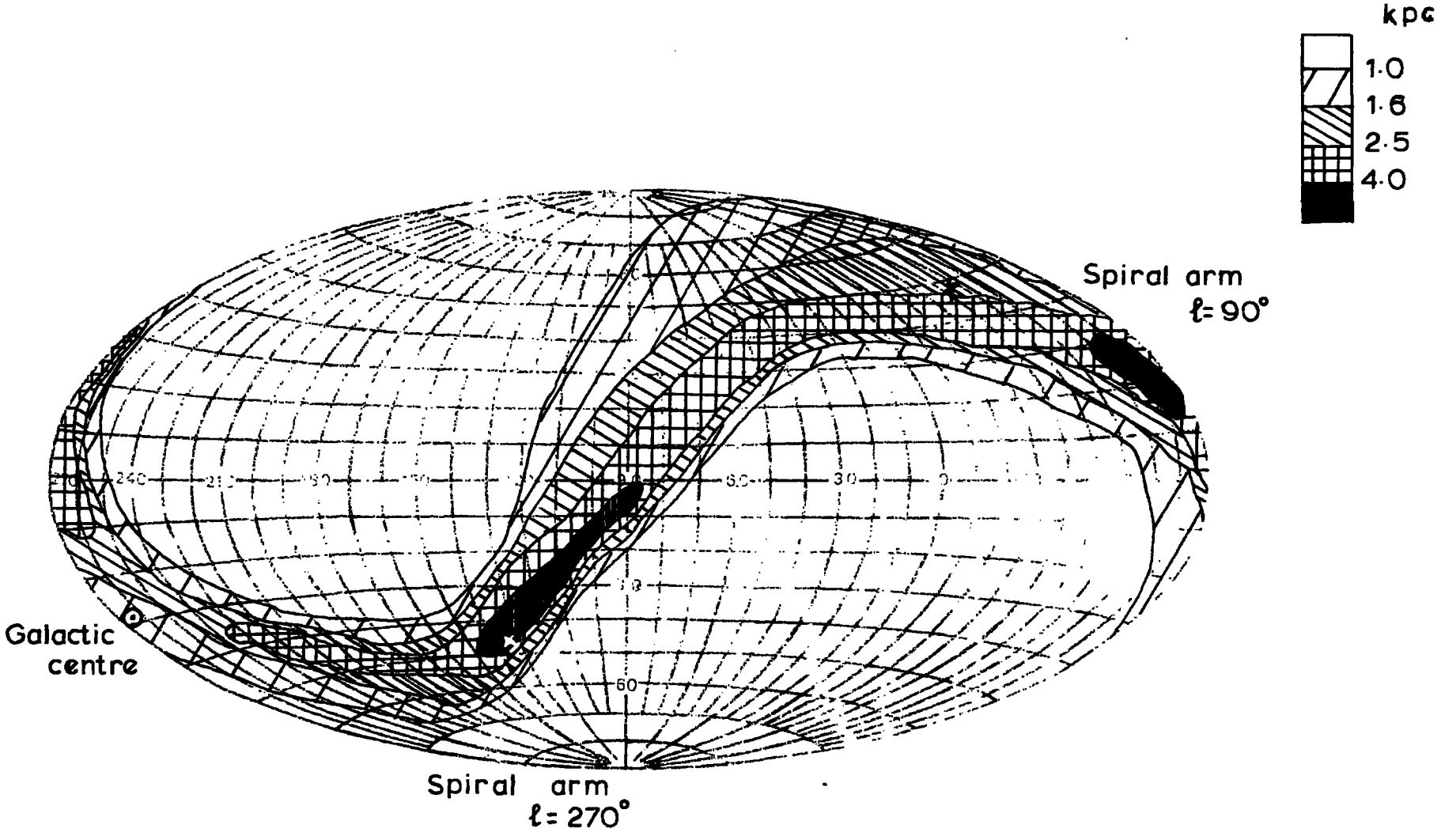

Figure 4.13 Plot in celestial coordinates of pathlengths in the disc for field B. $E/Z = 10^{19}$ eV.

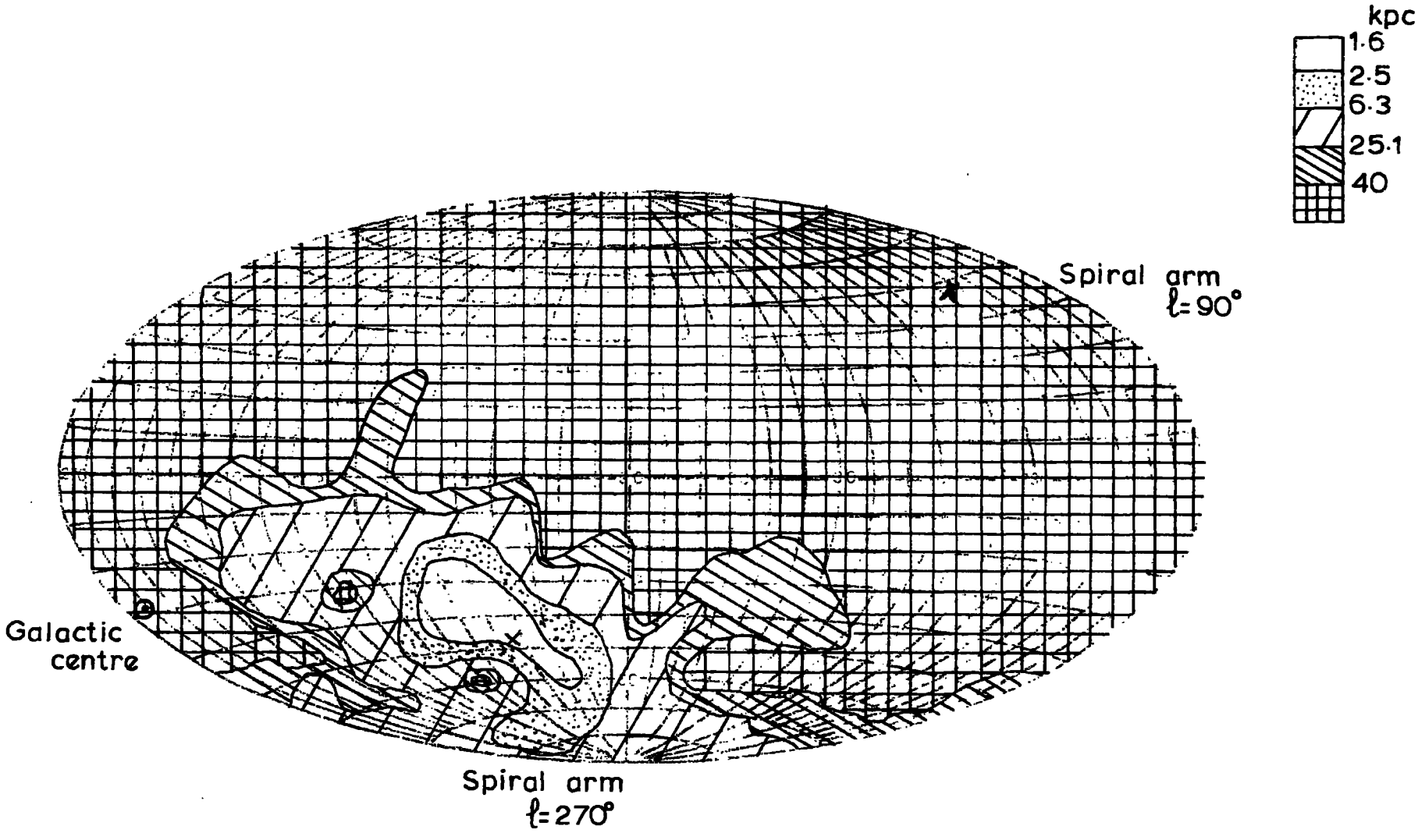

Figure 4.14 Plot in celestial coordinates of pathlengths in the disc for field C. $E/Z = 8.\ 10^{17}$eV

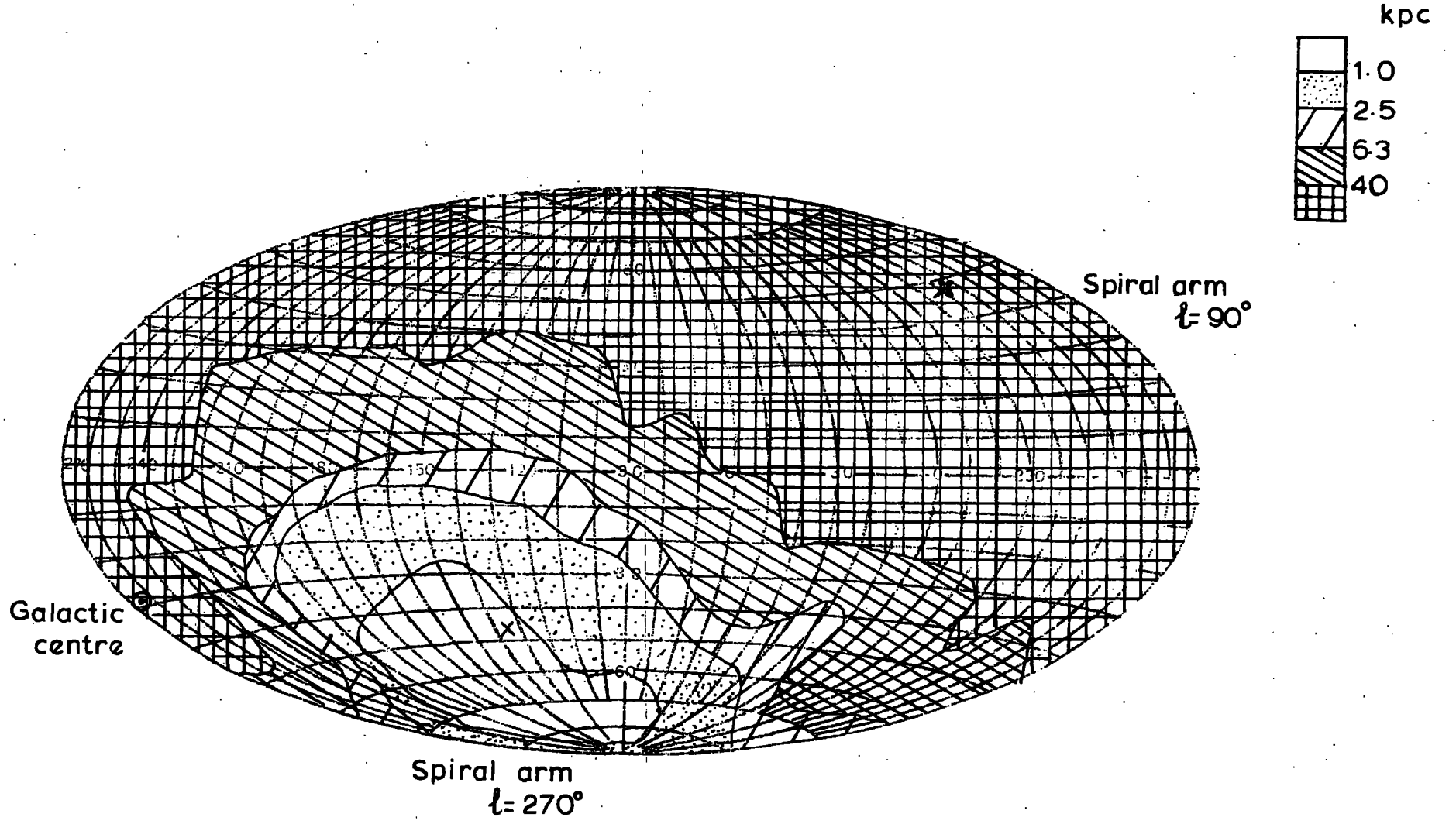

Figure 4.15 Plot in celestial coordinates of pathlengths in the disc for field C. $E/Z = 10^{18}$ eV

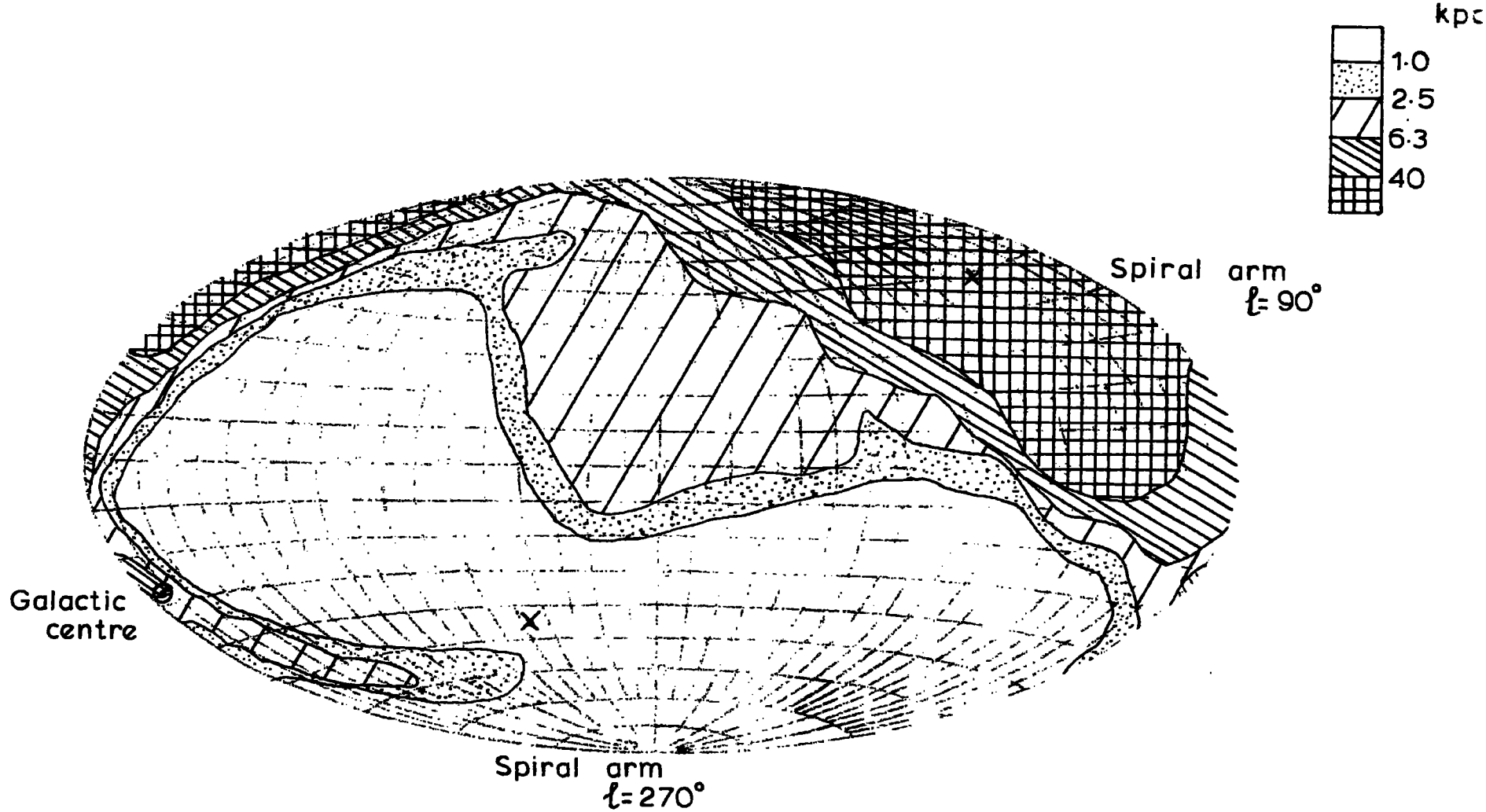

Figure 4. 16 Plot in celestial coordinates of pathlengths in the disc for field C. $E/Z = 3.\ 10^{18}$eV.

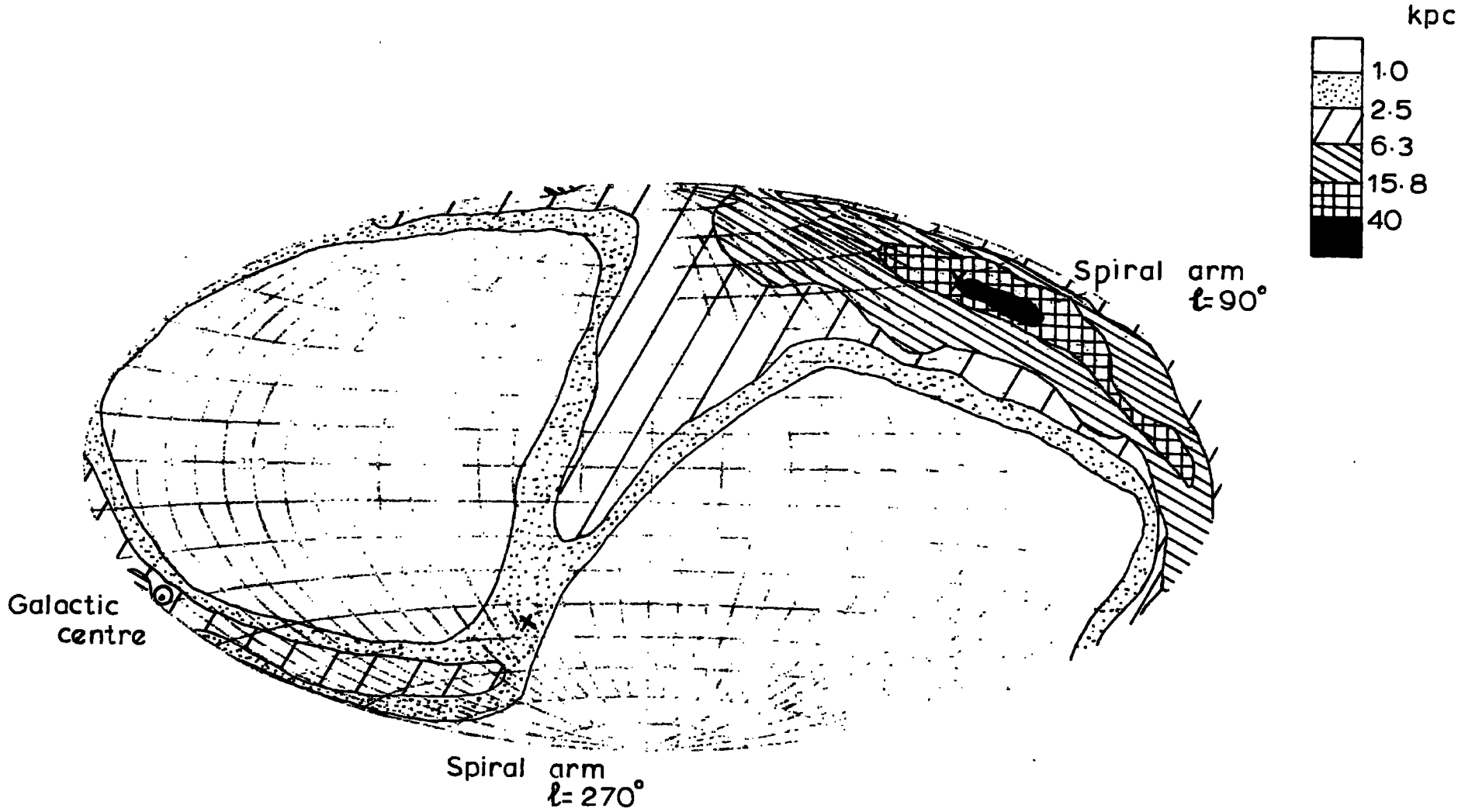

Figure 4.17 Plot in celestial coordinates of pathlengths in the disc for field C. $E/Z = 10^{19}$ eV.

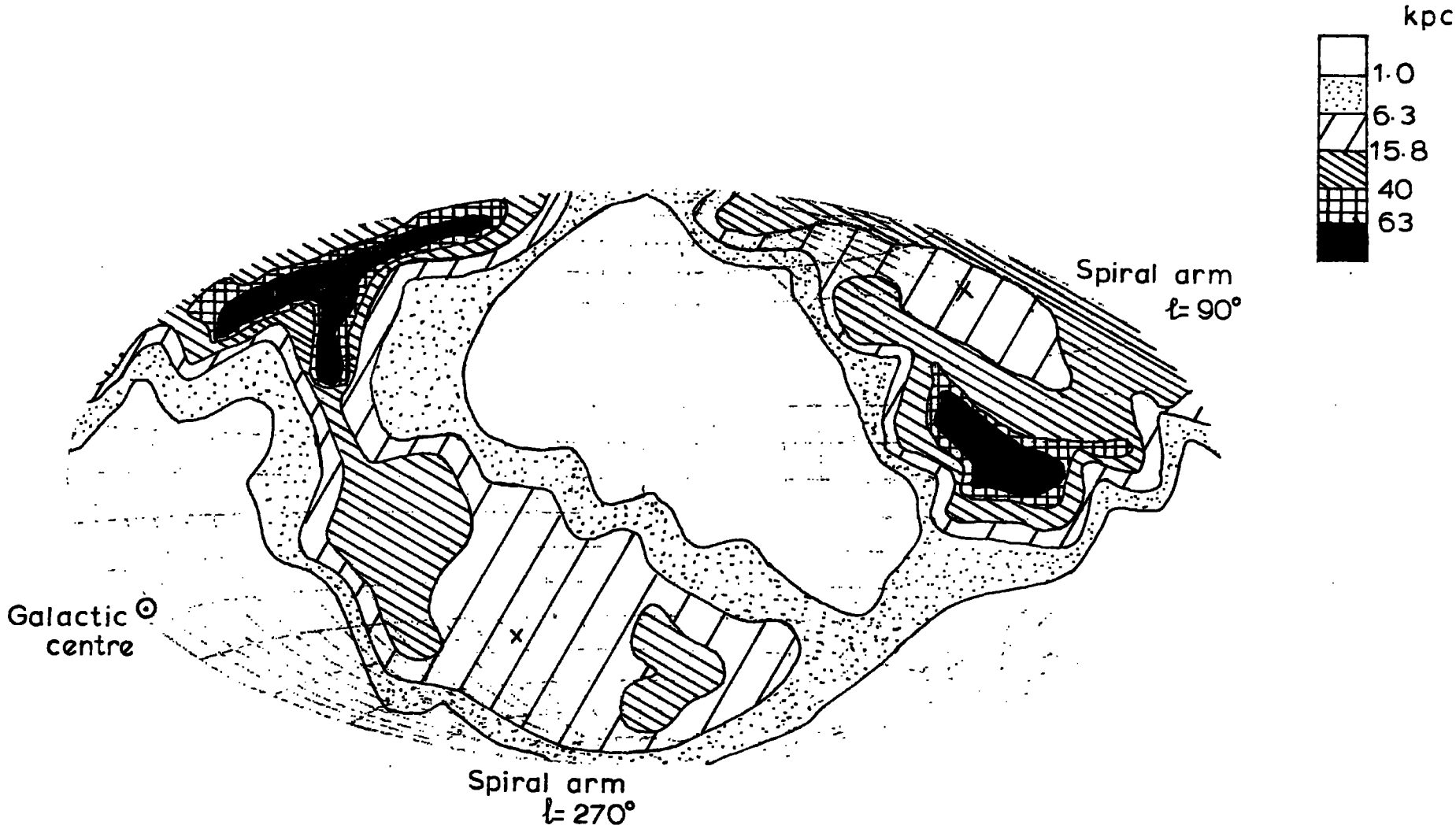

Figure 4.18 Plot in celestial coordinates of pathlengths in the disc for field D. E/Z = 10^{18}eV.

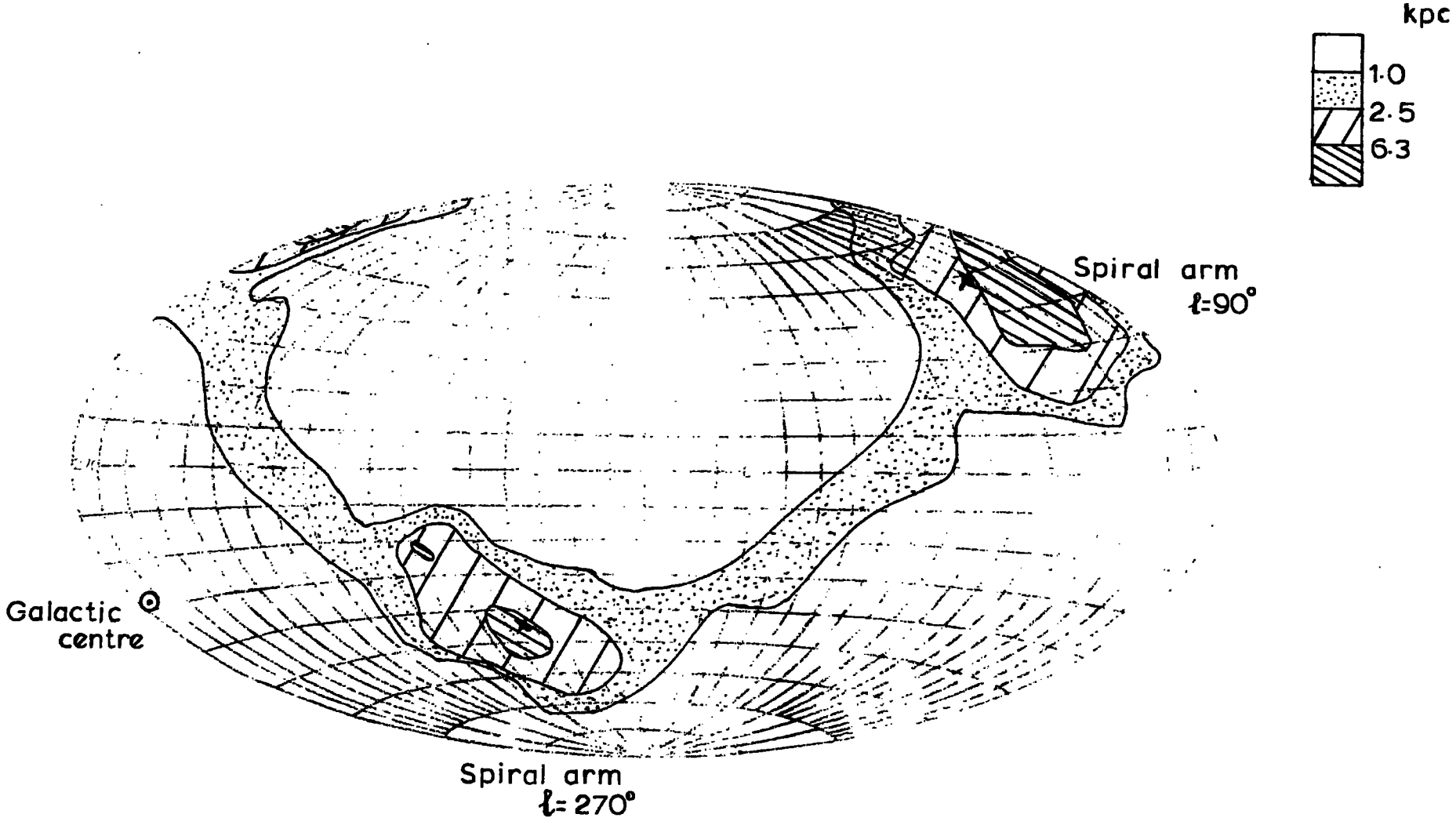

Figure 4.19 Plot in celestial coordinates of pathlengths in the disc for field D. $E/Z = 2.\ 10^{18}$ eV.

with the $\ell = 90^{\circ}$ spiral arm maximum tending to be larger and more extended than the $\ell = 270^{\circ}$ spiral arm maximum. At $E/Z = 6.\ 10^{17}$ eV the pathlengths in the direction of the galactic centre are very short and at higher energies this minimum becomes more extensive. Above 10^{18} eV the longest pathlengths tend to occur in a band about the galactic equator between $\ell \sim 90^{\circ}$ and $\ell \sim 270^{\circ}$. The width of this band decreases at higher energies and by $3\ 10^{18}$ eV all the pathlengths are < 1 kpc except for those in a narrow band ($b \sim \pm 30^{\circ}$) along the galactic equator in the direction of the anticentre. This band represents those directions in which particles are trapped in the spiral arm or oscillate about the plane so that they travel through successive spiral arms.

Above $3\ 10^{18}$ eV the addition of the 'halo' to field model A has little effect but at lower energies a third peak in the pathlength distribution occurs towards the galactic centre. Probably those particles which in field A are bent out of the disc are trapped in the spiral arms by this halo field.

For field B the peaks in the pathlength distribution are not so closely associated with the spiral arm directions as they are for model A, and their position varies with energy. Above $3\ 10^{18}$ eV the longest pathlengths are in a band about the galactic equator.

Field C traps particles much more easily than the other models. As mentioned in 4.2 there is tendency for particles to be trapped in the spiral arm and to follow it towards the galactic centre. As a result at $E/Z \lesssim 10^{18}$ eV the pathlength distribution shows a wide range of incident angles for which the pathlength in the disc is greater than 40 kpc. This region represents directions in which the particles are trapped in the spiral arms. At these energies the pathlength minimum occurs in the direction of the $\ell = 270^{\circ}$ spiral arm. As the energy increases the maximum contracts until, at 10^{19} eV, pathlengths > 40 kpc are only found in the direction of the $\ell = 90^{\circ}$ spiral arm, and the long pathlengths lie in a band along the galactic equator.

At this energy models B and C produce very similar pathlength distributions.

The model D pathlength distributions are similar to those of model B and this similarity becomes more marked at higher energies where the helical component of field B has less effect.

Above a few times 10^{19} eV, where the magnetic field has little influence on the particle trajectories, the pathlength distribution is independent of the field model and merely reflects the geometry of the Galaxy.

As mentioned above if cosmic ray sources are uniformly distributed within the regions considered, then for the energy band where the motion is quasirectilinear, the intensity of cosmic rays from a given direction is proportional to the maximum pathlength in these regions of particles from that direction. That is the contour maps of pathlength are also contour maps of cosmic ray intensity and can be used to predict anisotropies at the Earth. The predicted anisotropies at each energy for each field model can then be compared with observations.

CHAPTER 5

COMPARISON OF PREDICTED COSMIC RAY INTENSITIES WITH EXTENSIVE AIR SHOWER ARRIVAL DIRECTION MEASUREMENTS

The predicted variation of cosmic ray intensity with arrival direction obtained from each contour map of pathlength have been compared with extensive air shower measurements of the corresponding energy region.

5.1 Extensive air shower detectors

The measurements made by three air shower arrays, of the arrival directions of E.A.S. produced by cosmic ray primaries of energy $\geq 10^{17}$ eV, have been used. These arrays are the Massachusetts Institute of Technology array at Volcano Ranch, the Haverah Park array and the University of Sydney array at Pilliga Forest.

5.1.1 M.I.T. array at Volcano Ranch

Volcano Ranch is situated at latitude 30°N and at an atmospheric depth of 820 g/cm^2. The air shower array, which was in operation during 1960-61, had an area of 8 km^2 and consisted of a hexagonal arrangement of 19 solid scintillators, each with an area of 3.3 m^2.

The arrival direction data (Linsley, 1963 and private communication) covers declinations $+ 90^{\circ}$ to $- 30^{\circ}$.

For the comparison with predicted intensities, the energies of the Volcano Ranch data have been adjusted to be consistent with the Haverah Park values. Hillas (1969) first suggested that the use of different methods of analysis for the data from these two experiments was resulting in inconsistencies between them in the number spectrum and primary energy deduced. The reason for this is as follows. The energy of the primary particle is related to the size of the shower produced. To obtain the shower size from measurements of particle densities at the individual detectors it is necessary to assume some lateral distribution for the shower. The exact form of this lateral distribution is not well known and the use of different types of lateral distribution may result

in considerably different estimates for shower size. The lateral distribution used by Linsley with the Volcano Ranch data to obtain the size spectrum was of a different form from that employed at the Haverah Park and Sydney arrays. Hillas (1969) fitted a lateral distribution of the type used at Haverah Park to the Volcano Ranch data and obtained shower sizes approximately twice as large as those given by Linsley. Thus, in effect, the same detector response was interpreted as a shower of a different size produced by a primary particle of a different energy. Thus, to ensure consistency, the energies of the Volcano Ranch data have been adjusted to correspond to the Haverah Park values, for the purpose of this work of comparison with predicted intensities.

The adjustment was made by taking the "equivalent Haverah Park energy" as the energy given by the Haverah Park spectrum (Hillas et al., 1971) corresponding to the integral flux measured at Volcano Ranch for the unadjusted energy (Linsley, 1963).

The following groups of data were used for comparisons with predicted cosmic ray intensities.

TABLE 5.1

Volcano Ranch data groups

Number of Showers	Energy quoted by V.R.	"Equivalent H.P. energy"
538	$3.2\ 10^{17} - 6.4\ 10^{17}$ eV	$6.2\ 10^{17} - 1.18\ 10^{18}$ eV
409	$6.4\ 10^{17} - 2.5\ 10^{18}$ eV	$1.18\ 10^{18} - 3.65\ 10^{18}$ eV
90	$> 2.5\ 10^{18}$ eV	$> 3.65\ 10^{18}$ eV

5.1.2 The Haverah Park Array

Haverah Park is situated at latitude 54°N at approximately sea level (1030 g/cm^2). The air shower array covers an area of 11 km^2 and is composed of an inner 500 m array and an outer 2 km array. The 500 m array consists of four detectors, each composed of water Cerenkov tanks of depth 120 cm viewed by photomultipliers (Tennent, 1968). The arrival direction results obtained

in 1963-6 using this array are given by Hollows (1968). During 1967 the Haverah Park array was extended to include a 2 km array composed of six local arrays each of which contains four 13.5 m^2 detectors (Earnshaw et al., 1968). This extended array has been in operation since late 1967. Arrival direction data for the years 1963-70 has been obtained from Lapikens et al (1971) and by private communication. Only showers of zenith angle less than 60° have been included so the data covers declinations + 90° to - 6°.

The following groups of data were used for comparisons with predicted cosmic ray intensities.

TABLE 5.2

Haverah Park data groups

Number of showers	Energy range
2291	$5\ 10^{17}$ - 10^{18} eV
994	10^{18} - $3\ 10^{18}$ eV
172	$3\ 10^{18}$ - 10^{19} eV
29	> 10^{19} eV

5.1.3 The University of Sydney array at Pilliga Forest

Pilliga Forest is at latitude 30.5°S. The array covers an area of 40 km^2 and consists of a number of stations (34 by January 1969) arranged on a square grid. Each station comprises two 6 m^2 liquid scintillator tanks buried 50 m apart, at about 2 m below the surface of the ground.

Arrival direction results (Brownlee et al., 1970 and private communication) cover declinations + 30° to - 90°.

TABLE 5.3

Pilliga Forest data groups

Number of showers	Energy range
682	10^{18} - 10^{19} eV
86	> 10^{19} eV

5.2 Comparison of predicted cosmic ray intensities with experimental measurements

For the purpose of this comparison all these high energy cosmic rays were assumed to be protons (i.e. Z = +1).

Each pathlength contour map was divided into bins of 10° declination by 10° R.A. (15° R.A. for comparison with Haverah Park results) and the average pathlength in each bin was found. This pathlength was taken to be proportional to the intensity of cosmic ray protons and, by allowing for the solid angle contained in each bin, a value proportional to the number of protons of a particular energy expected to reach the Earth within each directional bin was obtained.

The predicted numbers apply to protons of galactic origin. Protons of metagalactic origin would arrive at the Earth isotropically. Of all the protons arriving G% were taken to be of galactic origin with an anisotropy as derived above, while (100 - G)% were taken to be of metagalactic origin arriving isotropically. For each field model and energy a range of values of G from 0 to 100% were used, and in each case a prediction of the number of protons expected in each bin was made to compare with experimental measurements.

In making this comparison it is necessary to take into account the variation with zenith and azimuth angle of the aperture of the air shower array. The aperture depends on the way in which the shower is propagated through the atmosphere and on the geometry of the array, and the exact form of this variation is difficult to obtain. However, if the predicted numbers of showers in all the declination bands are added for each right ascension band, the aperture variation only influences the weighting of the summation. Thus it is not important to know the exact form of the aperture variation if a comparison is made between the distribution in R.A. of the predicted and measured shower numbers. In fact it is possible to use an empirical aperture variation obtained from the observed zenith angle distribution. If an

expression which gives a good fit to the observed zenith angle distribution can be obtained then, assuming a uniform azimuth angle distribution it is possible to deduce a declination distribution. This can be used to give detection probabilities for the conversion of predictions of numbers of protons reaching the Earth in each bin to predictions of the numbers of showers detected by a particular array in each bin. Brownlee (1970) fitted a differential zenith angle distribution of the form $dN = (n+1)N \cos^n\theta \sin\theta \, d\theta$ to the Pilliga Forest data, where N is the number of showers and θ is the zenith angle. For an isotropic zenith distribution and no atmospheric attenuation of air shower muons n is predicted to be 1 giving

$$dN = 2 N\cos\theta \sin\theta \, d\theta.$$

A zenith angle distribution of this form was used in the present calculations to obtain detection probabilities. Despite the fact that Brownlee (1970) finds that the Pilliga Forest results indicate an exponent value of n = 2 over all energy ranges ($\gtrsim 10^{17}$ eV), for the higher energy band ($\gtrsim 5\ 10^{18}$ eV) he obtains $n = 1.0 \pm 1.0$, so that the use of n = 1 is not unreasonable, especially considering that the exact form of aperture variation is unimportant in this context. Hollows (1968) found that the zenith angle distribution of all 30556 showers observed at Haverah Park during 1963-6 could be represented by $P(>\theta) = 0.5\ (\cos^3\theta + \cos^4\theta)\ d\theta$, where $P(>\theta)$ is the probability of a shower arriving at a zenith angle greater than θ. Hollows deduced an expected declination distribution and found that the numbers of showers observed exceeded the predictions for declinations less than $+ 40^\circ$, with a corresponding deficit at larger declinations. This he interpreted as being due to a variation of the aperture of the array with azimuth angle, caused by its tilted position, rather than being the reflection of any large scale cosmic ray anisotropy. For comparisons with Volcano Ranch results the observed declination distribution was used to give detection probabilities.

When the predicted shower number for each 10^{o} x 10^{o} (or 15^{o}) bin had been obtained from a given contour map, for a particular value of G and for comparison with results from a particular array, the numbers corresponding to each declination band were added for each right ascension band to obtain the predicted distribution in R.A. of shower numbers.

Comparisons between predicted and measured R.A. shower number distributions were then made for the combinations shown in table 5.4, after normalizing the total number of predicted showers in each case to the corresponding number of observed showers. Each comparison was made using a range of values of G and a χ^2 test was utilized to obtain the G value that gives the best agreement between prediction and measurement. Figures 5.1, 5.2, 5.3, and 5.4 show plots of χ^2 against G for each of the comparisons made. The numbers refer to those listed in table 5.4. The Haverah Park results for 10^{18} eV to 3 10^{18} eV, were compared with predictions at 10^{18} eV and at 3 10^{18} eV, and those for 3 10^{18} eV to 10^{19} eV were compared with predictions at 3 10^{18} eV and at 10^{19} eV. In all cases the plots of χ^2 against G were very similar for the two prediction energies and those shown represent average values.

The minimum value of χ^2 occurs at the value of G for which there is the closest agreement between prediction and measurement. An upper limit to G is given by that corresponding to a χ^2 probability of 5% (χ^2 = 49.5 for 35 degrees of freedom (i.e. comparisons with Volcano Ranch and Pilliga Forest results) or χ^2 = 35.2 for 23 degrees of freedom (i.e. comparisons with Haverah Park results)). Table 5.4 shows best fit and upper limit (in parenthesis) values of G for each of the groups of data and field models. Negative values of G indicate an anti correlation between prediction and measurement but have no physical meaning. Since at energies greater than about 3 10^{18} eV the effects of field model D are basically the same as those of model B, the best fit and upper limit values of G will be similar for the two models above this energy.

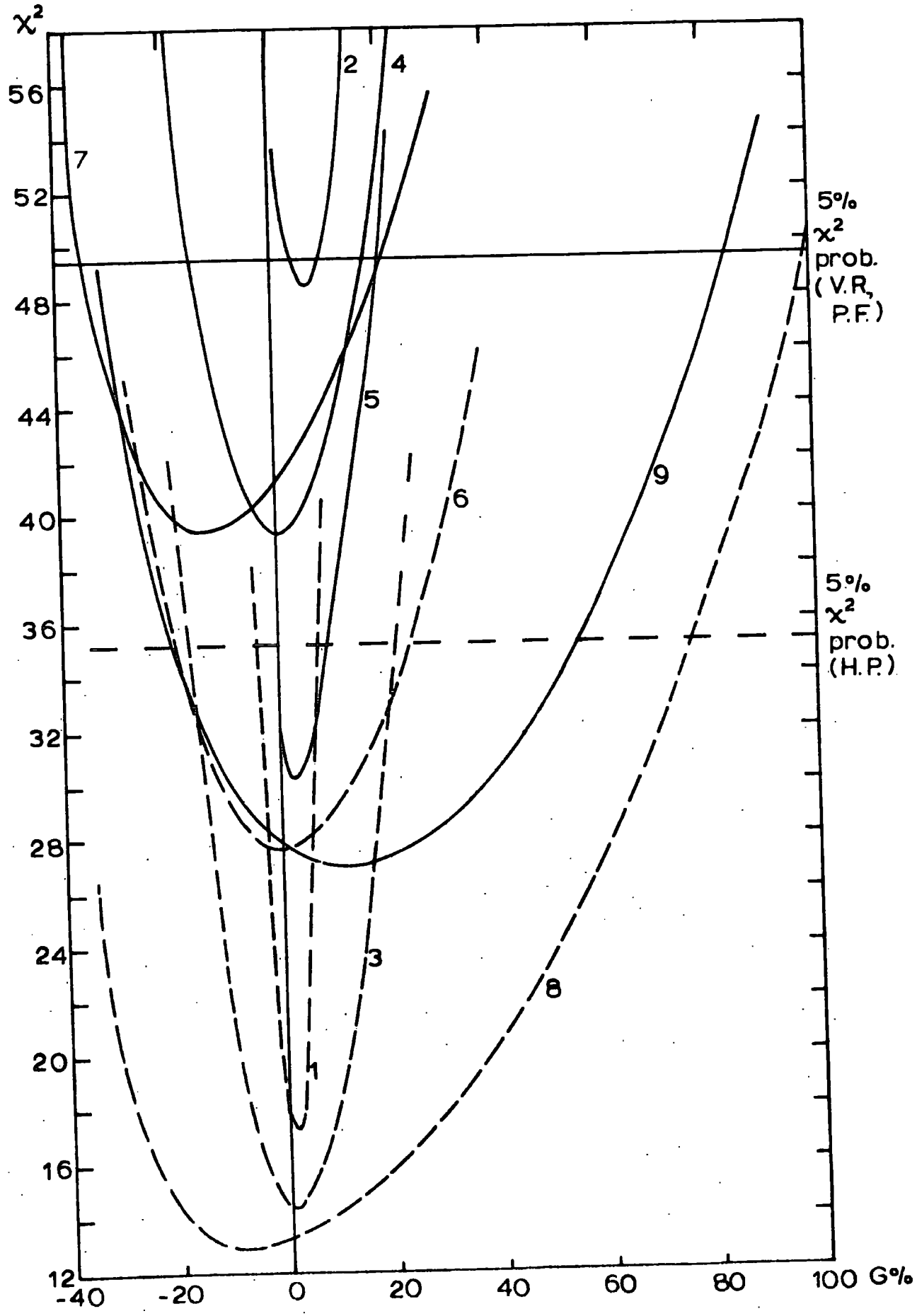

Figure 5.1. Plots of χ^2 against G for the predictions of field model A. Numbers refer to those listed in Table 5.4.

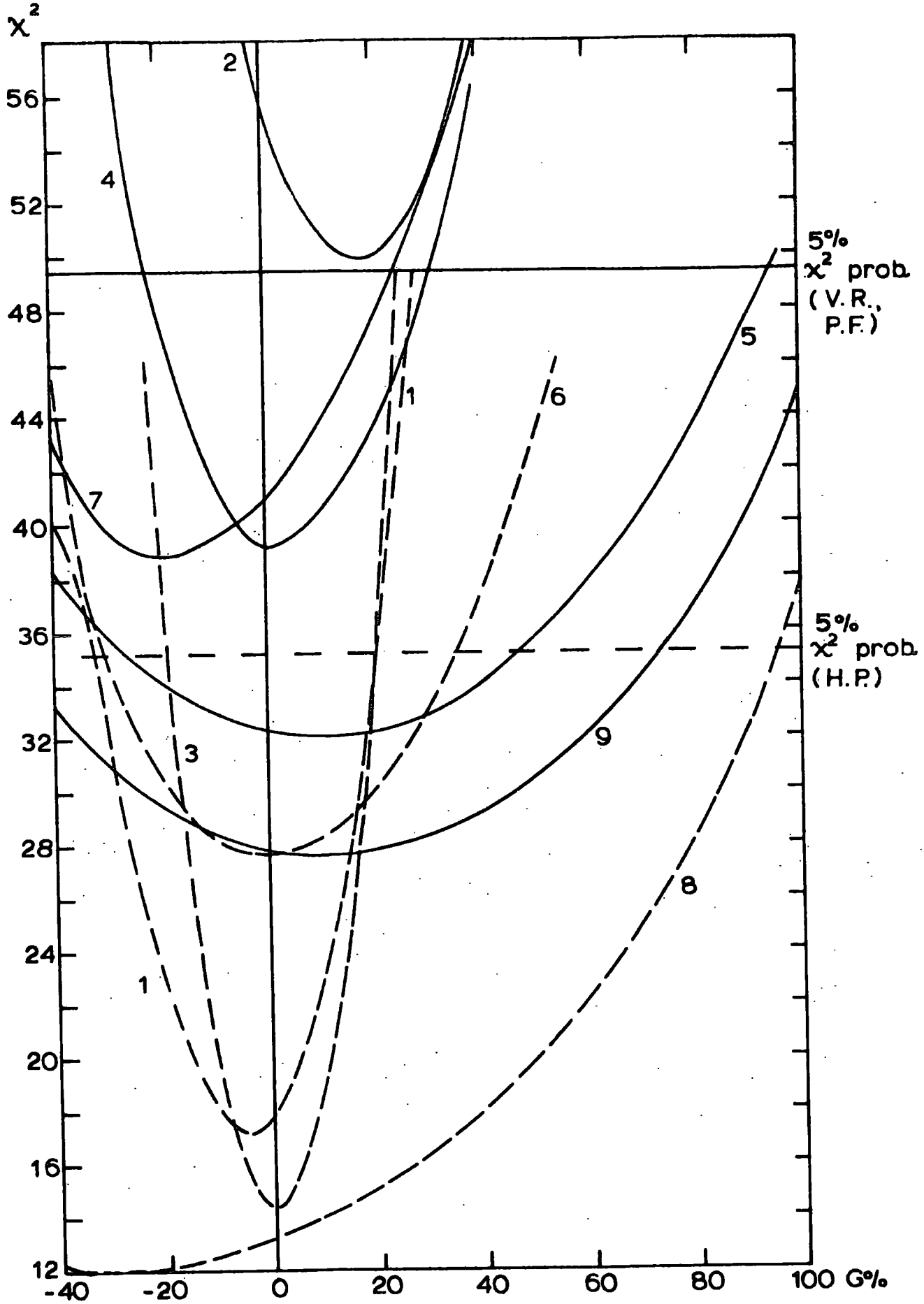

Figure 5.2. Plots of χ^2 against G for the predictions of field model B.

Numbers refer to those listed in Table 5.4.

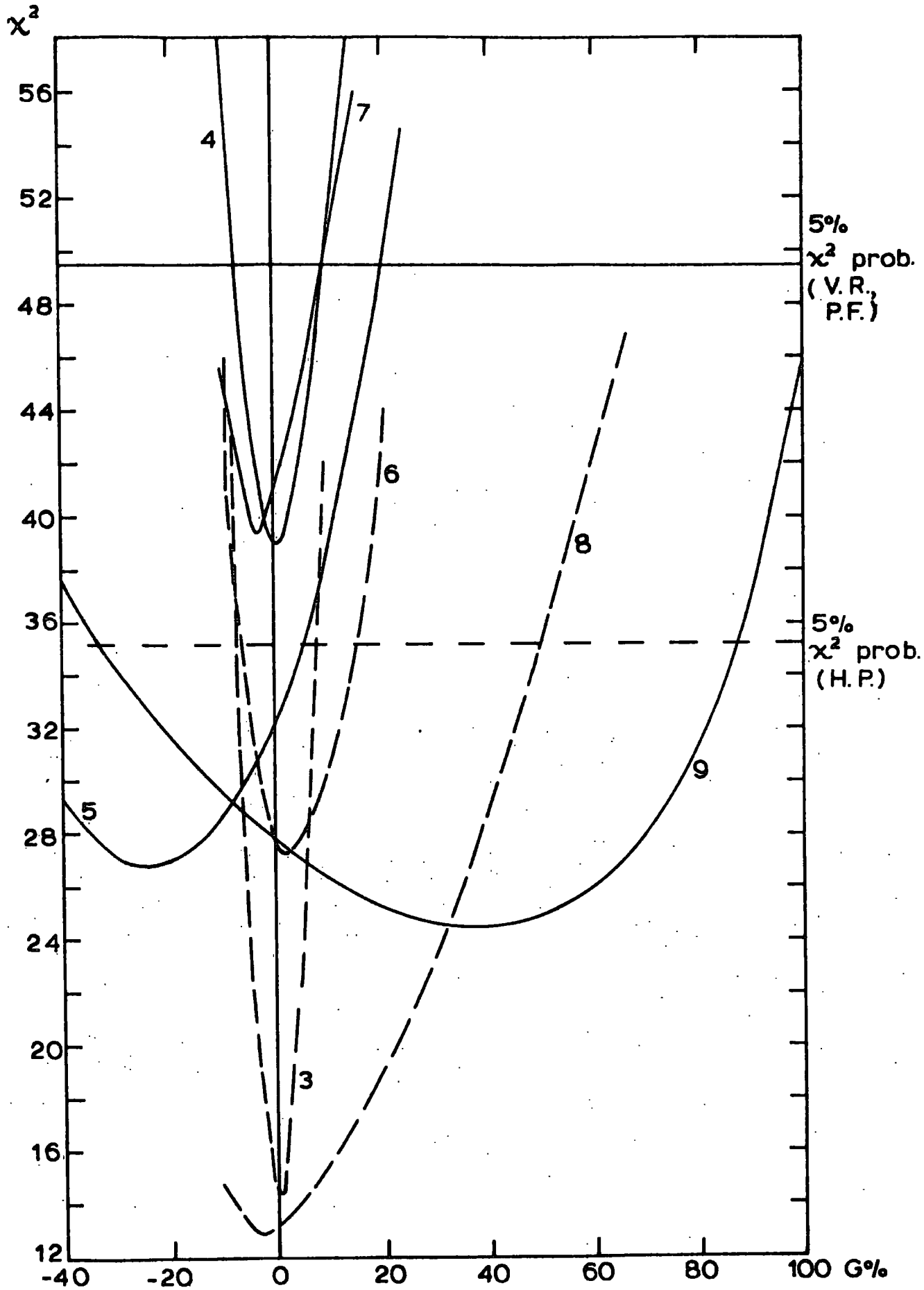

Figure 5.3. Plots of χ^2 against G for the predictions of field model C.

Numbers refer to those listed in Table 5.4.

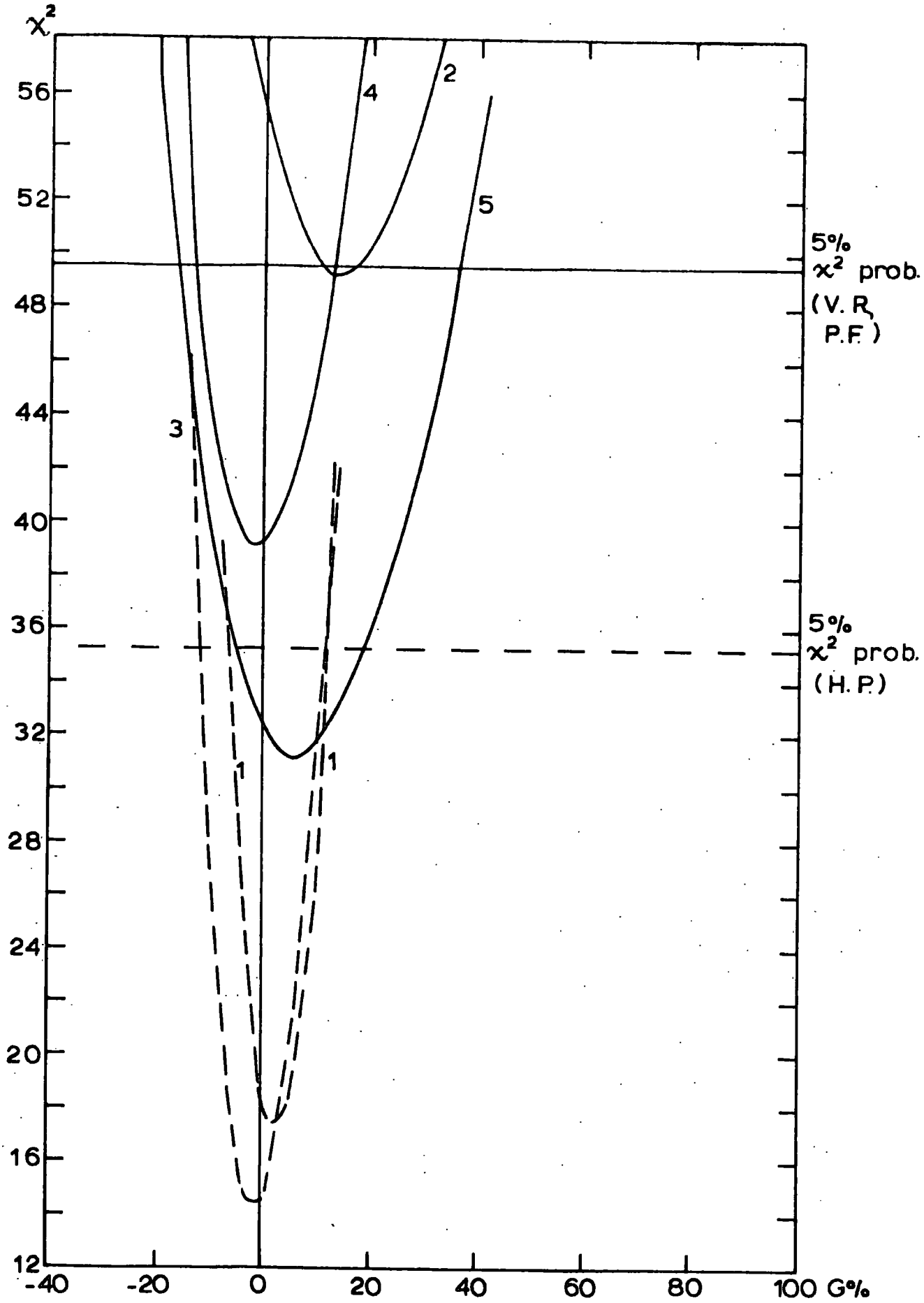

Figure 5.4. Plots of χ^2 against G for the predictions of field model D. Numbers refer to those listed in Table 5.4.

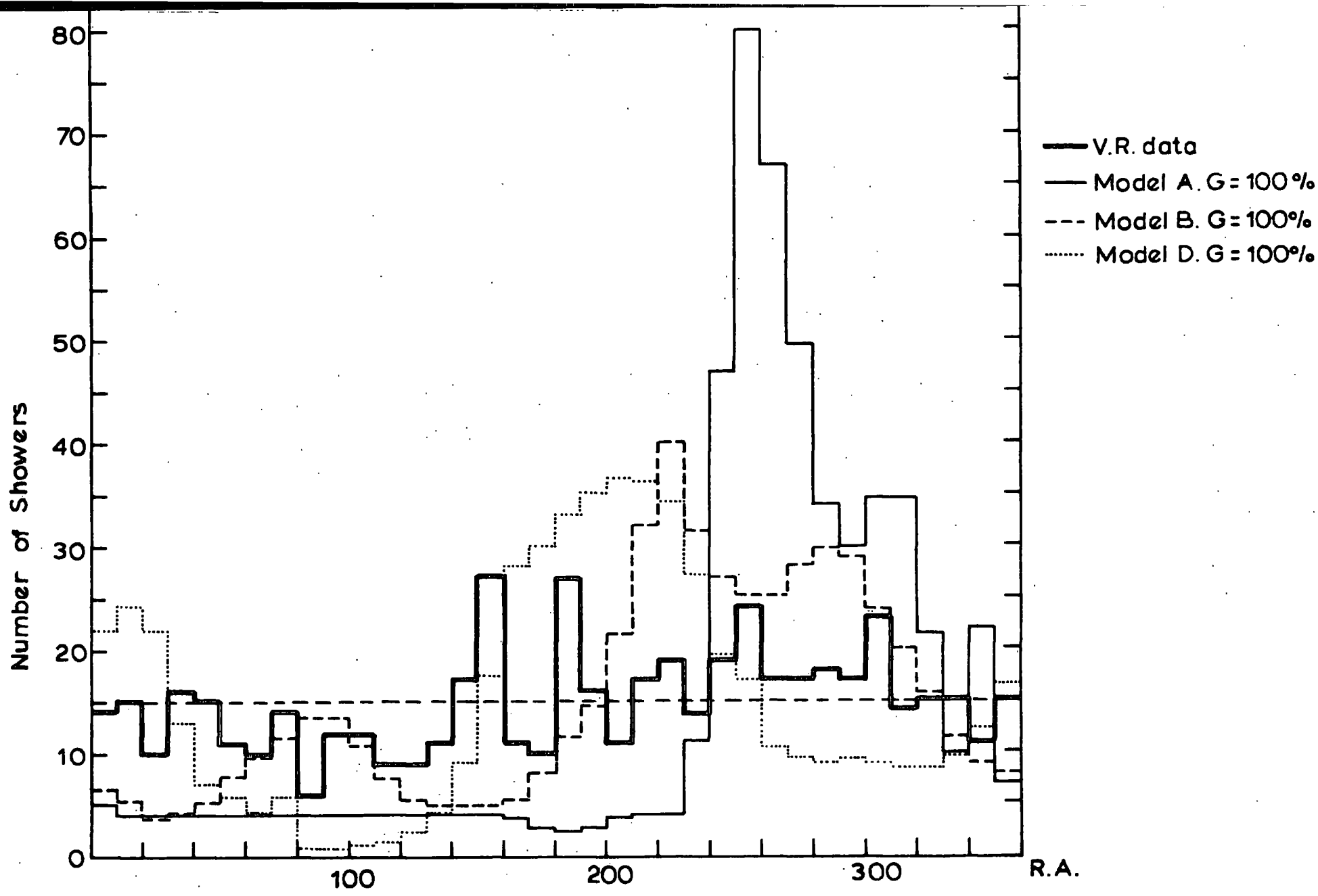

Figure 5.5. Volcano Ranch $6{\cdot}2\ 10^{17}$eV to $1{\cdot}18\ 10^{18}$eV data and corresponding model predictions.

At energies less than about 10^{18} eV field model C predicts very small anisotropies. The pathlength distribution is quite isotropic and by making the assumption that, while the cosmic ray intensity is proportional to pathlength for pathlengths less than 50 kpc, for longer pathlengths there is a uniform intensity, the anisotropy is underestimated. In fact at $8.\ 10^{17}$ eV the predicted galactic component observable at Volcano Ranch and Haverah Park is isotropic. Consequently at these energies field model C would allow a large galactic component. Values of G for field model C were thus only calculated for prediction energies $> 10^{18}$ eV.

The Volcano Ranch results for $6.2\ 10^{17}$ eV to $1.18\ 10^{18}$ eV show little agreement with the predictions of any field model. For field model B the minimum χ^2 occurs outside the 5% χ^2 probability limit ($\chi^2 = 50$) and the minimum χ^2 for the other models are also large (~ 48 for model A and 49 for model D). These results are also inconsistent with the G=0 prediction. This is probably due to the marked anisotropy of the $6.2\ 10^{17}$ eV $\rightarrow$ $1.18\ 10^{18}$ eV Volcano Ranch results.

The recorded shower numbers are below the mean for R.A. 330° to 150° and above the mean for R.A. 150° to 330° (Figure 5.5). However, this anisotropy does not correspond to that predicted by any of the models, thus making χ^2 large. All the other arrival direction measurements are compatible with G=0; that is with no galactic cosmic ray component.

At the higher energies larger upper limits of G are the result of the relatively isotropic predicted intensities. (However the shower numbers are small at the highest energies so that the use of a χ^2 test with 35 (or 23) degrees of freedom may be inappropriate).

In general model B seems to allow the largest galactic component above $\sim\ 10^{18}$ eV. Below this energy models A, B, and D predict small upper limits to G, due to the sharp peaks in the pathlength distributions. It is possible that the addition of an irregular field component, which could have considerable

TABLE 5.4 BEST FIT AND UPPER LIMIT VALUES OF G

Experiment	Energy Range of Measurements eV	Number of showers	Energy of prediction eV	Values of G.%			
				Field A	Field B	Field C	Field D
1 Haverah Park	$5\ 10^{17} \rightarrow 10^{18}$	2291	$6\ 10^{17}$ (Model A) $7.5\ 10^{17}$ (Models B,D)	1(7.5)	-5(20.5)	-	3(12)
2 Volcano Ranch	$6.2\ 10^{17} \rightarrow 1.18\ 10^{18}$	538	$6\ 10^{17}$ (Model A) $7.5\ 10^{17}$ (Models B,D)	6(9)	18(-)	-	14(17)
3 Haverah Park	$10^{18} \rightarrow 3\ 10^{18}$	994	$10^{18} + 3\ 10^{18}$	0(22)	0(20)	0(8.5)	-2(12)
4 Volcano Ranch	$1.18\ 10^{18} \rightarrow 3.65\ 10^{18}$	409	$3\ 10^{18}$	0(17)	1(31)	1(10)	-2(13)
5 Pilliga Forest	$10^{18} \rightarrow 10^{19}$	682	$3\ 10^{18}$	2(20)	10(95)	-25(21)	6(36)
6 Haverah Park	$3\ 10^{18} \rightarrow 10^{19}$	172	$3\ 10^{18} + 10^{19}$	0(24.5)	0(35)	2(16)	-
7 Volcano Ranch	$> 3.65\ 10^{18}$	90	10^{19}	-14(20)	-20(24)	-4(10)	-
8 Haverah Park	$> 10^{19}$	29	10^{19}	-10(75)	-30(96)	-4(51)	-
9 Pilliga Forest	$> 10^{19}$	86	10^{19}	12(84)	10(100)	38(100)	-

effect on the trajectories of protons of energy $\lesssim 10^{18}$ eV, would reduce the magnitude and increase the area of these peaks thus allowing a larger galactic component. The effect of irregularities is considered further in Chapter 6.

The addition of a halo magnetic field of the type mentioned in Chapter 4 has a considerable effect on the pathlength distribution maps below $\sim 3.\ 10^{18}$ eV. Despite this the pathlength distributions are rather non-uniform so that although a halo field would probably remove much of the anisotropy associated with the disc field models this halo model will not produce an isotropic distribution at the Earth, of cosmic rays of galactic origin at the energies considered ($\gtrsim 6\ 10^{17}$ eV). However, it is probable that a larger galactic cosmic ray component would be feasible if there were an extensive halo field.

It is possible that not all high energy cosmic ray particles are protons but that they are of a mixed composition, as at lower energies. To obtain a pathlength (i.e. intensity) distribution for such cosmic rays it is necessary to take a weighted sum of the distributions for a range of values of E/Z. However, as can be seen from the pathlength contour maps, this will not result in an isotropic distribution as the peaks in the distribution occur in approximately the same place for all values of E/Z. If, however, these cosmic rays are all heavy ($Z \geqslant 20$) particles then trapping by the galactic magnetic field could persist up to energies of the order of a few times 10^{18} eV, resulting in an isotropic intensity distribution below this energy.

If the primary particles are all heavy ($Z \geqslant 20$), then the presence of an extensive halo field could give sufficient isotropy in the intensity distributions to allow most of the cosmic rays with energy greater than $\sim 10^{18}$ eV to be of galactic origin. Without these conditions the majority of cosmic rays ($E \geqslant 10^{18}$ eV) would appear to be of metagalactic origin. Despite this it is possible that some of these cosmic rays are of galactic origin and the size of the galactic contribution compatible with the observed isotropic conditions is larger, if the galactic magnetic field has an irregular component. This will be considered in the next chapter.

CHAPTER 6

IRREGULARITIES IN THE GALACTIC MAGNETIC FIELD

6.1 Evidence for the existence of irregularities; their extent and field strength

6.1.1 Introduction

The magnetic field models considered so far assume that the magnetic field in the Galaxy is coherent and regular. However, there is evidence to suggest that this is not the case. For example the observed irregularity in the distribution of stars and clouds of dust and gas in the Galaxy suggests that the magnetic field is also irregular in form. Moreover, whereas Faraday rotation measurements, which give the average line of sight magnetic field, indicate a field $\sim$ 3 μgauss, measurements of synchrotron radiation could indicate larger values, - up to 10 μgauss (Anand et al. 1968b), for the magnetic field at the source of radiation. This would seem to show that there is a random component of the magnetic field.

In the present work a simplified model is taken where the random component is considered as consisting of cells of field, within each of which the field direction is constant but randomly orientated with respect to that of the other cells. In each cell the random field strength is assumed constant.

As far as the trajectories of cosmic ray particles of energy above about 10^{17} eV are concerned, only those irregularities of size greater than $\sim$ 10 pc will have any effect if the field strength is a few microgauss. Irregularities larger than 100 pc constitute a large scale change in field direction and strength. Thus, in this context, irregularities of 10 - 100 pc in extent are of interest.

Some information about the strength of field within the cells, and their sizes can be deduced from various observational results.

Observations of gas clouds suggest that, although there is a spectrum of cloud sizes, typical clouds are of radius 7 pc and are 125 pc apart. (i.e. 8

per kpc in the line of sight) (Spitzer 1968). These measurements indicate the type of values that might be expected for the separations and cloud sizes of polarizing material or material producing Faraday rotation.

Since there is probably some correlation between magnetic field and gas distribution it is not unreasonable to assume that each of these clouds contains a cell of irregular field.

6.1.2 Stellar polarization measurements

Stellar polarization measurements can give information about the size and strength of any irregular component of the magnetic field in regions occupied by dust grains.

Jokipii et al. (1969) considered the variation with distance of the mean stellar polarization and the variance of values about this mean. They predicted that the mean should increase linearly with distance. Defining a correlation length of the interstellar medium, which for the Davis-Greenstein mechanism is the correlation length of field or the distance between the dust clouds, whichever is the greater, they predict that this variance increases as the square of the distance for distances less than the correlation length, and increases linearly with distance for distances very much greater than the correlation length. Using polarization measurements given by Behr (1959) they considered directions approximately parallel or perpendicular to the spiral arm; that is $-25^{\circ} \leqslant b'' \leqslant 25^{\circ}$ and cones about $\ell = 80^{\circ}$, 170°, 260°, 350°. Each cone was divided into radial distance bins containing 10-20 stars to obtain the required variations with distance. From their results Jokipii et al., obtained a correlation length of 150 pc, which seems to correspond to distances between dust clouds (Spitzer, 1968). Consequently it appears that the correlation length of the field is less than this.

An independent analysis of the characteristics of the irregular field has been carried out in the present work, adopting the results of Mathewson and

Ford (1970). Mathewson and Ford plotted the electric vectors of the polarization of light from nearly 7000 stars. Separate plots were made for stars within each of the distance intervals 0-50, 50-100, 100-200, 200-400, 400-600, 600-1000, 1000-2000 and 2000 to 4000 pc. Mathewson and Ford interpreted these plots on the basis of their helical plus longitudinal model, to show that the extent of the helical component is about 600 pc. However, the helical field can be considered as a large scale irregularity and the polarization measurements can also give information about the smaller irregularities, if the distribution of the polarizing dust grains is known. In fact this is not well known but an approximation can be used and will be sufficiently accurate in this context. The electric vectors represent the component of the magnetic field perpendicular to the line of sight and they were plotted, by Mathewson and Ford, so that the lengths were proportional to the percentage polarization. If the total magnetic field is assumed to consist of a coherent field directed along the spiral arm, together with a randomly directed field, then in the direction of the local spiral arm, the amount of polarization indicates the mean strength between the star and the Earth, of the irregular magnetic field. However, perpendicular to the arm direction (in the galactic plane) the amount of polarization gives the strength of the coherent magnetic field.

It is assumed that the dust clouds are randomly separated with a mean separation L_s, and that the magnetic field within each cloud is uniform but randomly orientated with respect to that in all other clouds.

If f is the polarization produced per unit distance per unit field squared per unit dust density, then, if the field is sufficiently weak for the dust grains not to be completely aligned, the polarization produced by a single cell will be

$$P_i = f\rho L_c H_p^2 \quad \text{(Davis and Greenstein, 1951)}$$

where ρ is the mean grain density in a field cell (dust cloud) of length L_c and H_p is the field perpendicular to the line of sight.

In the direction of the arm only the irregular field contributes to the polarization. Adding the values of P_i vectorially, the resultant polarization

$$P_R = P_i \sqrt{N} \qquad \text{where N is the number of polarizing cells.}$$

Thus $P_R = P_i \sqrt{\frac{d}{L_s}}$ where d is the distance to the star. Hence

$$P_R = f \rho_o L_c \sqrt{\frac{d}{L_s}} \left(0{\cdot}7855\, H_R\right)^2$$ where H_R is the mean strength of the random field component and ρ_o is the grain density in clouds along the arm (assumed to be constant). Perpendicular to the spiral arms the coherent field produces a resultant polarization

$$P_c = f \frac{L_c}{L_s} \int_o^d \rho \left(X - X_\Theta, Y = Y_\Theta, Z = Z_\Theta\right) \cdot H_c^2 \left(X - X_\Theta, Y = Y_\Theta, Z = Z_\Theta\right) d(X - X_\Theta)$$

where X_Θ, Y_Θ and Z_Θ are the values of X, Y and Z at the Sun, and H_c is the coherent field strength. If the dust grain density falls off in the same way as the coherent field

$$\rho(X - X_\Theta, Y = Y_\Theta, Z = Z_\Theta) \propto H_c (X - X_\Theta, Y = Y_\Theta, Z = Z_\Theta)$$

Thus

$$P_c = \frac{f\rho_o}{H_c(0)} \frac{L_c}{L_s} \int_o^d H_c^3 (X - X_\Theta, Y = Y_\Theta, Z = Z_\Theta)\, d(X - X_\Theta)$$

where $H_c(0)$ is the value of H_c on the arm axis at $Y = Y_\Theta$, $Z = Z_\Theta$.

Using these expressions for P_R and P_c, and by considering stars at various distances and measuring the polarization of the light from those in the direction of the spiral arm and of those in the directions perpendicular to it(in the galactic plane) information about the random field component can be obtained.

Taking directions $-20^\circ \leqslant b'' \leqslant 20^\circ$ with $60^\circ \leqslant \ell \leqslant 90^\circ$ and $270^\circ \leqslant \ell \leqslant 300^\circ$ as being along the spiral arm, and directions $-20^\circ \leqslant b'' \leqslant 20^\circ$ with $-20^\circ \leqslant \ell \leqslant 10^\circ$ and $160^\circ \leqslant \ell \leqslant 190^\circ$ as being perpendicular to it, median values of P_R and P_c were

found from the data of Mathewson and Ford (1970), for stars in each of their distance ranges (0-50, 50-100, 100-200, 200-400, 400-600, 600-1000 pc).

Plots of these median values of the polarization versus distance for the two sets of directions are shown in figures 6.1 and 6.2. The errors show the range within which half the values lie.

Using the least squares method of fitting the measured values of P_c to those predicted by the expression above, it was found that

$$p_o \frac{L_c}{L_s} = 6{\cdot}24 \cdot 10^{-5} \text{ pc}^{-1} \mu G^{-2} \%.$$

So $P_R = 3{\cdot}85 \cdot 10^{-5} \sqrt{L_s}\ H_R^2 \sqrt{d}\ \%.$

Again using the least squares method to fit measured values of P_R to those predicted above it was found that

$$\sqrt{L_s}\ H_R^2 = 364 \text{ pc}^{\frac{1}{2}} \mu G^2.$$

If it is assumed that in any region $H_R = aH_c$ where a is constant, then using $H_c \simeq 6\mu G$ for the region near the spiral arm

$$a^2 \sqrt{L_s} \simeq 10 \text{ pc}^{\frac{1}{2}}$$

Taking $L_s \sim 100$ pc as is indicated by the dust cloud separations, this gives $a = 1{\cdot}0$. Thus it would seem that the mean random and mean coherent fields are approximately equal in magnitude.

6.1.3 Faraday rotation measurements: Pulsars

Further information about the extent and strength of magnetic field irregularities can be obtained from the measurement of the Faraday rotation of the polarized radiation from Pulsars. These measurements sample the field in the regions occupied by electrons.

As mentioned in 2.5.5. such measurements seem to indicate a longitudinal field directed along the local spiral arm towards galactic longitude $\ell = 90^\circ$.

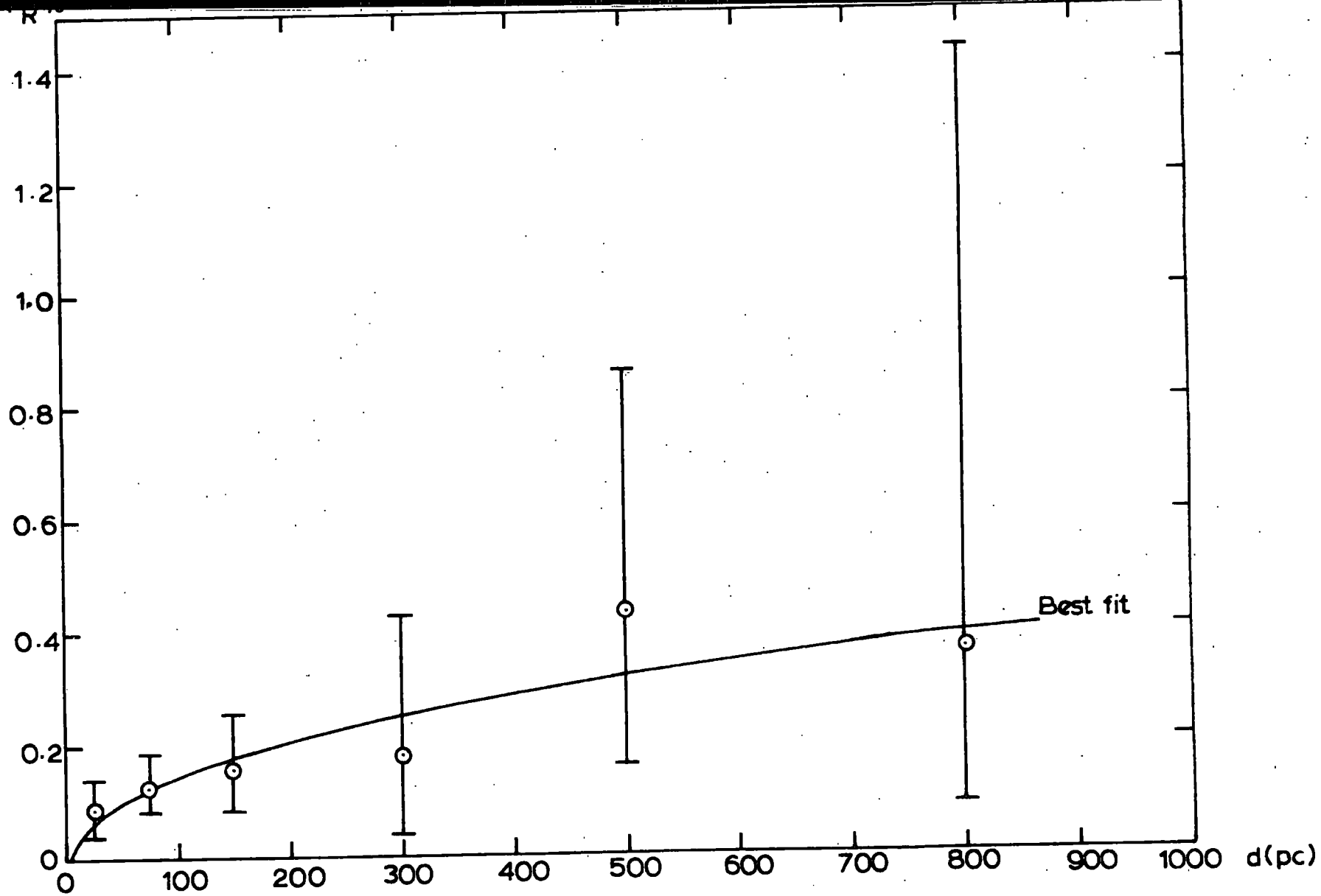

Figure 6.1. Median values of stellar polarization measurements along the spiral arm axis.

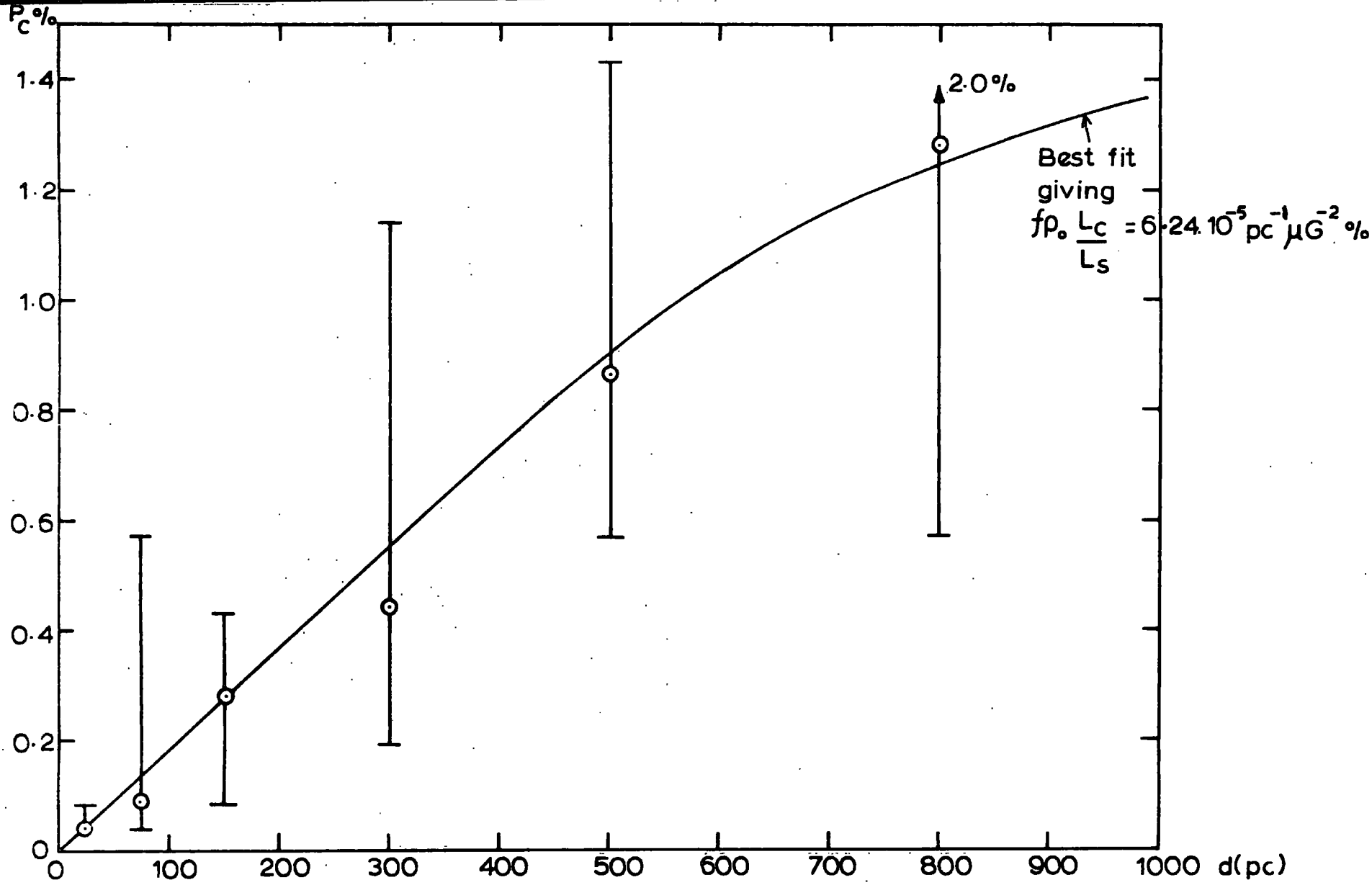

Figure 6.2 Median values of stellar polarization measurements perpendicular to the spiral arm axis

A comparison between the measured line of sight magnetic fields to 21 pulsars and the values expected from various coherent field models was carried out as described in 3.2. This comparison appears to show that the measurements are compatible with a longitudinal coherent field with a structure similar to that of either model A or model D. However, these models predict field strengths rather larger than the measured line of sight values and it was found that the measurements were best fitted if

$$H_A = 1{\cdot}69 \times \text{measured } \bar{H}_\ell$$

$$H_D = 1{\cdot}95 \times \text{measured } \bar{H}_\ell$$

where H_A and H_D are the values predicted by models A and D respectively for the mean line of sight field to the pulsar $\bar{H}_\ell$ That is the field strengths predicted by these models are approximately twice as large as those indicated by Faraday rotation of the radiation from pulsars. It may be that the fields that models A and D predict are too strong but this would not be very important so far as the trajectory calculations are concerned as it only involves a shift in energy. Predictions made from model A or D, for a particle of energy E, apply to an energy E/2 if the coherent longitudinal field strength is half that of the model value.

In this attempt to derive approximate information about field irregularities attention was confined to model D. However similar results would be obtained from the model A values. Figure 6.3 shows the amount of correlation between the line of sight component of the coherent field ($H_{CL} = H_{D/2}$) and the measured field strengths (H_{exp} = measured $\bar{H}_\ell$).

If only the coherent field is present and this model is a good representation of the coherent field, then all the values should lie on the line $H_{CL} = H_{exp}$. However, if an irregular field is also present it will cause scattering in the values of the predicted field. By applying a χ^2 test to the

Figure 6.3. Relation between predicted $\bar{H}_{\ell}$ to pulsars ($H_{CL} = H_{D/2}$) and observed values (H_{exp})

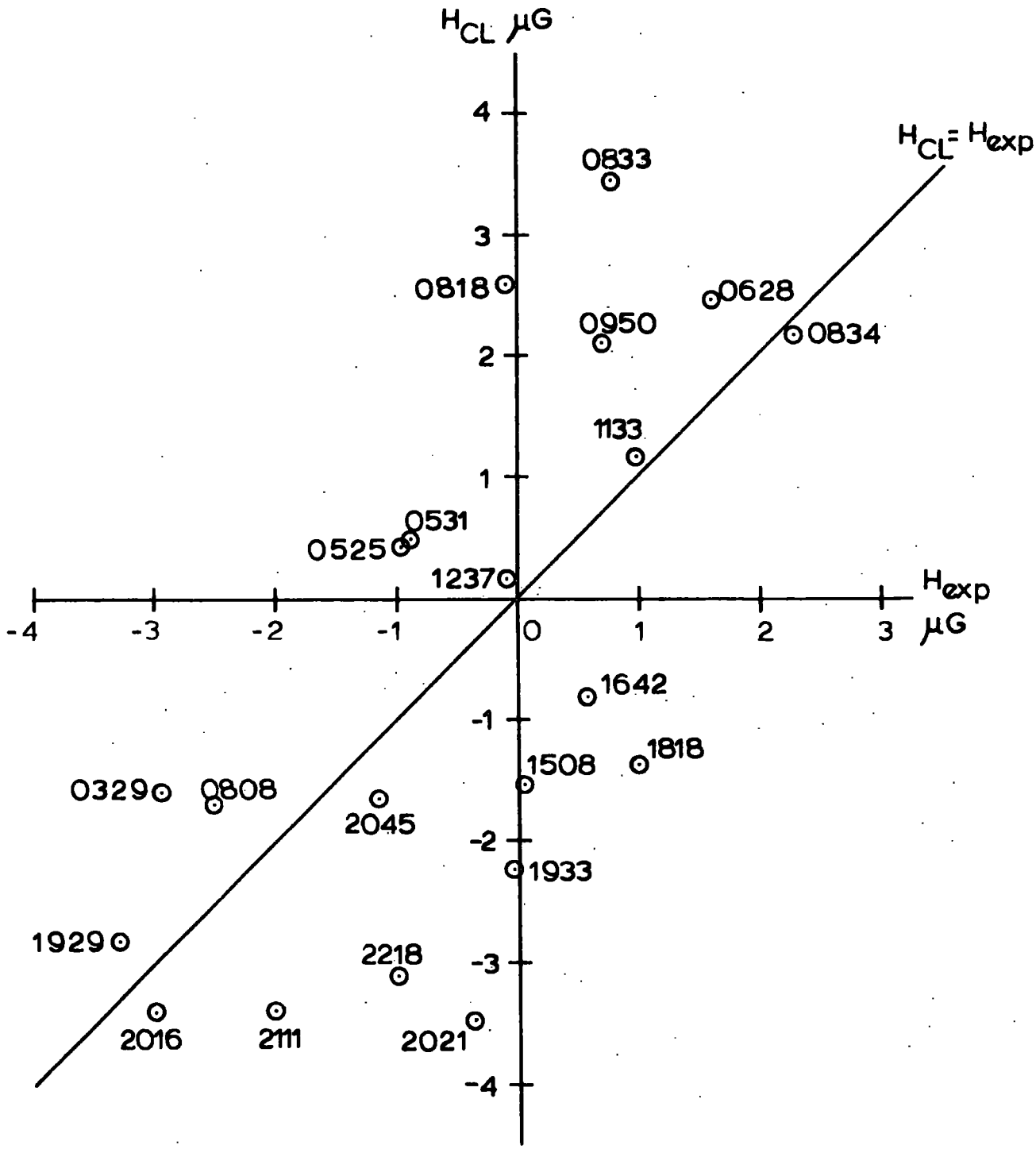

distribution of H_{CL} values about the line $H_{CL} = H_{exp}$, it is possible to find an upper limit to the strength of the irregular field consistent with Faraday rotation measurements.

Consider an electron distribution such that the irregular field is sampled by clouds of electrons of mean separation L_s. Assume each cloud contains a magnetic field which is uniform in the cloud but that different clouds have fields which are randomly orientated. The irregular field strength is related to the coherent field strength at any point by

$$H_R = aH_c, \text{ where a is a constant.}$$

The average line of sight component of the magnetic field to a pulsar at a distance d is then given by

$$H_{CL} \left(1 \pm 0{\cdot}886\ a \sqrt{\frac{L_s}{d}} \right)$$

For more distant pulsars this value approximates to H_{CL}. For a single pulsar, i,

$$\chi_i^2 = \left(\frac{H_{CL} - H_{exp}}{\sigma} \right)^2$$

where $\sigma = 0{\cdot}886\ a\ H_{CL} \sqrt{\frac{L_s}{d}}$

If values of H_{CL}, H_{exp} and σ are obtained for M pulsars the total $\chi^2 = \sum_{i=1}^{M} \chi_i^2$ and the most probable value of this occurs at $\chi^2 = M - 1$ (the number of degrees of freedom)

$$\chi^2 = \left(\frac{1}{0{\cdot}886\ a \sqrt{L_s}} \right)^2 \sum_i \left(\frac{(H_{CL} - H_{exp})}{H_{CL}} \quad d^{\frac{1}{2}} \right)_i^2$$

$$= \frac{1}{(a \sqrt{L_s})^2} \sum_i \omega_i^2$$

TABLE 6.1

(The convention used is that the field is negative if it is directed away from the observer)

Pulsar	H_{CL} μG	H_{exp} μG	d pc	ω^2 pc	
0329	-1.61	-2.93	435	371	
0525	+0.42	-0.96	800	10981	X
0531	+0.45	-0.92	810	9679	X
0628	+2.44	+1.6	560	85	
0808	-1.71	-2.5	100	27	
0818	+2.59	-0.08	665	900	
0833	+3.45	+0.8	810	609	
0834	+2.14	+2.3	215	23	
0950	+2.08	+0.7	55	31	
1133	+1.15	+0.99	85	2	
1237	+0.16	+0.07	155	64	
1508	-1.56	+0.05	320	434	X
1642	-0.80	+0.58	580	2205	X
1818	-1.39	+1.00	1370	5150	X
1929	-2.84	-3.3	65	2	
1933	-2.24	-0.015	2570	3230	X
2016	-3.41	-3.0	235	4	
2021	-3.49	-0.36	369	378	
2045	-1.65	-1.15	190	22	
2111	-3.42	-2.00	1620	381	
2218	-3.12	-1.0	705	415	

The sources of H_{exp} are given in Table 2.4, and the values of H_{CL} and d were calculated as described in 3.2.

Thus taking the measured values of H_{exp}, and the calculated values of H_{CL} and d, it is possible to find $\sum_i \omega_i^2$, and setting $\chi^2 = M - 1$, a value for $a\sqrt{L_s}$.

However, this is assuming that the coherent magnetic field between the Earth and the pulsars is fairly constant. In a direction perpendicular to the local spiral arm, in the galactic plane, the model D field falls off rapidly, so for pulsars in this direction at large distances from the arm, H_{CL} is much smaller than it would be in a uniform field. Thus σ is small and these pulsars contribute far more to the value of χ^2 than they would for a more constant H_c. For this reason pulsars 0525, 0531, 1642, 1818 and 1933 were not included in the χ^2 calculation. Pulsar 1508, which lies out of the galactic plane, was also rejected. (see figure 6.4).

From these values and taking $M - 1 = 14$, it was found that $a\sqrt{L_s} = 15\ pc^{\frac{1}{2}}$. However, not all the spread of the values about $H_{CL} = H_{exp}$ may be the result of field irregularities. There may be large intrinsic Faraday rotations associated with the pulsars or the coherent field model used may give incorrect coherent field directions. Thus the value of $a\sqrt{L_s}$ is an upper limit.

$$a\sqrt{L_s} \leq 15\ pc^{\frac{1}{2}}.$$

6.1.4 Faraday rotation measurements: Extragalactic sources

Jokipii and Lerche (1969) have studied the rotation measures of radiation from extragalactic sources in an attempt to derive information about field irregularities. They derive an expression for the variance, σ_R^2, of rotation measures along a certain path, the form of which depends on whether the correlation length of the rotating material, L_s, is less than or greater than the distance to the edge of the Galaxy in the direction of the source.

Hence they deduce that if

$T \gg L_s$, $|\sin b''|\sigma_R^2$ should be independent of galactic latitude, but if

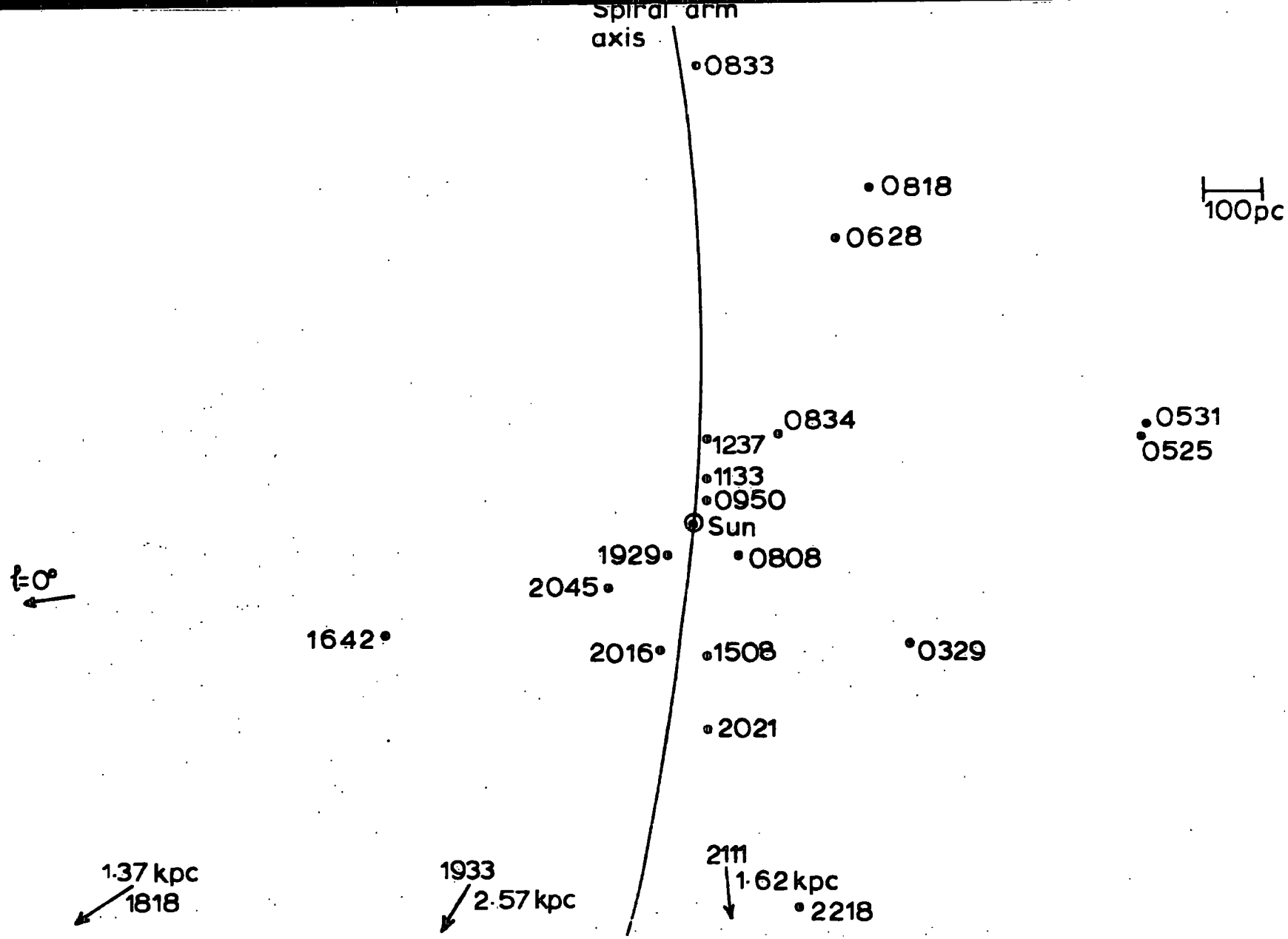

Figure 6.4. Positions of pulsars projected onto the galactic plane. N_e = 0.062 cm^{-3}

$T \sim L_s$, $|\sin b''|/\sigma_R^2$ should decrease with increasing latitude, where T is the thickness of the galactic disc. In each latitude band

$$\sigma_R^2 = \frac{1}{n-1} \sum (R_E - \langle R_E \rangle)^2$$

where n is the number of sources and $\langle R_E \rangle$ is the mean value in that band of the rotation measures R_E. Using 79 rotation measures given by Berge and Seielstad (1967), they then reach the conclusion that $L_s \sim T$.

This work has been updated by Osborne (private communication) who used the more recent data of Mitton (1972) (176 rotation measures). In these calculations he replaced $\langle R_E \rangle$ by R_p, the rotation measure predicted by a coherent field model. To obtain these predicted values Osborne used field models A and D and the three electron density distributions N_e1, N_e2 and N_e3 defined in 3.2. Before calculation of σ_R^2 the predicted values were approximately normalized to the measured values. An attempt was also made to eliminate sources with large intrinsic rotation measures by deleting all those with rotation measures more than 2.5 standard deviations above the mean in each latitude bin.

However, even with these adjustments a value of $L_s \sim T$ was not found to be unreasonable. That is $L_s \sim 250$ pc. This value is larger than the values obtained above, but since these calculations do not allow for discrete clouds of electrons and there are difficulties in eliminating the intrinsic rotations this is not surprising.

6.1.5 Conclusions

It appears that the galactic magnetic field measurements are not inconsistent with the presence of an irregular field. From measurements of the polarization of starlight $a^2\sqrt{L_s} = 10\ \mathrm{pc}^{\frac{1}{2}}$. The Faraday rotation measures of extragalactic radio sources give $L_s \sim 250$ pc, while those of pulsars suggest $a\sqrt{L_s} \leq 15\ \mathrm{pc}^{\frac{1}{2}}$.

Thus, in conclusion, it seems likely that a $\sim$ 1 and $L_s \sim 150$ pc. This value of a is not inconsistent with the synchrotron results.

Consequently a reasonable representation of the irregular field would appear to be one with 10 pc cells each containing a uniform field with strength similar to the coherent field but with random direction.

These cells, which are probably correlated with the dust and ionized gas distribution, would seem to be $\sim$ 100 pc apart. However, it is unlikely that the field is regular in the region between the dust and gas clouds. Thus, in an attempt to find an upper limit to the effect of the random component on cosmic ray trajectories, it has been assumed that the irregular field has the same form everywhere and consists of adjacent 10 pc cells of randomly directed field. In these cells the irregular field strength is equal to that of the coherent field at the same place.

6.2 Effect of irregularities in the magnetic field on particle trajectories and anisotropies

6.2.1 Calculation of trajectories

Trajectories were calculated for particles arriving at the Earth after travelling through an irregular magnetic field. In fact the trajectories of antiparticles, of given energy, starting from the Earth in particular directions were followed, until the particles left the galactic disc ($|z| > 0{\cdot}3$ kpc). For these calculations the basic coherent fields used were those of model A and model D. Added to this was an irregular field, which was reset at distance intervals of length L_c along each trajectory; the direction being chosen randomly, and the strength taken as aH_c, where H_c was the coherent field strength at the beginning of the irregular segment.

For each trajectory the pathlength to the edge of the galactic disc was found. Assuming a uniform distribution of cosmic ray sources in the disc,

the intensity of cosmic rays from a given direction is proportional to their pathlength in the disc. However, if a random field is present, then all the particles arriving in a particular direction, that is within a small solid angle $\delta\Omega$, will not have followed the same trajectory so that the cosmic ray intensity in that direction is represented, not by the pathlength of a single trajectory, but by the mean pathlength of several trajectories. In this case four trajectories were followed in each direction.

To find the effect of the random field on the anisotropy of cosmic rays arriving at the Earth, it is desirable to find the predicted intensities in as many directions as possible. In practice it was only feasible to follow trajectories in 25 directions. The directions were chosen to give a fairly uniform cover of the galactic latitude-longitude sphere, including directions near the pathlength maxima.

TABLE 6.2

Directions of trajectories calculated using an irregular magnetic field.

Galactic latitude	αc (galactic longitude $-173{\cdot}5^\circ$)	W(see 6.2.2)
$\pm 75^\circ$	0°	1
$\pm 45^\circ$	0°, 90°, 180°, 270°	1
$\pm 15^\circ$	0°, 72°, 144°, 216°, 288°	0·75
0°	36°, 108°, 180°, 252°, 324°	0·50

6.2.2 Anisotropies

An attempt was made to find the effect of the addition of an irregular field component with L_c = 10pc and a = 1, to the coherent field models A and D, on the predicted anisotropies of cosmic rays reaching the Earth. Calculations were made of pathlengths at several values of E/Z from 10^{19} eV to 6.10^{17}eV.

Initially an anisotropy coefficient A_n was defined such that maximum anisotropy or complete isotropy would be indicated by $A_n = 1$ or 0 respectively.

The pathlengths, ℓ, were calculated in the twenty five directions listed in Table 6.2 and weighted by factors W (shown in Table 6.2) to give equal representation to approximately equal areas of the galactic latitude-longitude sphere. Then

$$A_n = \frac{\sum_{i=1}^{25} |W_i(\ell_i - \bar{\ell})|}{1.9\, n_{\omega t}\, \bar{\ell}}$$

where $\bar{\ell} = \frac{\Sigma_i W_i \ell_i}{n_{\omega t}}$ and $n_{\omega t} = 20$

Each ℓ_i was the mean of the four pathlengths calculated in a particular direction. However it was found that the spread of these four values about their mean was sufficiently wide to produce a large noise ($\simeq A_n$ at $E/Z \lesssim 2.10^{18}$eV) in the calculated values of A_n.

This noise would mean that the calculated A_n could never fall below 0·1, that is indicate isotropy (which would be compatible with measurements of E.A.S.), however strong the random component. To reduce the noise it would be necessary to increase considerably the number of trajectories calculated in each direction. This was not practicable. Thus it would not seem possible to determine the anisotropies directly by this method.

However, it is possible to derive values for G, the percentage galactic component of cosmic rays compatible with the isotropic E.A.S. results, by relating pathlengths in the coherent field only to the corresponding pathlengths in the coherent field plus random field. Suppose it is possible to relate pathlengths calculated using the random plus coherent field, ℓ_R, to those

calculated using a coherent field only, ℓ_c, by $\ell_{R_i} = s\ell_{c_i} + t$ where s and t are constants for a given coherent field model and E/Z. Then the resulting cosmic ray intensity from a given direction, for the coherent plus random field model, can be considered as consisting of an isotropic component proportional to t and an anisotropic component proportional to $s\ell_{c_i}$. Thus for a given field model and E/Z, $(s\,\bar{\ell}_c)/(\bar{\ell}_R)$ gives a dilution factor D by which the anisotropy is reduced by the addition of a random field component.

$$\bar{\ell}_c = \frac{\Sigma_i W_i \ell_{c_i}}{20} \quad ; \quad \bar{\ell}_R = \frac{\Sigma_i W_i \ell_{R_i}}{20}$$

Then $G' = \frac{G}{D}$ where G' corresponds to the coherent + random field model.

Values of s and t were calculated using the least squares fitting method for field models A and D at energies from 6 10^{17} eV to 10^{19} eV. The values of 1/D found are listed in Table 6.3.

TABLE 6.3

1/D

E/Z eV	Field model D	Field model A
10^{19}	1·05 ± 0·02	1·04 ± 0·14
3 10^{18}	1·14 ± 0·13	1·24 ± 0·20
2 10^{18}	2·14 ± 0·34	-
10^{18}	2·73 ± 0·86	1·72 ± 0·36
8 10^{17}	5·26 ± 2·44	1·49 ± 0·13
6 10^{17}	-	2·09 ± 0·48

In an attempt to derive an absolute upper limit of G' the upper limits of 1/D were combined with the 5% χ^2 probability values of G. The resulting values of G', for protons, are shown in figures 6.5 and 6.6. These figures indicate the maximum percentage of cosmic rays that could be of galactic origin if the coherent plus random field configurations adopted are reasonable

Figure 6.5. Upper limits to G' (Protons). Field model A.

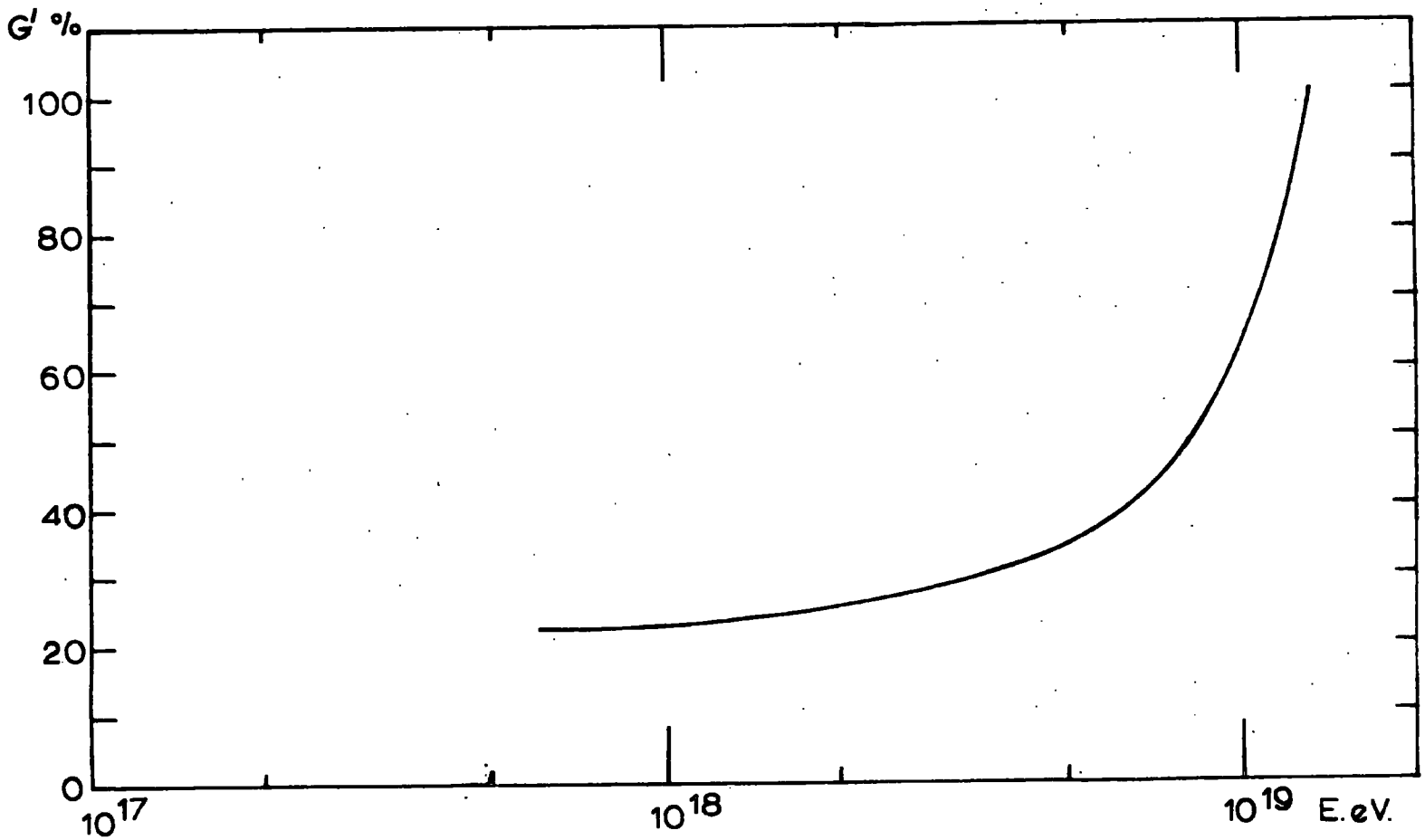

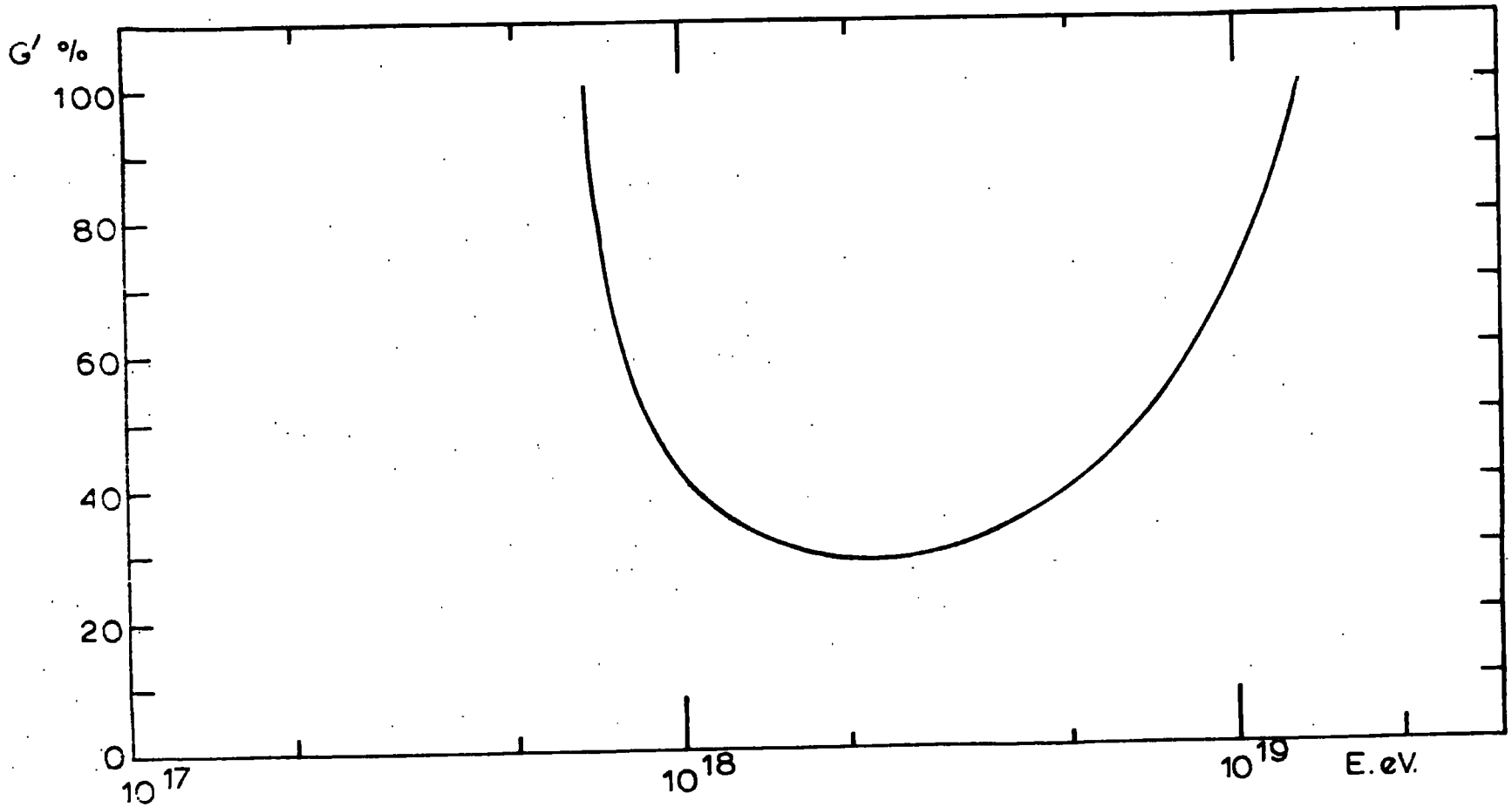

Figure 6.6. Upper limits to G´(protons) Field model D.

representations of the galactic magnetic field, and if these cosmic rays are all protons.

Thus for model D the bulk of cosmic rays of energy less than $\sim 6.\ 10^{17}$ eV could be of galactic origin, if they are protons, without causing a detectable anisotropy. Above this energy some must be of metagalactic origin. For model A the position is not quite so clear, as the calculations do not extend to sufficiently low energies to enable this limiting energy, E_L, to be determined. However, it is very probable that it occurs at about 10^{17} eV. Since the irregular field component configuration used probably produces a greater effect on the trajectories than the actual irregular field does on the cosmic rays, these values of E_L are upper limits to the possible extent of total galactic origin if the primaries are protons. For heavy primaries, the limiting energy increases to $\sim Z.\ E_L$, so that for model D it is possible for Z to be sufficiently large to allow all the particles to be of galactic origin without producing observable anisotropies. Thus the addition of irregularities to the coherent field models considerably reduces predicted cosmic ray anisotropies, and if the galactic field is accurately represented by field model D and the primaries are heavy, this reduction may be sufficiently large to allow compatibility between predictions for complete galactic origin and the measured extensive air shower isotropies.

CHAPTER 7

CONCLUSIONS

From the results of the various astronomical methods of measurement it is possible to deduce the strength and possible configurations of the galactic magnetic field. However, the measurements are somewhat ambiguous and have been interpreted, by different authors, to give four different basic field configurations. The longitudinal model suggested by Thielheim and Langhoff (1968) was initially based on a few extragalactic Faraday rotation measures. Although this model, which proposes a reversal of field direction about the galactic plane would seem to be incompatible with pulsar Faraday rotation measurements this is not the case if the Sun is situated sufficiently far below the galactic plane. A completely helical galactic field, such as suggested by Mathewson (1968), is in agreement with stellar polarization measurements and not incompatible with measurements of the Faraday rotation of radiation from extragalactic sources. However, the helical configuration is more likely to be just a local perturbation of a longitudinal field model (Mathewson and Ford, 1970).

Manchester (1972) interpreted his measurements of pulsar Faraday rotations as being consistent with a simple longitudinal field with no reversal of direction about the galactic plane. It would appear from a combination of all the evidence that the galactic magnetic field is most likely to be of a longitudinal type with the field directed along the local spiral arm towards $\ell = 90^{\circ}$. However, it is not possible to rule out a reversal of field direction above the galactic plane and there may be a local perturbation in the field, possibly of a helical nature. To cover all these possibilities field models A, B, C and D were developed, although models A and D are regarded as the more likely representations of the galactic field.

It is almost certain that the galactic field is not as regular as these models suggest but also contains small scale irregularities. If there is correlation

between the distributions of dust and gas and the magnetic field, then it is possible to assume that the largest magnetic field anomalies are associated with clouds of gas. Consequently it seems that these anomalies can be represented by 10 pc cells of randomly directed field approximately 100 pc apart superimposed upon the coherent field. Within each cell the field strength would appear to be about the same as that of the coherent field at the same point. However, the magnetic field is almost certainly not completely regular in the regions between the dust and gas clouds but no information can be obtained about the field here. An upper limit to the possible irregularity is given by a model in which the cells of irregular field described above exist in all regions occupied by the coherent field. The adopted (extreme) model for the irregular field component is thus one in which the irregular field changes direction every 10 pc and has a strength equal to that of the coherent field at any point.

It is not possible to completely rule out the possibility that, as well as the disc magnetic field, there is also a field in the galactic halo. However, the existence of an ordered galactic halo field appears unlikely.

Assuming that the adopted field models are reasonable representations of the galactic magnetic field it is possible to deduce the effect of this field on cosmic ray trajectories, and hence find the variation of intensity with arrival direction at the Earth for cosmic rays of galactic origin.

If it is assumed that there is a uniform distribution of cosmic ray sources within the possible source region (i.e. galactic centre, galactic disc or spiral arms), then, for cosmic rays of a particular energy and composition originating in this region, the intensity at the Earth at a given arrival direction will be proportional to the pathlength within the source region of particles from that direction, if the motion is reasonably quasirectilinear.

Initially the galactic magnetic field was assumed to be given completely by a coherent field model with no irregular component.

Under these assumptions the following effects have been observed.

For cosmic rays originating in the galactic centre there is an energy region within which none can reach the Earth. At higher energies the particles follow straight trajectories and may hit the Earth, while at lower energies the particles can travel from the centre along the spiral arms to the Earth. The energy range of this forbidden band depends on the field model used, but except in the extreme case of field model C, for which particles can follow the spiral arm up to $E/Z \sim 10^{19}$ eV, particles with 10^{18} eV $\lesssim E/Z \lesssim 3\ 10^{19}$ eV cannot reach the Earth from the galactic centre. Very large anisotropies are predicted for cosmic rays originating in the galactic centre.

Particles produced in the galactic disc or spiral arms reach the Earth isotropically at low energies ($E/Z <$ about 10^{16} eV) as they are completely trapped in the galactic magnetic field. For a completely regular field, such as represented by the adopted coherent models, the particles may never escape. However, for a more realistic field some escape will occur. In fact, for the actual field it is known that the cosmic ray lifetime in the Galaxy is $\lesssim 10^{7}$ years. Thus some anisotropy probably exists even at these energies. If $E/Z \gtrsim 10^{19}$ eV, for which the trajectories approximate to straight lines, the intensity distribution reflects the geometry of the source region, so that such cosmic rays arrive less anisotropically than at $E/Z \sim 10^{18}$ eV. However, at intermediate values of E/Z considerable anisotropy is produced by the action of the galactic magnetic field. (The effects described here apply to a field represented completely by a coherent model with no irregularities).

As extensive air shower arrival direction measurements indicate that there is no observable anisotropy at these energies it would seem impossible for all such cosmic rays to be of galactic origin, although a considerable proportion of them could be. The remainder must be metagalactic.

Assuming all these cosmic ray primaries to be protons an upper limit to the galactic component can be found by comparison of model predictions with

E.A.S. measurements. Above $\sim 10^{18}$ eV field model B allows the largest galactic component (a few per cent) but below this energy the somewhat unrealistic model C allows up to about 100% galactic origin. For the energy range of these calculations ($6\ 10^{17}$eV to 10^{19} eV) most of the protons must be of metagalactic origin if the galactic magnetic field is of the form of the more probable models A or D.

If the cosmic ray primaries are all heavy ($Z \gtrsim 20$) then entirely galactic origin is feasible up to energies $\sim 2.10^{18}$ eV if it is assumed that the particles are sufficiently trapped to arrive fairly isotropically. However no qualitative calculations have been made of the anisotropy for $E/Z < 6\ 10^{17}$ eV.

Larger galactic cosmic ray components would be feasible if there were an extensive halo field.

The above arguments apply to a purely coherent disc magnetic field. The effect of an irregular field of the extreme form described above is to enable almost all cosmic rays (if they are protons) with energies below $6.\ 10^{17}$ eV for model D, or about 10^{17} eV for model A, to have been produced in the Galaxy without producing a definitely detectable anisotropy. For a more reasonable irregular field configuration, in which the largest field anomolies occur at separations $\sim$ 100 pc, the limiting energies are lower. However, between these limiting energies and $\sim 10^{19}$ eV at least 80% of cosmic rays must be metagalactic if they are protons.

If the primaries are heavy particles then the limiting energies are a factor of $\sim$ Z higher.

Thus if all the primaries are iron nuclei, and the galactic magnetic field is accurately represented by coherent field model D with the extreme case of adjacent 10 pc cells of irregular field, there is some possibility that cosmic rays of galactic origin could reach the Earth isotropically. If these conditions are not fulfilled then the cosmic rays reaching the Earth isotropically cannot be entirely of galactic origin but must contain a metagalactic component.

APPENDIX I

THE CALCULATION OF THE MAGNETIC FIELD DIRECTION AND STRENGTH AT A POINT WITHIN A REGION OF HELICAL FIELD CONFIGURATION

Consider a point, Q, of coordinates X,Y,Z (or cylindrical coordinates R_q, ϕ, Z), lying within a spiral arm of the Galaxy (see Figure A.1.1). This point is assumed to lie on a helix such as described in section 3.1.2. Figure A.1.2 shows a cross section of the tube on which the helix lies. To determine the field direction at Q, the helix on which it lies must be known; that is the length of the minor axis of the elliptical cross section must be found. It is possible to evaluate b, if A is known. However, due to the 40° shearing, A cannot be calculated directly. A first approximation to A is given by p.

$$\phi_R = CR + \phi_o \qquad \text{where} \quad \phi_o = 0 \text{ or } \pi$$

(defining the two spiral arms).

If Q lies on the arm $\phi_R = CR$ then

$$2n - 1 < \frac{R_q C - \phi}{\pi} - \tfrac{1}{2} < 2n$$

(n is zero or a positive integer), and $R_o' = \dfrac{2n\pi + \phi}{C}$

If Q lies on the arm $\phi_R = CR + \pi$ then

$$2n < \frac{R_q C - \phi}{\pi} - \tfrac{1}{2} < 2n + 1$$

and $$R_o' = \frac{(2n+1)\pi + \phi}{C}$$

Then $p = R_q - R_o'$

Using p as a first approximation to A an iteration process can be used to find A.

This was done for a number of points and it was found that $A = dp + e$,

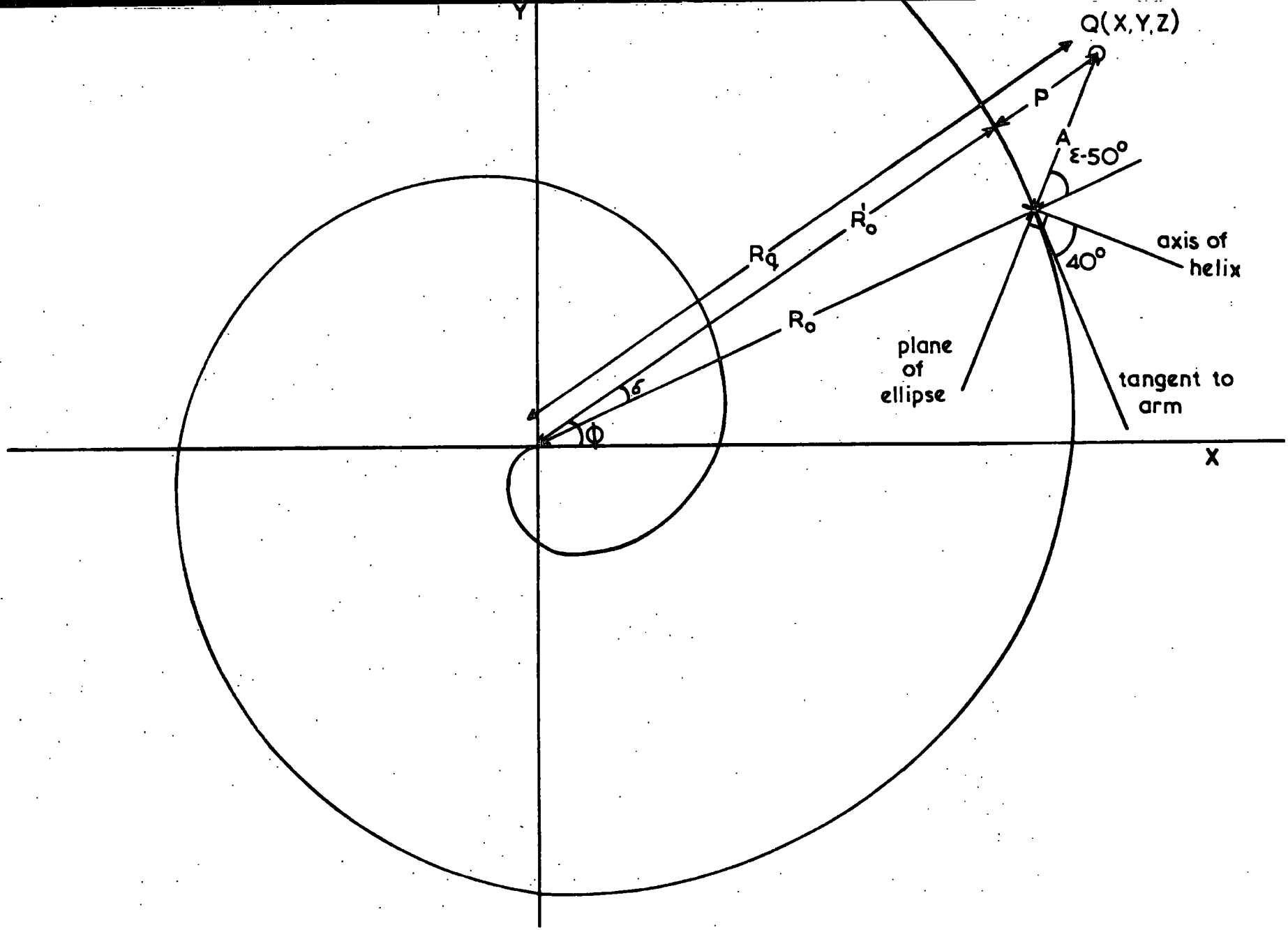

Figure A.1.1. Schematic diagram of the axis of a spiral arm of the Galaxy

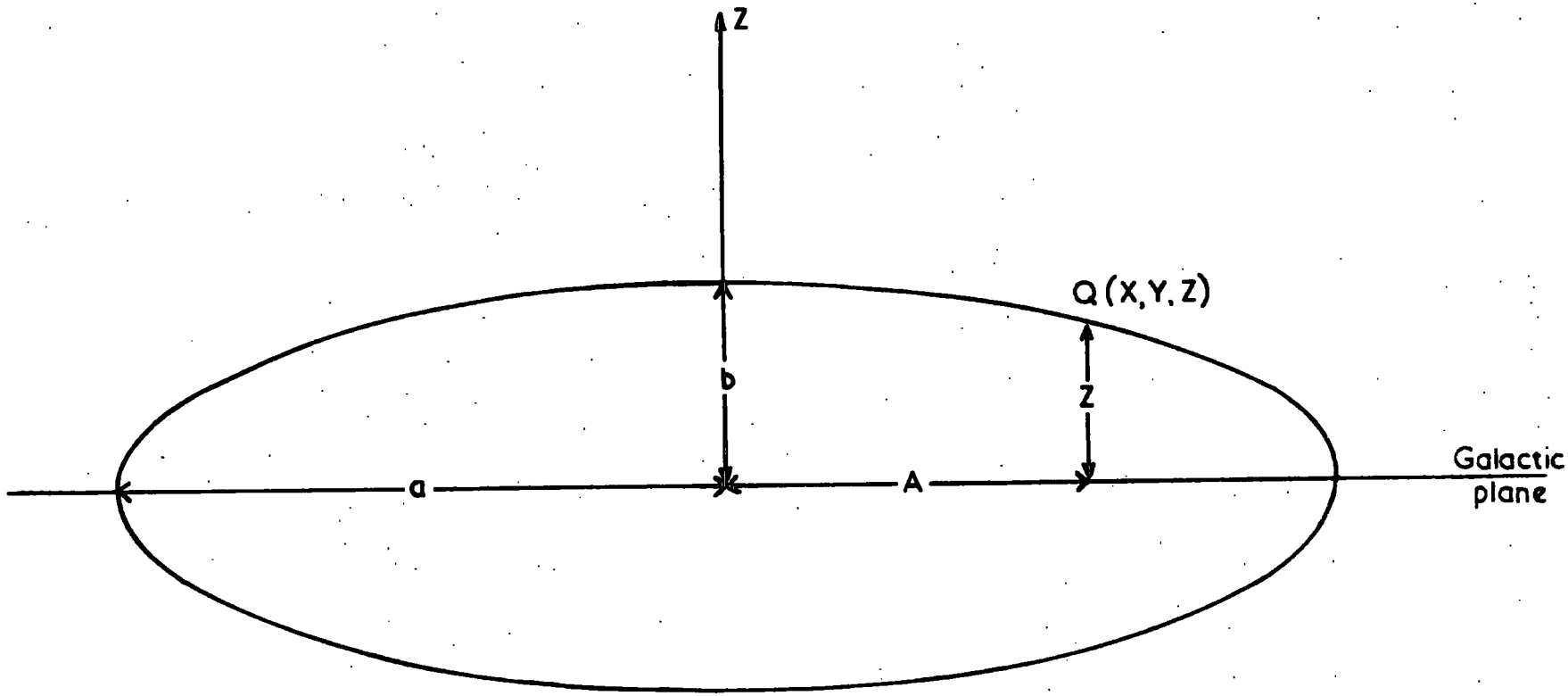

Figure A.1.2. Schematic diagram of a cross section of an elliptical tube.

where d and e are constants. Using a least squares fitting method

$$A = 1{\cdot}3319.\ p.$$

Then the equation of the ellipse is given by -

$$\left(\frac{A}{a}\right)^2 + \left(\frac{Z}{b}\right)^2 = 1$$

$$\text{so} \qquad b = \left(\frac{A^2}{9} + Z^2\right)^{\frac{1}{2}}$$

As the separation between arms is given by $\frac{\pi}{2C}$, the disc field is considered to exist only within the tube of elliptical semi-major axis of length $\frac{\pi}{2C}$. That is, if the ellipse corresponding to point Q has $b > b_{max} = \frac{\pi}{6C}$, Q lies outside the disc magnetic field.

If $b < 0{\cdot}001$ kpc, the field is also set at zero, since on the axis these helices give ambiguous field directions.

Initially setting $\varepsilon = 83{\cdot}95^{\circ}$ (the value at the Sun),

$$\sin\delta = \frac{|A|}{R_o} \sin(\varepsilon - 50)$$

$$R_o = R\cos\delta - A\cos(\varepsilon - 50)$$

$$\phi_{R_o} = CR_o + \phi_o$$

Then $\varepsilon = \tan^{-1} CR_o$ gives a better value for ε.

If the spiral arms are defined by $\phi_R = CR + \phi_o$, then the helical turns are described by

$$A = 3b \sin\left(\frac{2\pi C}{L\tan 7^{\circ}} R^2\right)$$

$$Z = b\cos\left(\frac{2\pi C}{L\tan 7^{\circ}} R^2\right)$$

where L is the circumference of the elliptical cross section and R corresponds to the centre of the ellipse.

$$X = R \cos \phi_R + A \cos (\phi_R + \varepsilon - 50)$$

$$Y = R \sin \phi_R + A \sin (\phi_R + \varepsilon - 50)$$

Hence setting $B = \dfrac{2\pi}{L \tan 7^\circ}$

$$\frac{\partial A}{\partial R} = 6ZBC\ R$$

$$\frac{\partial Z}{\partial R} = -\frac{2ABC\ R}{3}$$

$$\frac{\partial \varepsilon}{\partial R} = C \cos^2 \varepsilon$$

$$\frac{\partial X}{\partial R} = -CY + \cos \phi_R + \frac{\partial A}{\partial R} \cos (\phi_R + \varepsilon - 50)$$

$$-A \sin (\phi_R + \varepsilon - 50) \frac{\partial \varepsilon}{\partial R}$$

$$\frac{\partial Y}{\partial R} = CX + \sin \phi_R + A \cos (\phi_R + \varepsilon - 50) \frac{\partial \varepsilon}{\partial R}$$

$$+ \frac{\partial A}{\partial R} \sin (\phi_R + \varepsilon - 50)$$

Calculating $\dfrac{\partial X}{\partial R}$, $\dfrac{\partial Y}{\partial R}$, $\dfrac{\partial Z}{\partial R}$

and normalising by dividing by

$$M = \left[\left(\frac{\partial X}{\partial R} \right)^2 + \left(\frac{\partial Y}{\partial R} \right)^2 + \left(\frac{\partial Z}{\partial R} \right)^2 \right]^{\frac{1}{2}}$$

the magnetic field in the X, Y, and Z directions respectively is given by

$$H_X = \frac{H}{M} \frac{\partial X}{\partial R}$$

$$H_Y = \frac{H}{M} \frac{\partial Y}{\partial R}$$

$$H_Z = \frac{H}{M} \frac{\partial Z}{\partial R}$$

where H is the magnetic field strength.

Setting $R = R_o$, and substituting the values of X, Y, Z, A, b, etc. corresponding to point Q; H_X, H_Y, H_Z at Q can be determined in terms of the field strength at Q,

$$H = \gamma \frac{b_{max} - b}{b_{max}} \times \frac{1}{3} \left(1 + 8 \frac{Z^2}{b^2}\right)^{\frac{1}{2}}$$

The $\frac{1}{3} \left(1 + 8 \frac{Z^2}{b^2}\right)^{\frac{1}{2}}$ term gives Div $\underline{H} = 0$. On an ellipse of a particular b, the field corresponding to A, Z, must be

$\frac{1}{3} \left(1 + 8\frac{Z^2}{b^2}\right)^{\frac{1}{2}} H_{b_{max}}$ where $H_{b_{max}}$ is the field strength at $Z = b$, $A = 0$.

The $\frac{b_{max} - b}{b_{max}}$ term produces a reduction in the magnetic field strength as distance from the arm axis increases.

The field strengths are normalized by putting the maximum value of H (which is γ) equal to the maximum value on the Z axis through the Sun of H_{a_o} (model A).

Thus $\gamma = 6{\cdot}92$ μG.

Hence

$$H = 2{\cdot}3 \left(1 + 8 \frac{Z^2}{b^2}\right)^{\frac{1}{2}} \frac{b_{max} - b}{b_{max}} \quad \mu G$$

APPENDIX II

COSMIC RAY PROTONS FROM THE CRAB

The Crab Nebula is the remnant of a supernova explosion, the light from which was observed at the Earth in 1054 A.D. Any high energy protons produced in this explosion could also travel to the Earth. However, these protons will be affected by the galactic magnetic field and their path from the Crab to the Earth will be longer than the linear distance. Consequently these protons will arrive at the Earth later than the light from the explosion. In particular, those protons for which the path is 0·28 kpc longer than the linear distance to the Crab will be arriving at the Earth now. To investigate this effect, trajectories of protons from the Crab to the Earth were calculated for different field models at various energies.

The Crab is situated at $\ell = 184{\cdot}5^{\circ}$ and $b^{\prime} = -5{\cdot}8^{\circ}$. However, its exact distance from the Earth is uncertain by about 25%. (A recent distance estimate has been made by Trimble (1968), from measurements of the motion of filaments at the centre and at the edge of the nebula. The distance to the Crab nebula, assuming it to be either an oblate or prolate spheroid, was then deduced as $1{\cdot}38 \pm 0{\cdot}23$ kpc or $2{\cdot}02 \pm \begin{matrix}0{\cdot}24\\0{\cdot}27\end{matrix}$ kpc respectively. Trimble (1968) considered the latter case to be the more likely. Woltjer (1970), assuming smaller filament radial velocities obtained a distance of 1·68 kpc, but later measurements are interpreted by Trimble and Woltjer (1971) to give a distance $\sim$ 2 kpc). For the present calculations the Crab was taken to be at a distance of 1·70 kpc.

Trajectory calculations were performed using field models A and B, over a range of energies from 10^{19} eV down. In each case trajectories of antiprotons leaving the Earth over a range of directions were followed (as described in 4.2), and the minimum distance between each trajectory and the Crab was determined. Hence, by trial and error, the directions in which an antiproton must leave the Earth to hit the Crab was found.

TABLE A.2.1

DIRECTIONS OF ARRIVAL AT THE EARTH OF PROTONS FROM THE CRAB

FIELD MODEL A

Energy eV	Trajectory	Arrival direction at Earth ℓ	b^{II}	Length of trajectory from Crab. kpc
10^{19}		185·3°	- 22·4°	1·750
$3\ 10^{18}$	1	185·6°	33·5°	1·870
	2	188·2°	- 45·5°	1·760
	3	185°	26·5°	1·810
$2\ 10^{18}$	1	185·5°	33·5°	1·860
	2	192·7°	- 57·7°	1·760
	3	189·3°	53·4°	1·970
10^{18}	1	210·5°	76·4°	2·200
	2	191°	- 57·0°	2·040
	3	204°	- 73·4°	2·160
	4	260°	83·5°	2·190
	5	∿ 265°	∿ - 84·5°	∿ 1·80
$7{\cdot}5\ 10^{17}$	1	187°	48°	2·181
	2	336°	68·6°	2·385
	3	330·2°	- 67·2°	1·842
	4	331·5°	73·4°	2·526
	5	∿ 320°	∿ - 79°	∿ 2·35

TABLE A.2.2

DIRECTIONS OF ARRIVAL AT THE EARTH OF PROTONS FROM THE CRAB

FIELD MODEL B

Energy eV	Arrival direction at the Earth ℓ	b^{II}	Length of trajectory from Crab. kpc.
10^{19}	186·5°	- 17·8°	1·710
$6\ 10^{18}$	188·3°	- 24·7°	1·720
$3\ 10^{18}$	194·1°	- 38·0°	1·755
$2\ 10^{18}$	202·1°	- 48·9°	1·785
10^{18}	250·3°	- 63·0°	1·875
	328·0°	38·2°	2·885
$7\ 10^{17}$	292·5°	- 51·2°	1·960
$6\ 10^{17}$	305·6°	- 36·3°	2·030

Field Model A

This field model was used for calculations at 10^{19}eV, 3 10^{18}eV, 2 10^{18}eV, 10^{18}eV and 7·5 10^{17} eV.

The arrival directions are listed in Table A.2.1.

Due to the position of the Crab and the oscillation of trajectories about the galactic plane described in 4.2., there are several directions in which protons of a given energy (below about 3 10^{18} eV) can arrive at the Earth from the Crab.

These trajectories are shown in figures A.2.1 to A.2.4., which illustrate that protons from the Crab reach the Earth after making one or more oscillations about the galactic plane.

Thus for field model A, at least within this energy range, there is no unique direction or energy at which protons produced in the Crab supernova reach the Earth now.

Field Model B

The arrival directions at the Earth of protons from the Crab, for this field model are listed in Table A.2.2.

At energies 3 10^{17} eV and below the antiprotons followed are found to be completely trapped in the spiral arms. Some of the trajectories from the Crab are shown in figure A.2.5. In this case there are no oscillations about the galactic plane and at each energy considered, except 10^{18} eV, there is a unique path along which protons travel from the Crab to the Earth. The protons of 10^{18}eV which reach the Earth at $\ell = 328.0^{\circ}$, $b' = 38.2^{\circ}$, follow a long path from the Crab, and if they were produced in the Crab supernova will arrive at the Earth in $\sim$ 4900 A.D. For all the other trajectories followed there is a simple relationship between energy and trajectory length, as shown in figure A.2.6.

At very high energies the trajectory length approaches the straight line

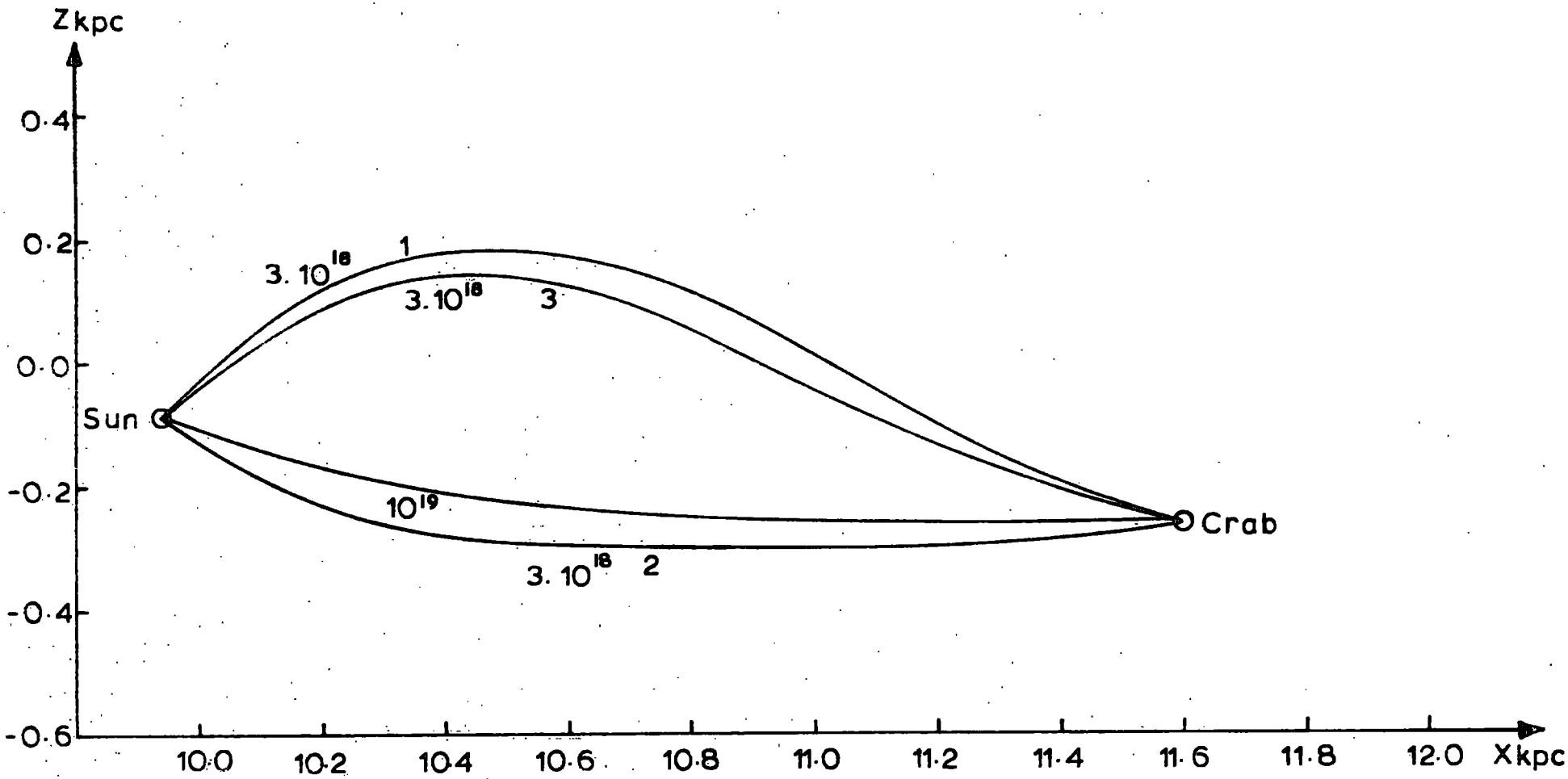

Figure A.2.1. Trajectories from the Crab to the Earth of protons of energy 10^{19} eV and $3.\ 10^{18}$ eV. Field model A.

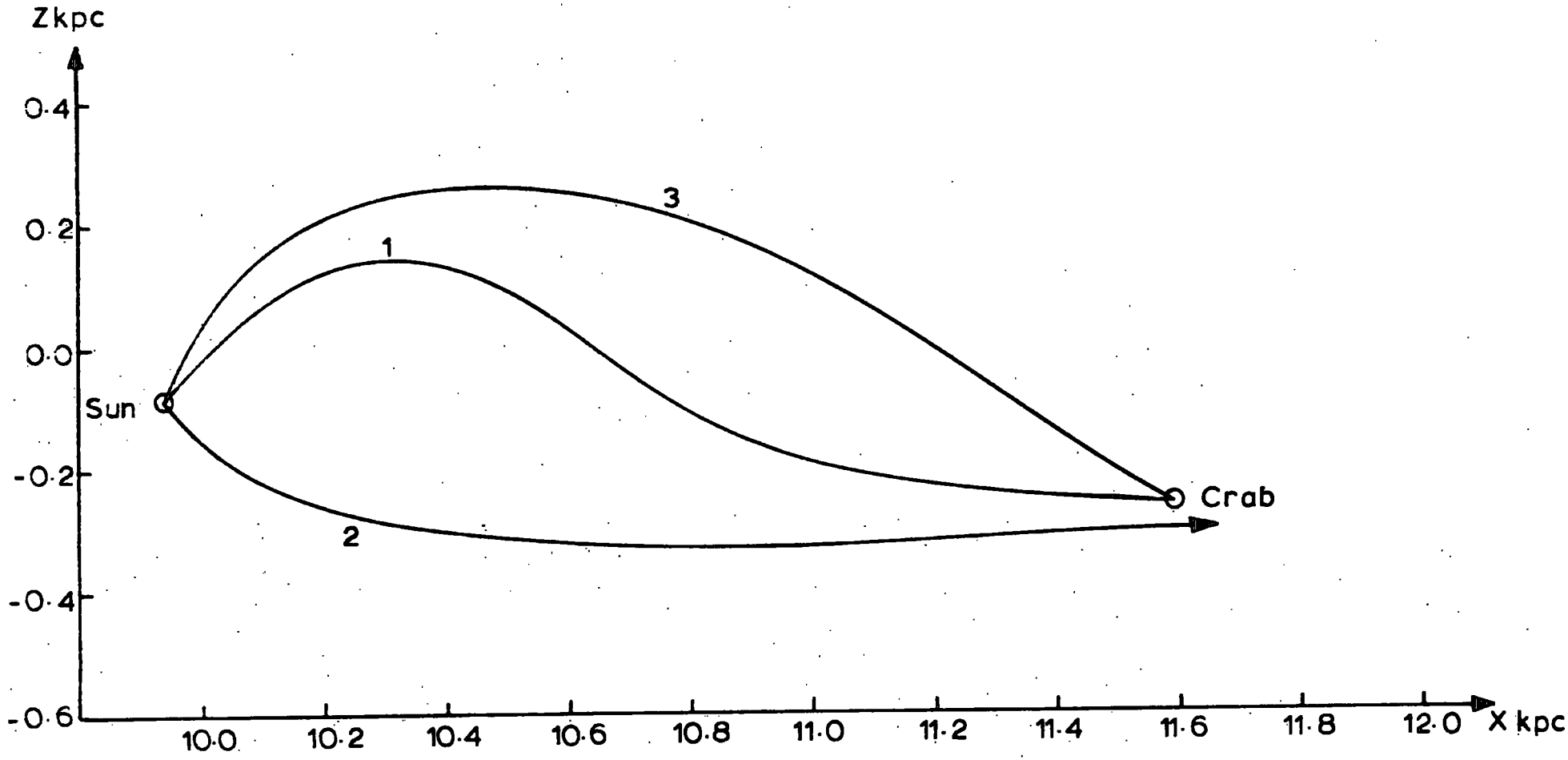

Figure A.2.2. Trajectories from the Crab to the Earth of protons of energy 2. 10^{18} eV.
Field model A.

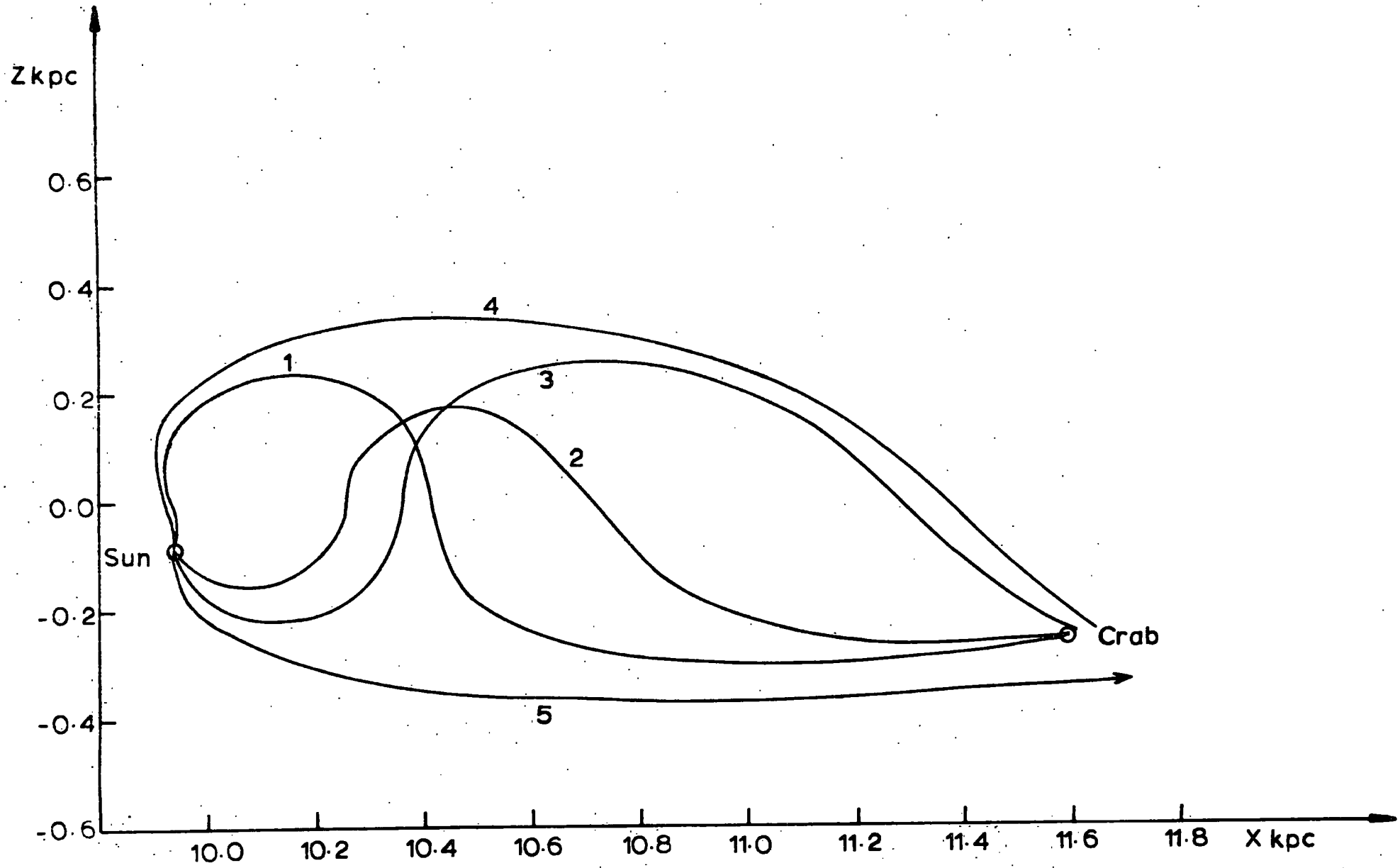

Figure A.2.3. Trajectories from the Crab to the Earth of protons of energy 10^{18} eV. Field model A.

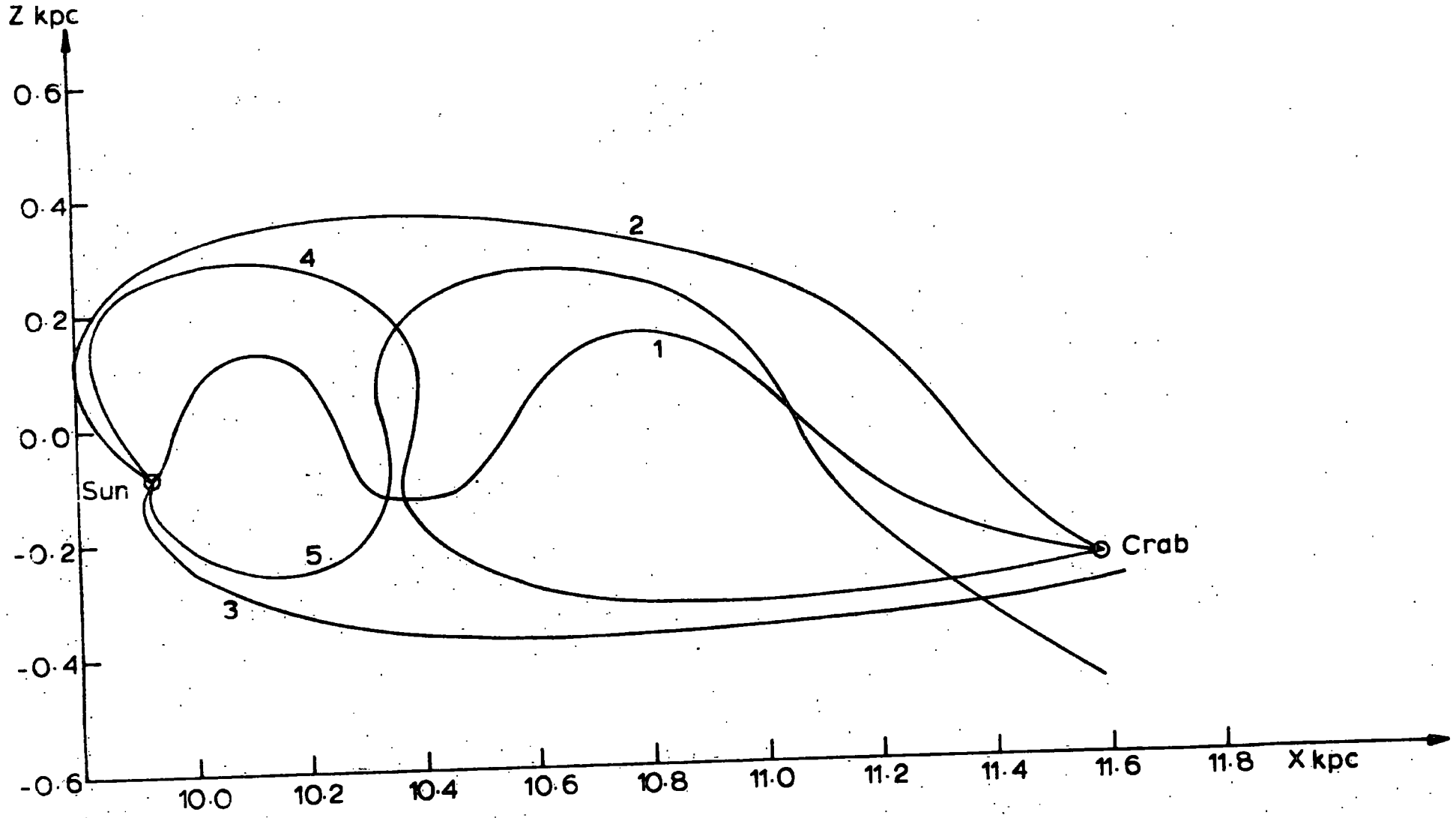

Figure A.2.4. Trajectories from the Crab to the Earth of protons of energy $7{\cdot}5\ 10^{17}$ eV. Field model A,

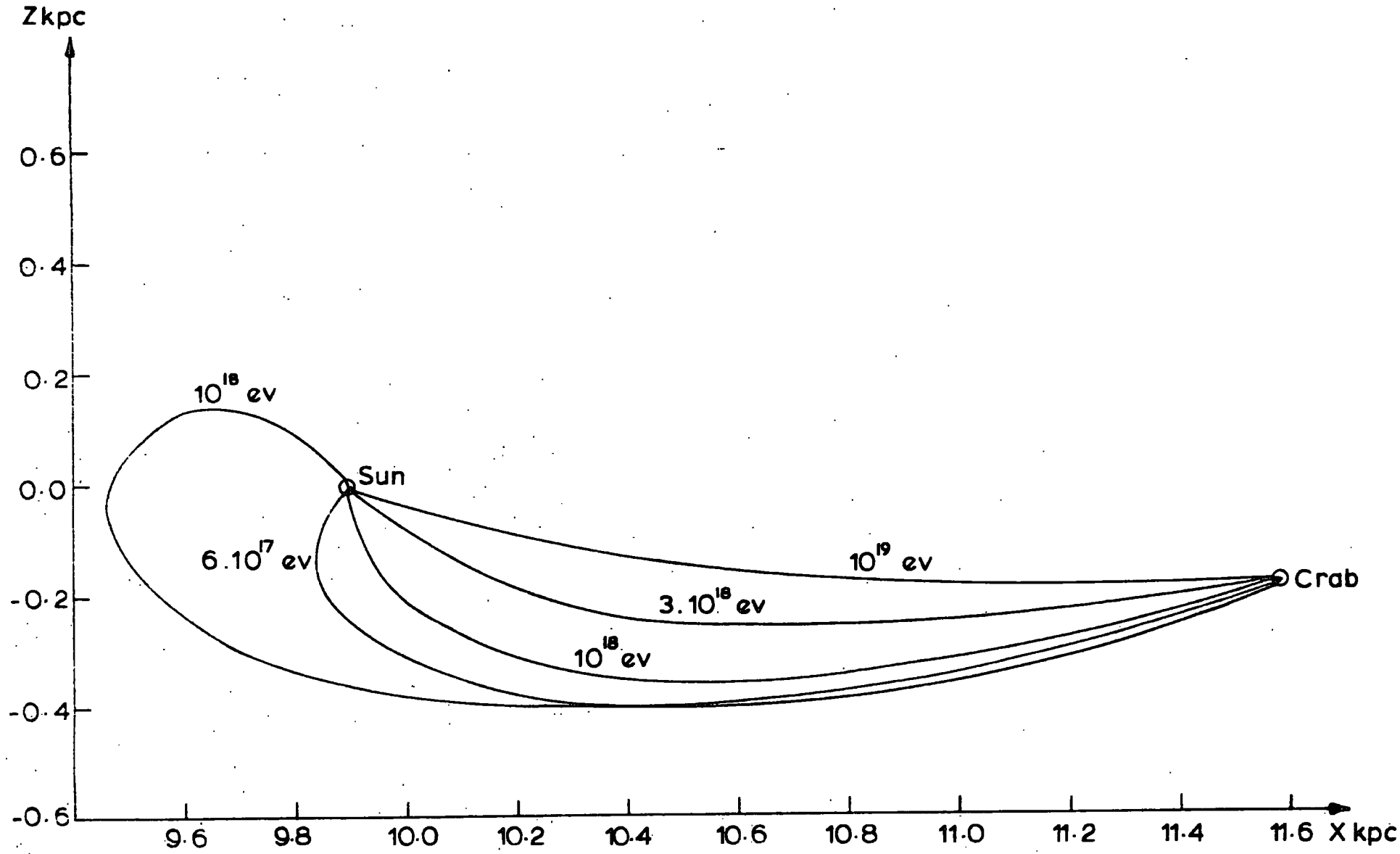

Figure A.2.5. Trajectories from the Crab to the Earth of protons. Field model B

Figure A.2.6. Trajectory lengths and arrival times at the Earth of protons from the Crab Supernova. Field model B.

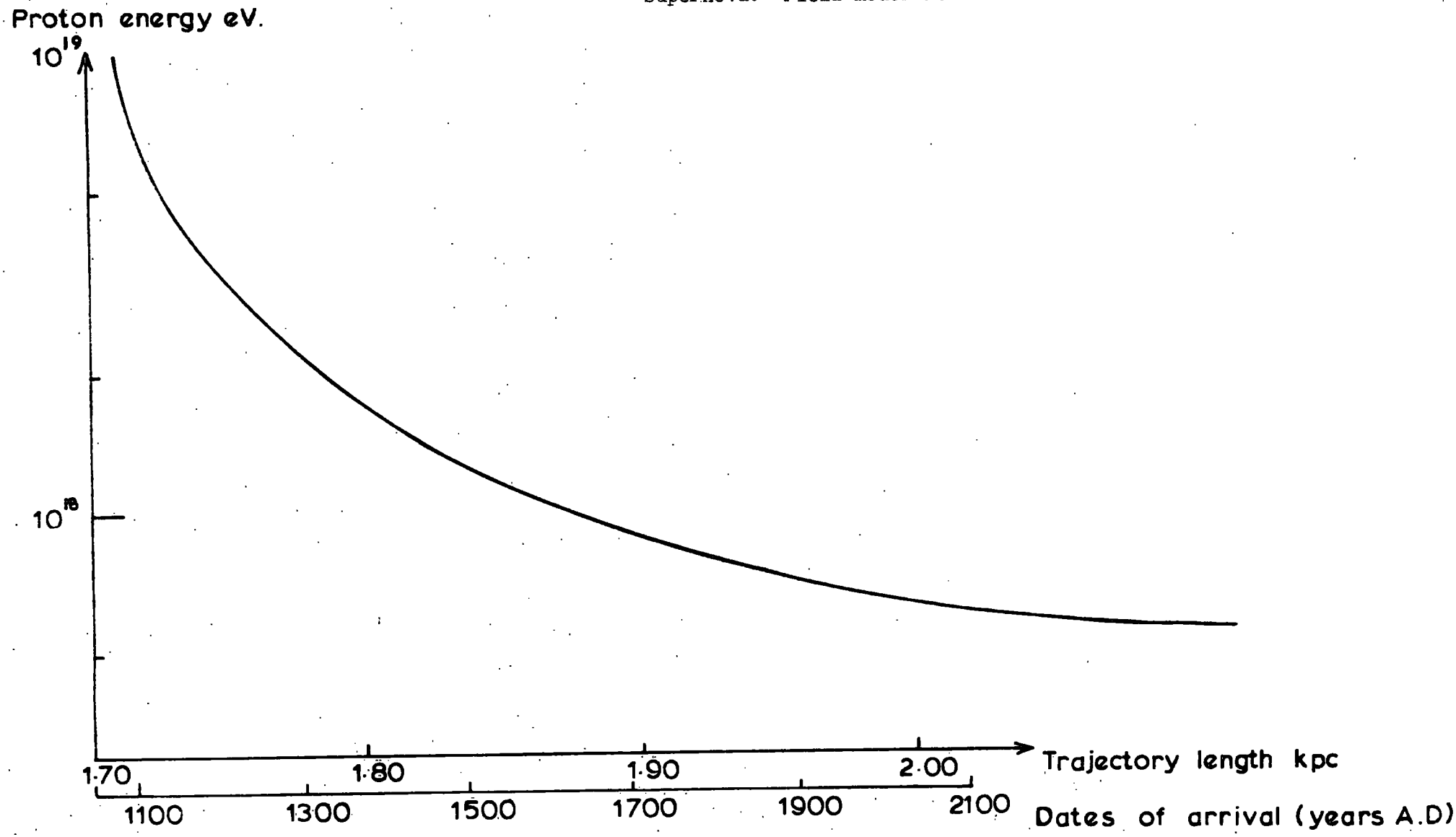

distance of 1·70 kpc, while protons of energy $\lesssim 5\ 10^{17}$ eV are unable to reach the Earth from the Crab, if field B is an accurate representation of the galactic field.

Protons arriving at the Earth now would have a trajectory length of 1·98 kpc and thus an energy of $6{\cdot}6\ 10^{17}$ eV. (Due to the form of the trajectories it is very probable that if the Crab is at a greater distance than 1·70 kpc, then the protons arriving now from the supernova would not have an energy much greater than this). These protons would appear to come from a point source at $\ell = -297^{\circ}$ and $b' = -49^{\circ}$. (R.A. = 26° and declination = -68°).

The proton flux is given by

$$\frac{N(E(R_t))}{4\pi R_t^2} \cdot \frac{dE(R_t)}{dT}\ m^{-2}\ s^{-1}$$

where $E(R_t)$ is the energy of protons having a trajectory of length R_t, T is the time taken to arrive at the Earth, and N(E) is the differential spectrum per ev of protons produced in the supernova.

Values of $\frac{dE(R_t)}{dT}$ were obtained from figure A.2.6. and the predicted flux at $6{\cdot}6\ 10^{17}$ eV was found to be $3{\cdot}7\ 10^{-34}\ N(E = 6{\cdot}6\ 10^{17}\ eV) m^{-2} s^{-1}$.

$E(R_t) \Big/ \frac{dE(R_t)}{dT}$ is typically $\sim 10^{10}$ seconds for $E(R_t)$ between $6\ 10^{17}$ eV and 10^{19} eV. Thus the supernova, which lasted for a much shorter time than this, can be considered to produce instantaneous emission.

Even if the actual field structure is not exactly as predicted by model B the flux of protons at $6.6\ 10^{17}$ eV will probably not be very different from the value above. However, the arrival direction may be changed considerably. For this reason it was taken that a point source would be observable in air shower measurements at these energies, if the intensity in a 10° R.A. by 10° declination bin exceeds the isotropic background by a factor of two.

The flux of the isotropic background in a 10° x 10° bin in an energy range 5 10^{17} eV to 10^{18} eV is $\sim 3.4\ 10^{-13} m^{-2} s^{-1}$. Thus the fact that no point source is observed gives an upper limit of $N(E = 6.6\ 10^{17}\ eV) \lesssim 6\ 10^{20}\ eV^{-1}$.

Assuming that the Crab Supernova produced protons such that for energies greater than 10^{9} eV

$$N(E) \propto E^{-2.6}$$

and that the total energy of these protons is 10^{49} ergs, then $N(E = 6.6\ 10^{17} eV) \sim 4\ 10^{19}\ eV^{-1}$. Thus the fact that no point source is observed does not rule out the Crab supernova as a source of high energy protons.

REFERENCES

ANAND, K.C., DANIEL, R.R., and STEPHENS, S.A., 1968, Phys. Rev. Letters, 20, 764.

ANAND, K.C., et al., 1968b, Proc. Ind. Acad. Sci., 67, 267.

ANAND, K.C., DANIEL, R.R., and STEPHENS, S.A., 1970, Proc. 11th Int. Conf. on Cosmic Rays (Budapest), Acta. Phys. Hung., 29, Suppl. 1, 229.

ANDREWS, D., et al., 1968, Nature 219, 343.

BALDWIN, J., 1955, Observatory, 75, 229.

BALDWIN, J.E., 1955, Mon. Not. R. Astr. Soc., 115, 690.

BEHR, A., 1959, Nach. Akad. Wiss. Gottingen (Sonderabdruck), 126, 201.

BEREZINSKII, V.S., and ZATSEPIN, G.T., 1969, Physics Letters, 28B, 423.

BEREZINSKII, V.S., and ZATSEPIN, G.T., 1971, Sov. Journal of Nuclear Physics, 13, 453.

BERGE, G.L., and SEIELSTAD, G.A., 1967, Astrophys. J., 148, 367.

BERKHUIJSEN, E.M., 1971, Astron. and Astrophys., 14, 359.

BIERMANN, L., and DAVIS, L., 1960, Zeitschrift fur Astrophysik, 51, 19.

BINGHAM, R.G., 1966, Mon. Not. R. Astr. Soc., 134, 327.

BINGHAM, R.G., and SHAKESHAFT, J.R., 1967, Mon. Not. R., Astr. Soc., 136, 347.

BOLTON, J.G., and WILD, J.P., 1957, Astrophys. J., 125, 296.

BRIDLE, A.H., and VENUGOPAL, V.R., 1969, Nature, 224, 545.

BROWNLEE, R.G., 1970, Ph.D. Thesis, University of Sydney.

BROWNLEE, R.G., et al., 1970, Proc. 11th Int. Conf. on Cosmic Rays (Budapest), Acta. Phys. Hung., 29, Suppl. 3, 383.

BROWNLEE, R.G. et al., 1970a, Proc. 11th Int. Conf. on Cosmic Rays (Budapest), Acta. Phys. Hung., 29, Suppl. 3, 377.

CAVALLO, G., 1971, Nature Physical Science 231, 35.

CHANDRASEKHAR, S., 1946, Astrophys. J., 103, 351.

CHANDRASEKHAR, S., and FERMI, E., 1953, Astrophys. J., 118, 113.

COOPER, B.F.C., and PRICE, R.M., 1962, Nature, 195, 1084.

COSTAIN, C.H., 1960, Mon. Not. R. Astr. Soc., 120, 248.

CRITCHFIELD, C.L., NEY, E.P., and OLESKA, S., 1952, Physical Rev., 85, 461.

DAVIES, J.G., and LARGE, M.I., 1970, Mon. Not. R. Astr. Soc., 149, 301.

DAVIES, J.G., et al., 1968, Nature, 217, 910.

DAVIES, R.D., 1964, Mon. Not. R. Astr. Soc., 128, 133.

DAVIES, R.D., 1965, Proc. 9th Int. Conf. on Cosmic Rays (London), (Institute of Physics and the Physical Society), Vol. 1, 35.

DAVIES, R.D., 1968, Nature, 218, 435.

DAVIES, R.D., 1969, Nature, 223, 355.

DAVIES, R.D., and HAZARD, C., 1962, Mon. Not. R. Astr. Soc., 124, 147.

DAVIES, R.D., and SHUTER, W.L.H., 1963, Mon. Not. R. Astr. Soc., 126, 369.

DAVIES, R.D., et al., 1960, Nature, 187, 1088.

DAVIES, R.D., et al., 1962, Nature, 196, 563.

DAVIES, R.D., et al., 1963a, Mon. Not. R. Astr. Soc., 126, 343.

DAVIES, R.D., et al., 1963b, Mon. Not. R. Astr. Soc., 126, 353.

DAVIES, R.D., et al., 1968, Nature, 220, 1207.

DAVIS, L., and GREENSTEIN, J.L., 1951, Astrophys. J., 114, 206.

EARL, J.A., 1961, Physical Review Letters, 6, 125.

EARNSHAW, R.A., et al., 1968, Proc. 10th Int. Conf. on Cosmic Rays, Canadian Journal of Physics, 46, S5.

GALT, J.A., et al., 1960, Mon. Not. R. Astr. Soc., 120, 187.

GARDNER, F.F., and DAVIES, R.D., 1966, Aust. J. Phys., 19, 129.

GARDNER, F.F., and WHITEOAK, J.B., 1963, Nature, 197, 1162.

GARDNER, F.F., et al., 1967, Nature, 214, 371.

GARDNER, F.F., et al., 1969a, Aust. J. Phys., 22, 79.

GARDNER, F.F., et al., 1969b, Aust. J. Phys., 22, 107.

GARDNER, F.F., et al., 1969c, Aust. J. Phys., 22, 813.

GARDNER, F.F., et al., 1969d, Aust. J. Phys., 22, 821.

GINZBURG, V.L., and SYROVATSKII, S.I., 1971, Lebedev Physical Institute, Theoretical Dept., Preprint No. 77.

GOLD, T., 1969, Nature, 221, 25.

GOLDSTEIN, S.J., and JAMES, J.T., 1969, Astrophys. J., 158, L179.

GREISEN, K., 1966, Physical Review Letters, 16, 748.

GUNN, J.E., and OSTRIKER, J.P., 1969, Physical Review Letters, 22, 728.

HADDOCK, F.T., and HOBBS, R.W., 1963, Astron. J., 68, 75.

HALL, J.S., 1958, Pub. U.S. Naval Obs., 17, part VI.

HALL, J.S., and SERKOWSKI, 1963, Stars and Stellar Systems (University of Chicago Press), Volume 3, Basic Astronomical Data, Ch. 16, Polarization of Starlight.

HARWIT, M., 1970, Nature, 226, 61.

HENRY, J., 1958, Astrophys. J., 128, 497.

HEWISH, A., 1970, Annual Review of Astron. and Astrophys. 8, 265.

HILLAS, A.M., 1968, Proc. 10th Int. Conf. on Cosmic Rays (Calgary), Canadian Journal of Physics, 46, S623.

HILLAS, A.M., 1969, Proc. 11th Int. Conf. on Cosmic Rays (Budapest), Acta. Phys. Hung., 29, Suppl. 3, 355.

HILLAS, A.M., et al., 1971, Proc. 12th Int. Conf. on Cosmic Rays (Hobart), (Hobart: University of Tasmania), Vol. 3, 1001.

HILTNER, W.A., 1949, Astrophys. J., 109, 471.

HILTNER, W.A., 1956, Astrophys. J., Suppl. 2, 389.

HOAG, A.A., 1953, Astron. J., 58, 42.

HOLLINGER, J.P., et al., 1964, Astrophys. J., 140, 656.

HOLLOWS, J.D., 1968, Ph.D. Thesis, University of Leeds.

HORNBY, J.M., 1966, Mon. Not. R. Astr. Soc., 133, 213.

HOYLE, F., and IRELAND, J.G., 1961, Mon. Not. R. Astr. Soc., 122, 35.

IRELAND, J.G., 1961, Mon. Not. R. Astr. Soc., 122, 461.

JOKIPII, J.R., and LERCHE, I., 1969, Astrophys. J., 157, 1137.

JOKIPII, J.R., et al., 1969, Astrophys. J., 157, L119.

KARAKULA, S., et al., 1971, Proceedings 12. Int. Conf. on CR., Hobart: Uof Tasmania, Vol. 1., 310

KARAKULA, S., et al., 1971a, J. Phys. A.: Gen. Phys., Vol 5, 904

KULIKOV, G.V., et al., 1969, Soviet Physics - J.E.T.P. Letters, 10, 222.

LANDECKER, T.L., and WIELEBINSKI, R., 1970, Australian J. Phys., Suppl. 16.

LAPIKENS, J., et al., 1971, Proc. 12th Int. Conf. on Cosmic Rays (Hobart), (Hobart: University of Tasmania), Vol. 1, 316.

LARGE, M.I., MATHEWSON, D.S., and HASLAM, C.G.T., 1961, Mon. Not. R. Astr. Soc., 123, 123.

LINSLEY, J., 1963, Proc. 8th Int. Conf. on Cosmic Rays, (Jaipur), (Bombay: Tata Inst. Fund. Research), Vol. 4, 77.

LINSLEY, J., and SCARSI, L., 1962, Phys. Rev. Letters, 9, 123.

LYNE, A.G., and RICKETT, B.J., 1968, Nature 219, 1339.

LYNE, A.G., et al., 1971, Mon. Not. R. Astr. Soc., 153, 337.

MALTBY, P., and SEIELSTAD, G.A., 1966, Astrophys. J., 144, 216.

MANCHESTER, R.N., 1971a, Astrophys. J., 167, L101.

MANCHESTER, R.N., 1971b, Nature Physical Science, 231, 189.

MANCHESTER, R.N., 1972, Astrophys. J., 172, 43.

MARTIN, P.G., 1971, Mon. Not. R. Astr. Soc., 153, 279.

MATHEWSON, D.S., 1968, Astrophys. J., 153, L47.

MATHEWSON, D.S., 1969, Proc. Australian Ast. Soc., 1(5), 209.

MATHEWSON, D.S., BROTON, N.W., and COLE, D.J., 1966, Aust. J. Phys., 19, 93.

MATHEWSON, D.S., and FORD, V.L., 1970, Mem. R. Astr. Soc., 74, 139.

MATHEWSON, D.S., and MILNE, D.K., 1964, Nature, 203, 1273.

MATHEWSON, D.S., and NICHOLLS, D.C., 1968, Astrophys. J., 154, L11.

MATHEWSON, D.S., and ROME, J.M., 1963, Observatory, 83, 20.

MAYER, C.H., et al., 1962, Astron. J., 67, 581.

MAYER, C.H., et al., 1964, Astrophys. J., 139, 248.

MEYER, P., and MÜLLER, D., 1971, Proc. 12th Int. Conf. on Cosmic Rays (Hobart), (Hobart: University of Tasmania), Vol. 1, 117.

MEYER, P., and VOGT, R., 1961, Physical Review Letters, 6, 193.

MILLS, B.Y., 1959, Proc. I.A.U. Paris Symposium on Radio Astronomy, 431, Ed. R.N. Bracewell (Stanford: Stanford University Press).

MILLS, B.Y., 1970, I.A.U. Symposium No. 38, The Spiral Structure of our Galaxy, (D. Reidel Pub. Company, Dordrecht-Holland), 178.

MITTON, S., 1972, Mon. Not. R. Astr. Soc., 155, 373.

MORRIS, D., and BERGE, G.L., 1964, Astrophys. J., 139, 1388.

MORRIS, D., RADHAKRISHNAN, V., and SEIELSTAD, G.A., 1964, Astrophys. J., 139, 758.

OSBORNE, J.L., and ROBERTS, E., 1971, Proceedings 12. Int. Conf. on CR., Hobart: Uof Tasmania, Vol 1, 340

PARKER, E.N., 1965, Astrophys. J., 142, 584.

PARKER, E.N., 1968, Astrophys. J., 154, 49.

PARKER, E.N., 1969, Astrophys. J., 157, 1129.

PAULINY-TOTH, I.I.K., and SHAKESHAFT, J.R., 1962, Mon. Not. R. Astr. Soc., 124, 61.

PENZIAS, A.A., and WILSON, R.W., 1965, Astrophys. J., 142, 419.

PRENTICE, A.J.R., and ter HAAR, D., 1969, Mon. Not. R. Astr. Soc., 146, 423.

RADHAKRISHNAN, V., and COOKE, D.J., 1969, Astrophys. Letters, 3, 225.

RADHAKRISHNAN, V., et al., 1969, Nature, 221, 443.

ROSE, W.K., et al., 1963, Astron. J., 68, 78.

SCHWARZ, U.J., and MORRIS, D., 1971, Astrophys. Letters, 7, 185.

SEIELSTAD, G.A., et al., 1963, Astrophys. J., 138, 602.

SEIELSTAD, G.A., et al., 1964, Astrophys. J., 140, 53.

SEYMOUR, P.A.H., 1969, Mon. Not. R., Astr. Soc., 142, 33.

SHITOV, Yu. P., 1971, Nature Physical Science, 229, 179.

SMITH, E. Van P., 1956, Astrophys. J., 124, 43.

SMITH, F.G., 1961, Nature, 191, 1381.

SMITH, F.G., 1968a, Nature, 218, 325.

SMITH, F.G., 1968b, Nature, 220, 891.

SPITZER, L., 1954, Astrophys. J., 120, 1.

SPITZER, L., 1956, Astrophys. J., 124, 20.

SPITZER, L., 1968, Diffuse Matter in Space (John Wiley, New York).

SPITZER, L., and TUKEY, J.W., 1951, Astrophys. J., 114, 187.

SPOELSTRA, T.A.TH., 1971, Astron. and Astrophys., 13, 237, and Private Communication.

STAELIN, D.H., and REIFENSTEIN, E.C., 1969, Astrophys. J., 156, L121.

SYROVATSKII, S.I., 1969, Lebedev Institute, Preprint No. 151.

TAYLOR, J.H., 1969, Astrophys. Letters, 3, 205.

TENNENT, R.M., 1968, Proc. 10th Int. Conf. on Cosmic Rays, Canadian Journal of Physics, 46, S1.

THIELHEIM, K.O., and LANGHOFF, W., 1968, J. Phys. A: Gen. Phys., 1, 694.

THIELHEIM, K.O., and LANGHOFF, W., 1969, Proc. 11th Int. Conf. on Cosmic Rays (Budapest), Acta. Phys. Hung., 29, Suppl. 1, 549.

THIELHEIM, K.O., et al., 1971, Proc. 12th Int. Conf. on Cosmic Rays (Hobart), (Hobart: University of Tasmania), Vol. 1, 395.

TRIMBLE, V., 1968, Astron. J., 73, 535.

TRIMBLE, V., and WOLTJER, L., 1971, Astrophys. J., 163, L97.

VERSCHUUR, G.L., 1968, Physical Review Letters, 21, 775.

VERSCHUUR, G.L., 1969a, Astrophys. J., 156, 861.

VERSCHUUR, G.L., 1969b, Astrophys. J., 155, L155.

VERSCHUUR, G.L., 1970, I.A.U. Symposium No. 39, Interstellar Gas Dynamics, (D. Reidel Pub. Comp., Dordrecht-Holland), 150.

VITKEVICH, V.V., and SHITOV, Yu. P., 1970, Nature, 226, 1235.

WEINREB, S., 1962, Astrophys. J., 136, 1149.

WESTERHOUT, G., et al., 1962, Bull. Astr. Inst. Neth., 16, 187.

WICKRAMASINGHE, N.C., 1969, Nature, 224, 656.

WIELEBINSKI, R., and SHAKESHAFT, J.R., 1964, Mon. Not. R. Astr. Soc., 128, 19.

WOLTJER, L., 1961, Astrophys. J., 133, 352.

WOLTJER, L., 1965, Stars and Stellar Systems, (University of Chicago Press), Volume 5.

WOLTJER, L., 1970, I.A.U. Symposium No. 37, Non Solar X and γ Ray Astronomy (D. Reidel Pub. Comp., Dordrecht-Holland)

YATES, K.W., and WIELEBINSKI, R., 1966, Aust. J. Phys., 19, 389.

ZATSEPIN, V.I., 1971, Proc. 12th Int. Conf. on Cosmic Rays (Hobart), (Hobart: University of Tasmania), Vol. 1, 116.

ZATSEPIN, G.T., and KUZMIN, V.A., 1966, Soviet Phys. - J.E.T.P. Letters, 4, 78.

ACKNOWLEDGEMENTS

The author wishes to thank Professor G. D. Rochester, F.R.S., for the provision of facilities to carry out this work.

She would also like to thank her supervisor Professor A. W. Wolfendale.

She is indebted to Dr. J. L. Osborne for his invaluable help and advice at all stages of the work.

The valuable discussions with Dr. J. Wdowczyk, Dr. S. Karakula and Mr. W. Tkaczyk of the Lodz Cosmic Ray Research Group are acknowledged with gratitude.

The Institute of Nuclear Physics in Poland is thanked for its hospitality.

The author would also like to thank Dr. A. A. Watson and Professor J. Linsley for supplying data from the Haverah Park and Volcano Ranch E.A.S. arrays, respectively.

The assistance of the staff of the Durham University Computing Unit and the Institute of Nuclear Physics, Lodz, Computer Unit is gratefully acknowledged.

The author is very grateful to Mrs. P. Russell for preparing the diagrams and to Mrs. J. Moore for her typing of this thesis.

The Science Research Council is thanked for the provision of a Research Studentship during the period of this work.

Finally, the author would like to thank all those who encouraged her throughout the work described in this thesis and during the preparation of the thesis, particularly Mrs. A. Bowcott.